REPORT DOCUMENTATION PAGE	Form Approved OMB No. 0704-0188

Public reporting burden for this collection of information is estimated to average 1 hour per response, including the time for reviewing instructions, searching existing data sources, gathering and maintaining the data needed, and completing and reviewing the collection of information. Send comments regarding this burden estimate or any other aspect of this collection of information, including suggestions for reducing this burden, to Washington Headquarters Services, Directorate for Information Operations and Reports, 1215 Jefferson Davis Highway, Suite 1204, Arlington, VA 22202-4302, and to the Office of Management and Budget, Paperwork Reduction Project (0704-0188), Washington, DC 20503.

1. AGENCY USE ONLY (Leave blank)

2. REPORT DATE: Mar 95

3. REPORT TYPE AND DATES COVERED

4. TITLE AND SUBTITLE: Flow & Visualization of vorticity Cancellation of Jets in Cross flow

5. FUNDING NUMBERS

6. AUTHOR(S): Anthony G. Simpson

7. PERFORMING ORGANIZATION NAME(S) AND ADDRESS(ES): AFIT Students Attending: Univ of Washington

8. PERFORMING ORGANIZATION REPORT NUMBER: AFIT/CI/CIA 94-004

9. SPONSORING/MONITORING AGENCY NAME(S) AND ADDRESS(ES):
DEPARTNEMT OF THE AIR FORCE
AFIT/CI
2950 P STREET, BDLG 125
WRIGHT-PATTERSON AFB OH 45433-7765

10. SPONSORING/MONITORING AGENCY REPORT NUMBER

11. SUPPLEMENTARY NOTES

12a. DISTRIBUTION/AVAILABILITY STATEMENT:
Approved for Public Release IAW AFR 190-1
Distribution Unlimited
BRIAN D. GAUTHIER, MSgt, USAF
Chief Administration

12b. DISTRIBUTION CODE

13. ABSTRACT (Maximum 200 words)

14. SUBJECT TERMS

15. NUMBER OF PAGES: 93

16. PRICE CODE

17. SECURITY CLASSIFICATION OF REPORT

18. SECURITY CLASSIFICATION OF THIS PAGE

19. SECURITY CLASSIFICATION OF ABSTRACT

20. LIMITATION OF ABSTRACT

DISCLAIMER NOTICE

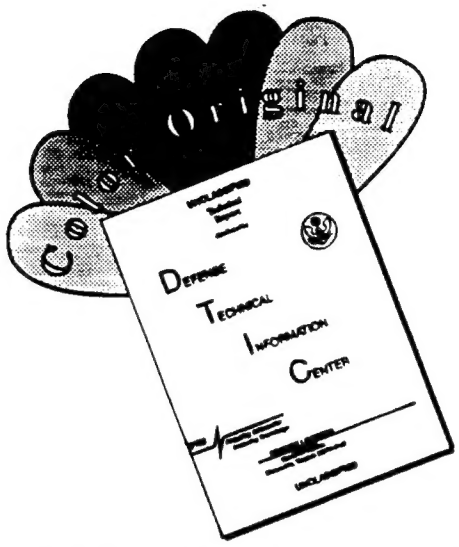

THIS DOCUMENT IS BEST QUALITY AVAILABLE. THE COPY FURNISHED TO DTIC CONTAINED A SIGNIFICANT NUMBER OF COLOR PAGES WHICH DO NOT REPRODUCE LEGIBLY ON BLACK AND WHITE MICROFICHE.

University of Washington

Abstract

Flow Visualization of Vorticity Cancellation of Jets in Crossflow

by Anthony G. Simpson

Chairperson of Supervisory Committee: Professor Mitsuru Kurosaka
Dept. of Aeronautics and Astronautics

An experimental apparatus was designed and constructed for water tunnel flow visualization of multiple, staggered and in-line row jet injection in crossflow. Specifically, a physical explanation was sought for existing film cooling performance results from turbine test rigs. Experiments were conducted in the University of Washington low-speed, free surface water tunnel facility having a 3.0x0.7x0.7 meter test section and a speed capability of up to 0.7 m/s. Jet injection was controlled for each row independently at blowing ratios from 0.5 to 2.5, with the jet development length to diameter ratio set at 6.0. Flow visualization using both colored dye and fluorescent laser sheeting was accomplished to track vortex structure and interaction in the flow. The results indicate that vorticity cancellation is a factor in improved cooling performance over single row injection through a reduction in both jet lift off from the surface and entrainment of the main flow toward the surface.

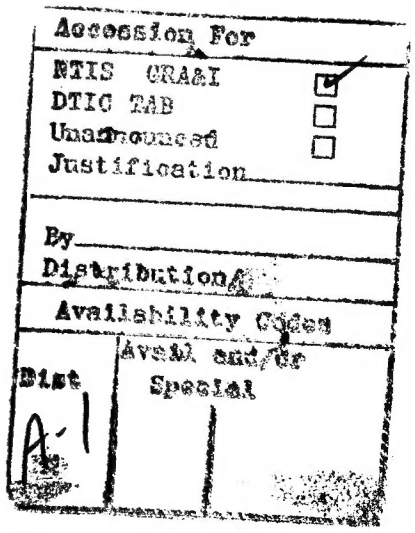

Flow Visulization of Vorticity Cancellation of Jets in Crossflow

by

Anthony G. Simpson

A thesis submitted in partial fulfillment
of the requirements for the degree of

Master of Science in Aeronautics and Astronautics

University of Washington

1995

Approved by _____
(Chairperson of Supervisory Committee)

Program Authorized
to Offer Degree Department of Aeronautics and Astronautics

Date 1/4/95

In presenting this thesis in partial fulfillment of the requirements for a Master's degree at the University of Washington, I agree that the Library shall make its copies freely available for inspection. I further agree that extensive copying of this thesis is allowable only for scholarly purposes, consistent with "fair use" as prescribed in the U.S. Copyright Law. Any other reproduction for any purposes or by any means shall not be allowed without my written permission.

Signature _____

Date _____

Table of Contents

List of Figures

List of Tables

Acknowledgements

First, I'd like to thank all the people who helped make this thesis possible. Without the belief of Professor Kurosaka and the educational guidance and proofreading of Captain Brenda Haven this paper would not have happened.

Next, I truly thank Bill Lowe for his chastisement in the machine shop. I certainly learned more about mill and lathe operation than I did about vortex theory.

On a more personal level, I extend a hearty thanks to all my peers. Lt. Paul Scott's invaluable assistance in high speed interference effects research was invaluable. Also, Anhtuan Ngo receives my sincerest thanks for reminding me that data is the plural of datum.

Finally, many thanks to the United States Air Force Institute of Technology for my personal funding, time and tuition. I hope to repay you many times over.

For Blythe; you are everything to me.

Chapter 1: Introduction

1.1 Film Cooling

Modern aircraft gas turbine engine fuel economy and thrust to weight performance are largely dependent on attaining a high turbine inlet temperature. Although materials research continues to yield significant increases in material allowable temperatures, turbine blade and combustor liner cooling have allowed for the increase of turbine inlet temperature to around 2000 °K, which is several hundred degrees above the maximum allowable temperature of the materials utilized in turbine blade manufacture (Kerrebrock 296) .

Much of this cooling in the turbine section is performed through film cooling in which compressor bleed air is ejected from the rotor and stators near the leading edge and mid-chord regions and passed over the exterior of the blade as shown in figure 1-1. This reduces the advective heating of the surface by the hot gas and cools the blade through advection with the "cool" gas. Although film cooling efforts have allowed significant turbine inlet temperature increases, turbine inlet temperatures as high as 2400 °K are envisioned for future engines operating at near-stoichiometric combustion (Kerrebrock 296). Despite the past performance of film cooling and the burden it is expected to carry in the future, much of the knowledge concerning film cooling being applied is purely empirical. For example, in the voluminous 1990 Rolls Royce report entitled "Turbine Cooling System Design", the authors presented results of heat transfer performance both in a wind tunnel and a turbine test rig (Norton iii). No effort was made to describe the underlying physical phenomena which determine the performance. An understanding of these phe-

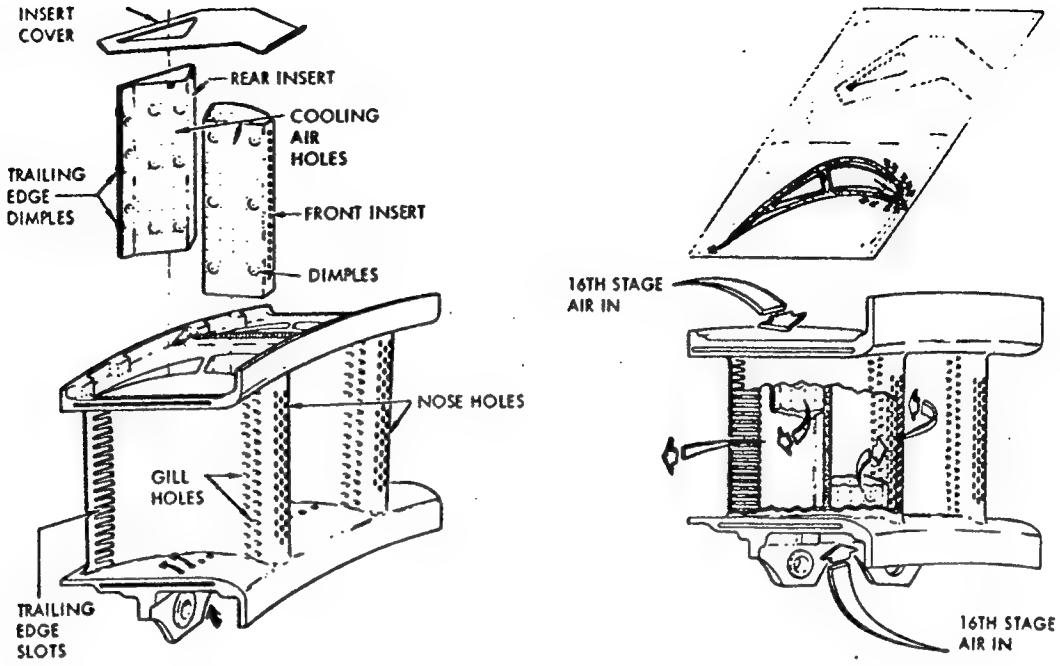

Figure 1-1: Film cooling schematic.

nomena will be critical for achieving the engine performance goals set by the Air Force and engine companies desiring to reach near-stoichiometric combustion (Koop).

1.2 Research Efforts

A continuing program of investigation directed at understanding and improving the efficiency of turbine cooling schemes is underway at the University of Washington, Department of Aeronautics, Propulsion Laboratory, under the supervision of Professor Mitsuru Kurosaka. Investigation of film cooling is being primarily undertaken by doctoral candidate Brenda Haven. The principal areas of interest are presented in a 1994 grant proposal to the Air Force Office of Scientific Research (Kurosaka 25-28). This research is planned through approximately 1997.

First will be flow visualization research of circular and shaped holes at both perpendicular and 30° injection angles. Experiments will be conducted with multiple and single jets, for blowing ratios from 0.2 to 2.0 and at a variety of jet development length to diame-

ter (l/d) ratios. During these experiments, both near field and far field vorticity data will be acquired. Finally, a multiple row, shaped, angled injection apparatus will test vorticity cancellation between the rows based on results of the present research detailed in this thesis. The final objective is to achieve an understanding of the sources and influences of vorticity in an effort to improve boundary layer code prediction of film cooling flow in turbine blades and to present criteria for optimizing film cooling schemes.

This thesis details preliminary research conducted for the vorticity cancellation experiments of the overall experimental plan. Chapter 2 briefly describes the apparatus and flow visualization techniques employed. Chapter 3 gives the barest essentials of vorticity theory necessary to understanding the data contained and analyzed in Chapter 4. Finally, Chapter 5 provides a summary and proposes areas for further research.

Chapter 2: Experimental Facility and Techniques

Water tunnel flow visualization experimentation was the tool used throughout this investigation. Jets were transversely injected into the main flow in the test section of the University of Washington Flow Visualization Water Tunnel Facility. Far field flow structure resulting from the interaction of steady jets in a uniform crossflow were studied using both colored dye and laser induced fluorescence techniques. This chapter describes the water tunnel facility and the visualization techniques employed.

2.1 Water Tunnel and Jet Supply

The University of Washington Flow Visualization Water Tunnel Facility is a horizontal, recirculating facility with a 3.0 m x 0.7 m x 0.7m test section and a maximum flow speed of 70 cm/s. A simplified sketch showing major components is given in figure 2-1. Tunnel speed is controlled by a variable frequency drive unit which controls the recirculating pump speed. A complete description of the water tunnel is contained in "An Experimental Investigation of Entrainment and Mixing in Pulsed and Transverse Jets" by Adnan Eroglu (7-13). Through his efforts, velocity calibration and turbulence levels are well documented.

The jet fluid is supplied by an air driven setup as shown in figure 2-2. The major components of this setup are preparation and pressurization tanks, a distribution manifold with shutoff valves and flow meters with fine adjustment valves for accurate establishment of jet blowing ratios. Water is drawn into the pressurization tank via connection of a vacuum pump in lieu of the pressurized air line. Once the air line is connected and the manifold

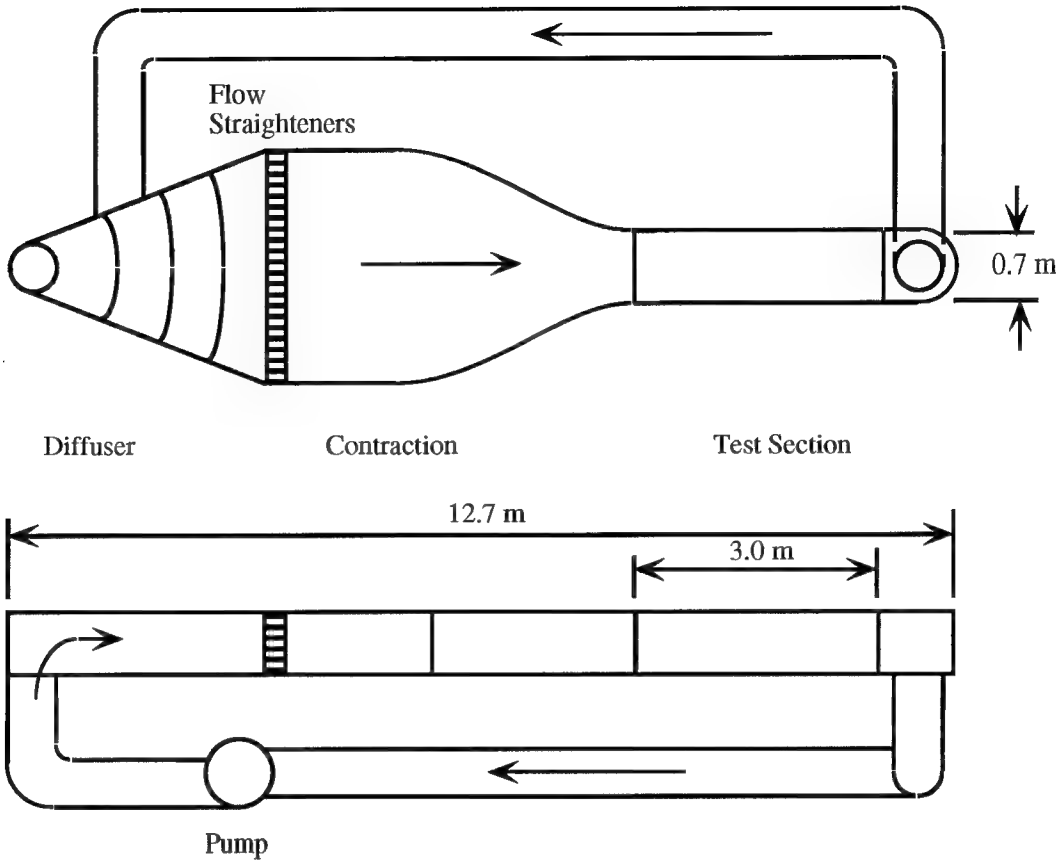

Figure 2-1: University of Washington Flow Visualization Water Tunnel Facility.

valves are opened, precise flow control may be accomplished through valves contained in the flow meters. This flow rate is subject to decrease with the reduction in hydraulic head which occurs in the pressurization tank. As the level in the tank falls, outlet pressure and hence flowrate decrease. The large free surface area of the pressurization tank, along with the free surface pressure at a nominal 2.06×10^5 N/m^2 minimizes this effect however. Given the possible head height change of the pressurization tank at approximately 0.70m, the maximum head loss over an experiment using the entire tank would be 6727 N/m^2 or 3.3% that of the free surface pressure. Experiment showed a flow rate change of 3.4% during the discharge of the entire tank at the intermediate flow rate of 2.0 gal./min. Typical experiments used approximately 4% of the tank capacity and therefore, flow rate decrease over an experiment can be characterized as nominally 0.136%. At flow rates below 2.0 gal./min., less head height change occurs as a result of less fluid being used, while the

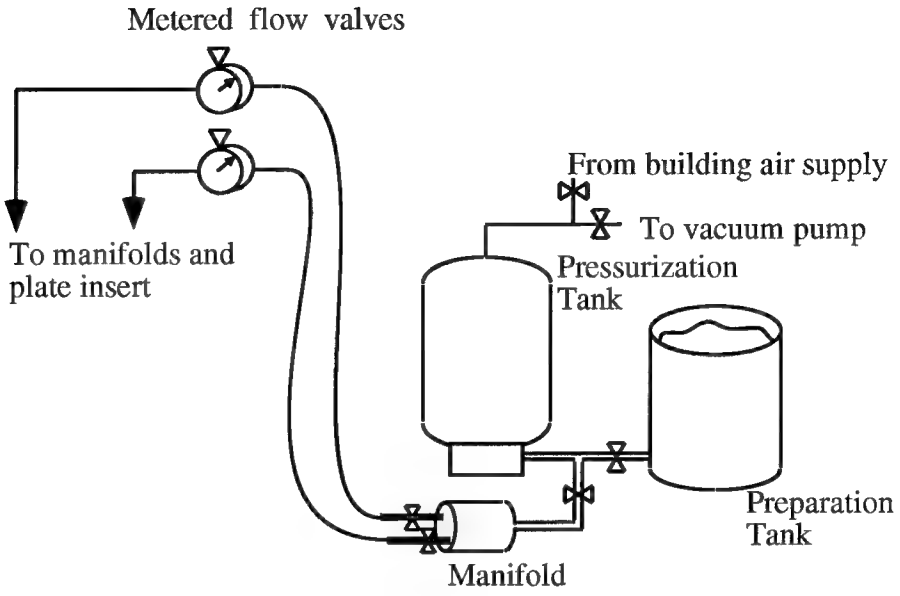

Figure 2-2: Jet supply system schematic.

opposite is true at higher flow rates. The flow rate change and the flow rate are directly related such that the percent variation over an experiment should match this nominal value. Earlier experiments by Eroglu estimated the maximum flowrate change over an experiment as 0.7% (Eroglu 14). However, no discussion of the jet fluid supply system, flowrate or constraints was given.

From the flow meters, the jet flow is distributed again for the leading and trailing rows of jets by manifolds constructed of plexiglass. Flexible hoses then connect to the stovepipes in the insert plate where the flow is restarted by flow straighteners to establish a specific development length at the exit. The plexiglass manifolds and the stovepipe/plate inserts are interchangeable to allow for examination of various inter-row and intra-row spacings as well as staggered and in-line arrangements.

2.2 Flow Visualization Techniques

2.2.1 Colored Dye Technique

Initial experiments were conducted using Schilling's food coloring to dye the jet flows in a

variety of manners. In all cases, generalized lighting was used to highlight the entire flow field while seeking to eliminate shadows. The typical concentration was nominally 0.299 grams of Schilling's liquid food coloring per liter of jet fluid.

Dying of the jet fluid was accomplished by several methods. In the preliminary experiments, the preparation tank was dyed, resulting in a single color dying of both the leading and trailing row of jets. Next, dying was accomplished at each of the manifolds to allow for separate color selection and thus differentiation of the individual rows in the data. The primary advantage of this system was its relatively minor impact on flow rates as the dye could be injected at its full concentration. However, this method led to incomplete mixing of the dye, at times leaving entire jets undyed. The final method employed diluted the dye with water at the rate of 14.2 grams per liter. This dye was then injected immediately beyond the leading row flow meter by means of a centrifugal pump. This increases the flow rate over that shown on the flow meter at the most 7% based on the flow rate/pump speed combinations used. This minimal impact on flow rate is offset by the head loss issue discussed earlier. Experiments could be reconducted adjusting for the error introduced in this manner. This technique does allow for control of the dye concentration by way of a rheostat and ensures complete mixing of the dye with the jet fluid.

Color dye taping was accomplished with a Panasonic VHS video camera placed abeam the leading row or at an oblique angle. This data was then converted to still photographs via a Quick Image 24 frame grabber card and Photoshop 2.5. In this manner, several frames could be examined to find a representative example and adjustments made to color saturation, contrast and brightness.

2.2.2 Laser Induced Fluorescing Technique

In a manner similar to that described above in subsection 2.2.1, the entire jet supply could be dyed with fluorescein sodium salt at a rate of 7.9×10^{-4} grams per liter. In general, the minimum concentration necessary for fluorescing is desirable in that it prevents shadowing of the light source. Additionally, fluorescein dying was also accomplished in approximately the same ratio through use of the centrifugal pump described earlier. The same advantages and drawbacks presented in subsection 2.2.1 are present for this case except

that pump speed was sufficiently slow as to prevent the introduction of discernible error into the flow rate.

Once the jet fluid was seeded with fluorescein, a two dimensional sheet of light was produced by projecting the output of the 5 watt argon-ion laser onto an oscillating mirror. By selective placement of the mirror and through a moveable calibrated shuttle, precise placement and alignment of the laser sheet is possible. Generally, sheets were taken perpendicular to the crossflow. By placing a mirror downstream of the insert, a perpendicular videotaping of this sheet was possible as shown in figure 2.3. The camera used was a high

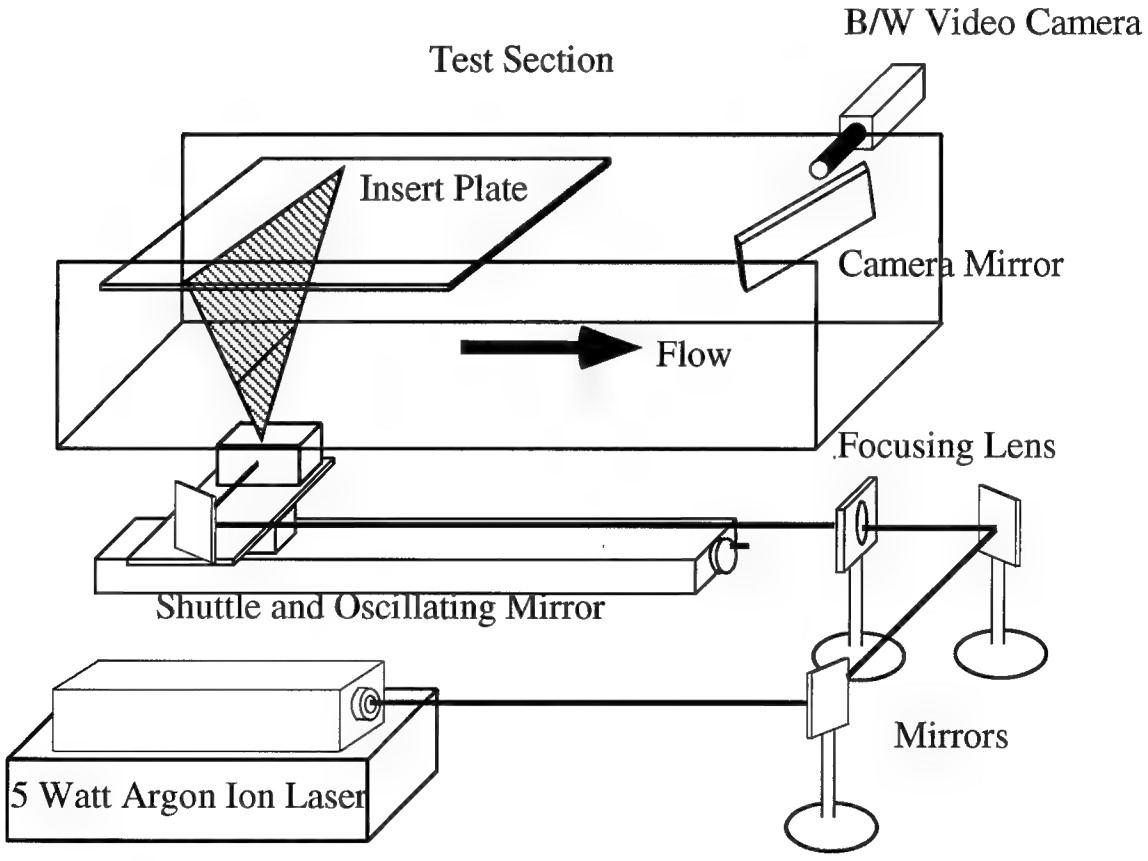

Figure 2-3: Laser sheeting apparatus and video imaging arrangement.

resolution Sony black and white camera connected to a Sony SVHS tape machine. Again, these video images were processed in a manner similar to that described in sub section 2.2.1 with the exception that no color adjustments were made.

Chapter 3: Jet Vortex Theory

The structure and vortex composition of a single jet in crossflow has been well examined by Thomas Fric in his 1990 paper entitled "Structure in the Near Field of the Transverse Jet". That paper examined not only the near field vortex structure of jets but also touched upon the kidney shaped vortices which dominate the far field structure. That paper examined blowing ratios from 2 to 10 in air using smoke wire flow visualization and wholesale seeding of the jet flow (Fric 2,13-15). This chapter sets forth the dynamic equations governing vortex behavior and then looks at the far field interaction of the kidney shaped vortices which are known to exist within jets in crossflow.

3.1 Vorticity

The vorticity vector, $\vec{\omega}$, is a measure of the solid body like rotation of a fluid particle and may be expressed as:

$$\vec{\omega} = \vec{\nabla} \times \vec{v}. \tag{3-1}$$

This basic equation states that vorticity, or the solid body like rotation of a fluid, exists only where cross derivatives of velocity exist.

The dynamic equation which governs vorticity transport is formed by taking the cross product of the gradient operator, $\vec{\nabla}$, and the momentum equation to yield:

$$\frac{\rho D(\vec{\omega}/\rho)}{Dt} = \left(\vec{\omega} \bullet \vec{\nabla}\right)\vec{v} + \frac{1}{\rho}\vec{\nabla} \times \vec{\nabla} \bullet \underline{R} - \left(\vec{\nabla} \bullet \underline{R} - \vec{\nabla}p\right) \times \vec{\nabla}\left(\frac{1}{\rho}\right) + \vec{\nabla} \times \vec{f}, \tag{3-2}$$

where $\underline{R}$ is the friction stress tensor. For the present flow this equation may be simplified

greatly by making the typical assumption of a Newtonian, barotropic, isothermal and incompressible flow field in the absence of body forces. This leads to the more familiar vorticity transport equation:

$$\frac{D\vec{\omega}}{Dt} = \left(\vec{\omega} \bullet \vec{\nabla}\right)\vec{v} + \upsilon\nabla^2\vec{\omega} \tag{3-3}$$

This equation contains no vorticity generation or source terms and says only that vorticity may be stretched, convected, rotated and diffused. The second term in eq. 3-3 which represents vortex stretching and rotation can only be nonzero in three dimensional flows and, by virtue of containing the term $\vec{\nabla}\vec{v}$, must be zero at solid surfaces. The last term represents the diffusion and convection term and allows for the transport of vorticity perpendicular to streamlines and for the crossing of vorticity of opposite sign (Fric 30).

3.2 The Kidney Vortex and Lift-off by Mutual Induction

Thomas Fric's 1990 paper discussed the issues contained in section 3.1 in depth and showed that in the far field of a transverse jet, the vortical structure of the jet could be idealized as consisting of the so-called kidney vortex. The kidney vortex is actually a pair of counter-rotating vortices whose vectors are parallel to the centerline of the jet as shown in figure 3-1.

Figure 3-2 examines an isolated kidney vortex next to a wall where the wall has been replaced by a mirror image plane and the corresponding mirror kidney vortex. This figure corresponds to a sheet taken from figure 3-1 in the y-z plane.

The induced velocity for a vortex varies inversely with the radial distance from the vortex. The induced velocity on vortex number 2 by the other vortices is then as shown. The resultant induced velocity on vortex number 1 in figure 3-2 will similarly be a mirror image of that on vortex number 2. This induction of velocity away from the wall is called lift-off by mutual induction and results in the jet being further lifted off the wall (Kurosaka 14).

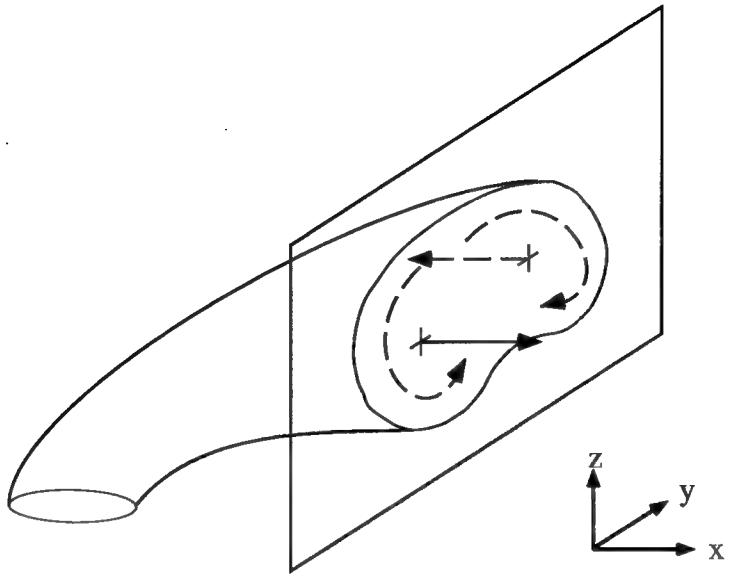

Figure 3-1: Vortex structure of a single jet in crossflow showing kidney vortex.

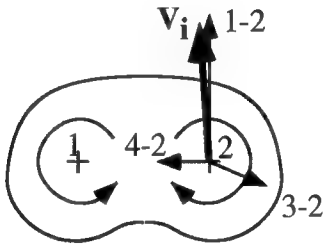

Wall or mirror image surface

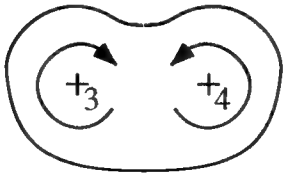

Figure 3-2: Isolated kidney vortex next to a wall showing resultant induced velocity.

The induced velocity, in addition to its inverse relationship with radial distance is directly related to the vortex strength. Thus, reducing the strength of the vortex pair will

reduce lift-off by mutual induction which, in a film cooling application, should prove to be beneficial.

3.3 Vorticity Cancellation of Multiple Jets

3.3.1 Single Row

In the case of a single row of transverse jets as shown in figure 3-3, an analysis similar to

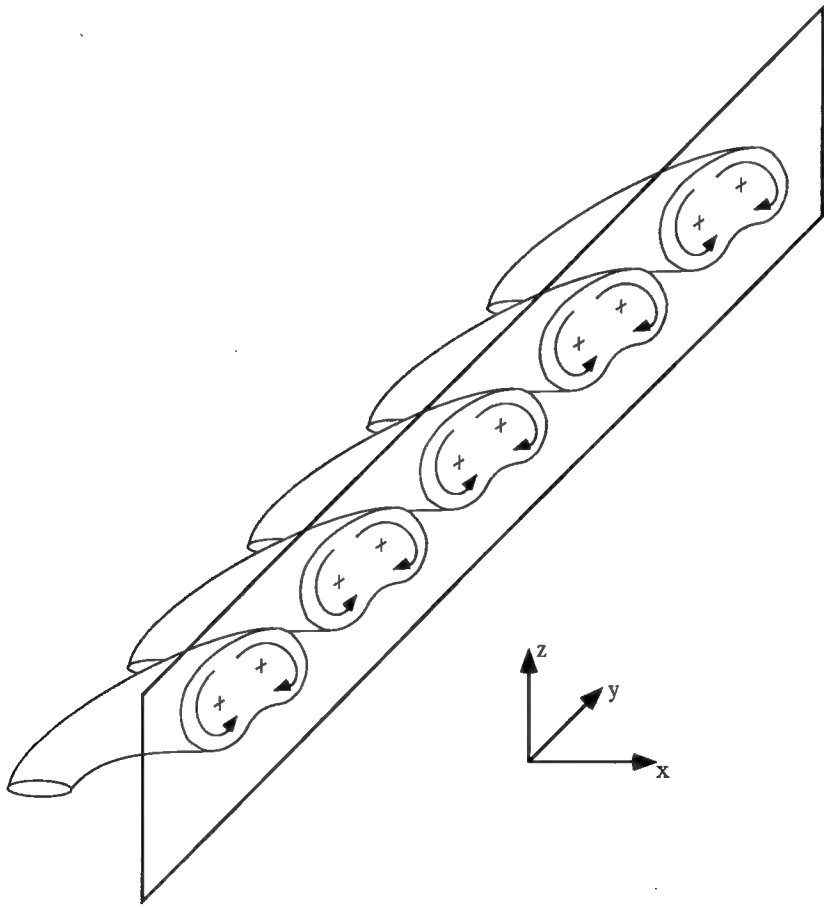

Figure 3-3: Kidney vortex alignment for a single row of jets.

that performed for a single jet may be accomplished as shown in figure 3-4. Unlike the case for a single kidney vortex, for an infinite array of closely spaced kidney vortices

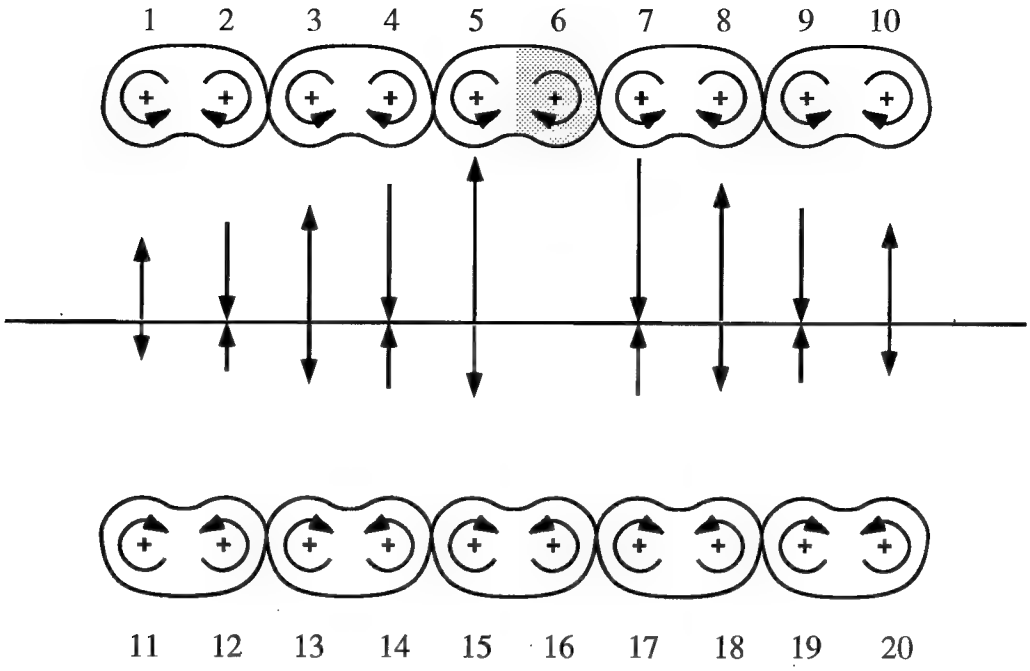

Figure 3-4: Vortex distribution for a single row of jets. The induced vertical velocity on vortex number 6 by each vortex is shown by the arrows.

whose individual vortices are equally spaced, there is no lift-off by mutual induction due to cancellation by vortices on either side of vortex 6. In figure 3-4 note that the equally spaced vortices on either side of vortex 6 cancel each other resulting in the only contributing vortices being numbers 1 and 11. In an infinite array, the horizontal distance would become very large compared to the vertical separation. Thus, in the infinite limit, the number 1 and number 11 vortex would also cancel. However, as the distance between each kidney vortex is increased, the limit of the single vortex next to a wall as described in section 3.2 will be reached where lift-off is at a maximum.

The existence or lack of lift-off does not speak to the issue of entrainment of hot gas toward the surface. This will continue whether or not the kidney vortex has been lifted off and results due to the existence of the kidney vortex as shown in figure 3-5.

3.3.2 Staggered Rows

Consider now the case in which two rows of transverse jets are being injected from a configuration as shown in figure 3-6. This is called staggered row injection and will result in

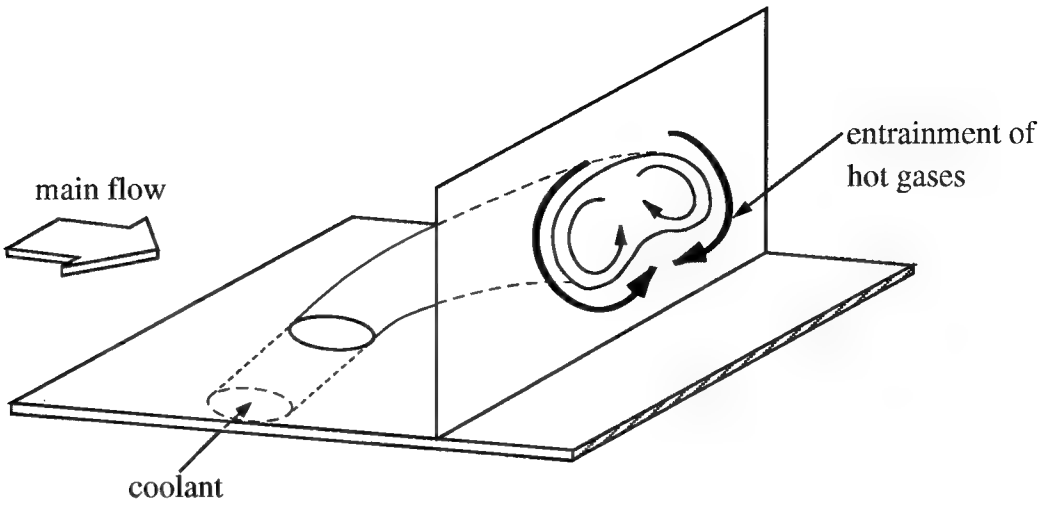

Figure 3-5: Kidney vortex showing entrainment of main flow toward the surface (Haven 4).

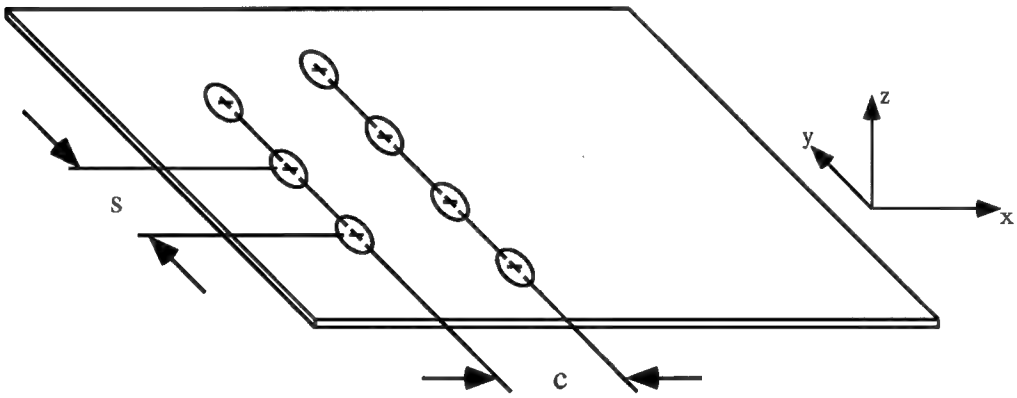

Figure 3-6: Staggered row injection.

the jet alignment and kidney vortex distribution as shown in figure 3-7. In the cross section, note that, depending on spacing within each row, lift-off by mutual induction may be present. However, if the second row vortices have the same x-component vortex strength, $|\omega_x|$, as the first row and align themselves in such a manner as to create the 'best case' of a single row of equally spaced vortices, the lift-off by mutual induction would be eliminated. Though perhaps not to the extent of this 'best case' condition, the second row injection will tend to reduce lift-off by mutual induction by reducing the spacing between vortices.

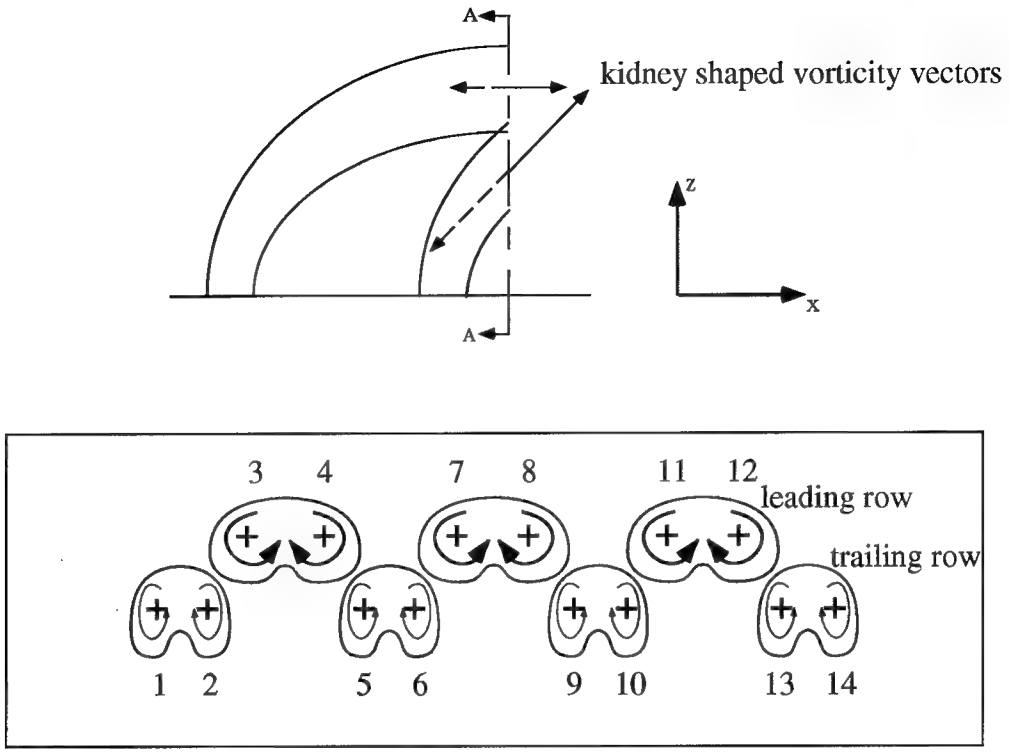

Section A - A

Figure 3-7: Staggered row injection showing lateral view of jet trajectory and cross section showing kidney vortex alignment.

More importantly, if in figure 3-7 the number 2 and number 3 vortices and other geometrically similar combinations can be brought into close proximity and be made to cancel, the absence of vorticity in the x direction will cease entrainment of 'hot' gas toward the surface.

3.3.3 In-line Rows

Finally, consider the case in which two rows of transverse jets are injected into the main flow in-line with each other as shown in figure 3-8. The resultant jet trajectory and orientation of the kidney vortices is shown in figure 3-9. Again, the intra-row distance, s, will determine if lift-off by mutual induction is operating. However, the downstream row can only serve to increase lift-off by mutual induction. This is the case because the downstream row is injected directly beneath the existing jets which cannot induce a velocity

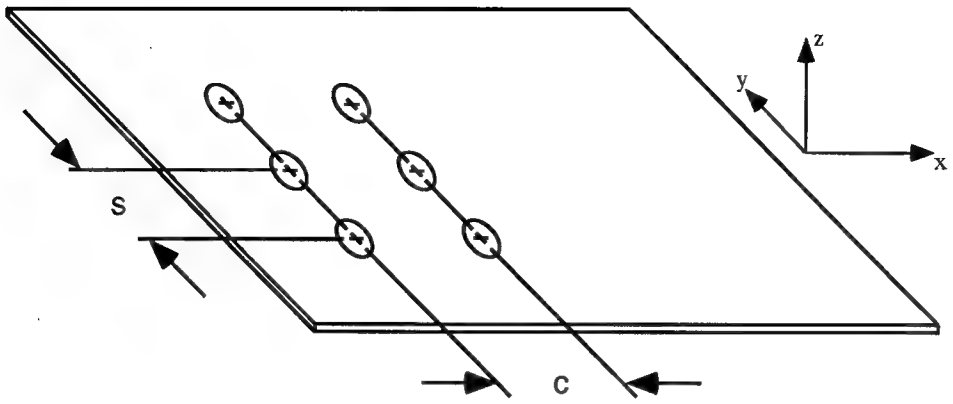

Figure 3-8: In-line row injection.

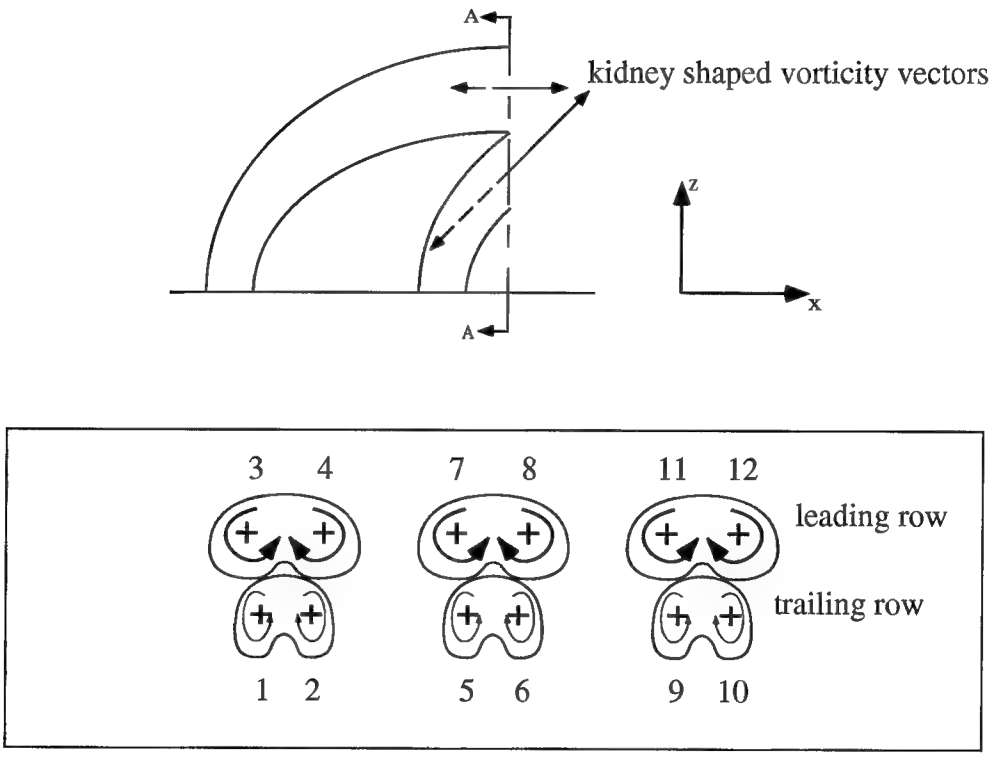

Figure 3-9: In-line row injection showing lateral view of jet trajectory and cross section showing kidney vortex alignment.

toward the wall. In a situation where the intra-row spacing, s, is set to obtain the 'best case' situation described in subsection 3.3.2, the addition of a second row will not produce

lift-off by mutual induction. This results due to the same type of cancellation that produced the 'best case' situation in the first place. As this spacing is increased, the addition of a second row does increase lift-off because the adjacent vortices are too far away to cancel the one injected directly beneath the vortex of interest. Thus, lift-off by mutual induction may only remain the same or increase with the addition of a second row in-line with the first.

Next, the vorticity interaction between the jets of each row must be considered. Recall that in the staggered case, the x-component of vorticity strength , $|\omega_x|$, was reduced by the interaction of vortices from the leading and trailing rows of jets. For this case of in-line rows, as shown in figure 3-9, the vortices number 1 and number 3 will interact. Being of the same sign, the result will be a summation rather than a cancellation. Compared to the staggered case, this will increase $|\omega_x|$, thereby increasing entrainment of 'hot' fluid toward the surface and reducing cooling effectiveness as was shown in figure 3-5.

Chapter 4: Experimental Results

This chapter begins with a discussion of the experimental parameters used in gathering data and then examines the results. First, the results from the staggered and in-line rows will be compared to single row data and then compared to each other. This chapter includes figures representative of the general trends to be discussed. The complete set of figures is contained in Appendix A.

4.1 Experimental Parameters and Nomenclature

The two physical configurations investigated were one with staggered rows as depicted in figure 4-1, and one with in-line rows with the trailing row containing three jets directly behind the front jets. Figure 4-1 shows the major dimensions of the staggered case. For

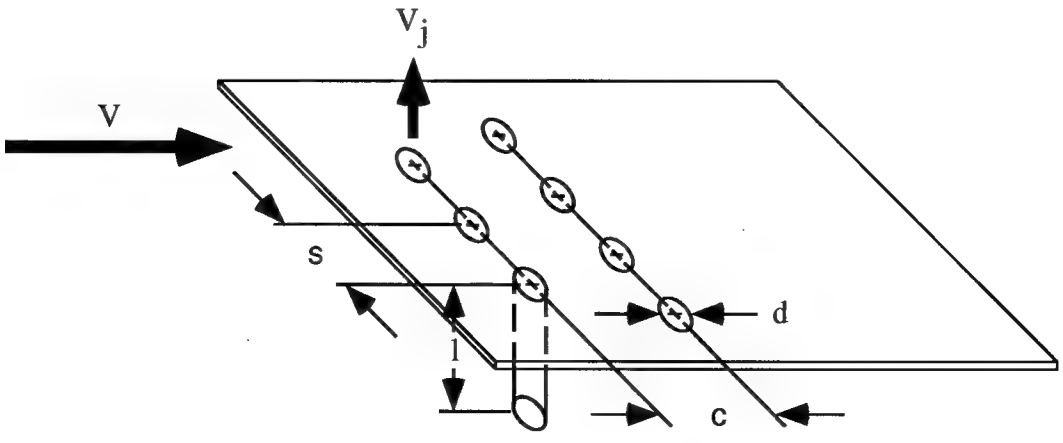

Figure 4-1: Staggered row injection apparatus showing key nomenclature.

brevity, the reader is referred to figure 3-7 for the in-line schematic. For this thesis, both the intra-row and inter-row spacing ratios, s/d and c/d respectively, were 3.5. The flow within the jetting pipes was restarted by the placement of a honeycomb-like structure to provide a consistent development length, l. The development length ratio, l/d, was maintained at 6.0 in all cases. Dimensions of the apparatus investigated are shown in Table 4-1.

Table 4-1: Dimensions of experimental apparatus

s	c	d	l
1.75 inches	1.75 inches	0.5 inches	3.0 inches

From the outset, the primary objective was to examine blowing ratios, M, between 0.5 and 2.5. As a constant main flow velocity was considered desirable to eliminate Reynold's number as a consideration, the blowing ratio range dictated a tunnel speed of 26.7 cm/s because of jetting apparatus limitations. The leading row blowing ratio, M_L, is the leading row jet velocity, V_j, divided by the main flow velocity, V. Similarly, the trailing row blowing ratio, M_T, is V_j of the trailing row of jets divided by V.

In all the figures that follow in this chapter and those contained in Appendix A, lateral photographs were taken abeam the trailing jet, while lasersheets were taken at 10 diameters (5.0 inches) downstream of the trailing row centerline. These lasersheets were obtained opposite the main flow direction as described in chapter 2.

4.2 Comparison of Staggered Row Results to Single Row Data

Figures A-1, A-7, A-13, A-19, and A-25 show lateral color dye photographs and lasersheet photographs for a single row at blowing ratios from 0.5 to 2.5. As expected, as the blowing ratio is increased, momentum of the jet carries the trajectory further away from the wall resulting in less contact with the surface. Due to the distance downstream at which the lasersheets were taken, accurate placement of vortex centers is not possible, but as discussed in chapter 3, some of the increase in displacement may be attributable to an increase in lift-off by mutual induction. This is likely because with $s/d = 3.5$, the spac-

ing between vortices within each kidney should be less than the distance between vortices of adjacent kidney vortices. This, coupled with an increase in vortex strength with blowing ratio, M, increases lift-off by mutual induction.

Examining figure 4-2, where a second staggered row is added, its addition doesn't seem to significantly change the jet trajectory as traced by the color dye present in only the leading row. In figure 4-2, M_L is so low (M_L=0.5) that displacement from the surface is almost nonexistent and does not appear to be affected by the presence of a second row of staggered jets, regardless of the trailing row blowing ratio as seen in figures 4-2b through 4-2d. However, examining the lasersheets for these same cases shows more interaction as shown in figure 4-3, where, as for all lasersheets, only the leading row is dyed with fluorescein. As M_T increases, there is an initial tendency towards smearing of the leading row of jets. In figure 4-3c, for M_L=0.5 and M_T=1.0, the axial component of vorticity, $|\omega_x|$, of the leading row of jets appears to be cancelled by the $|\omega_x|$ of the downstream row as illustrated earlier in figure 3-5. As M_T is further increased, as in figure 4-3d, $|\omega_x|$ of the trailing row becomes greater than $|\omega_x|$ of the leading row and four coherent vortical structures begin to appear corresponding to the number of jets in the trailing row.

Thus, even at low leading row blowing ratios where displacement from the wall is not present, evidence of vorticity cancellation is evident in smearing of the leading jet. As M_L is increased, the interaction begins to clarify as may be seen in Appendix A and will be elaborated upon here.

For example, Figure 4-4 shows trajectories for M_L=1.0 and various M_T's. Note in figure 4-4a, for the case of no trailing row blowing, the trajectory shows a thin, but noticeable space beyond the downstream row location indicating the lift-off of the leading row of jets. As the downstream row of staggered jets increases in blowing ratio, the colored jet becomes scalloped where the second row interacts with it and the concentration of dye becomes greater at the wall as in figures 4-4b and 4-4c. This indicates reattachment of the jet to the wall. At the same time, the lasersheets show a progression towards smearing of the leading row of jets which appears to be maximized at M_T=1.5 as also shown in figure 4-5c. Again, as shown in figure 4-5d with M_T=2.5, at higher trailing row blowing ratios, $|\omega_x|$ of the trailing row is greater than that of the leading row and coherent vortical struc-

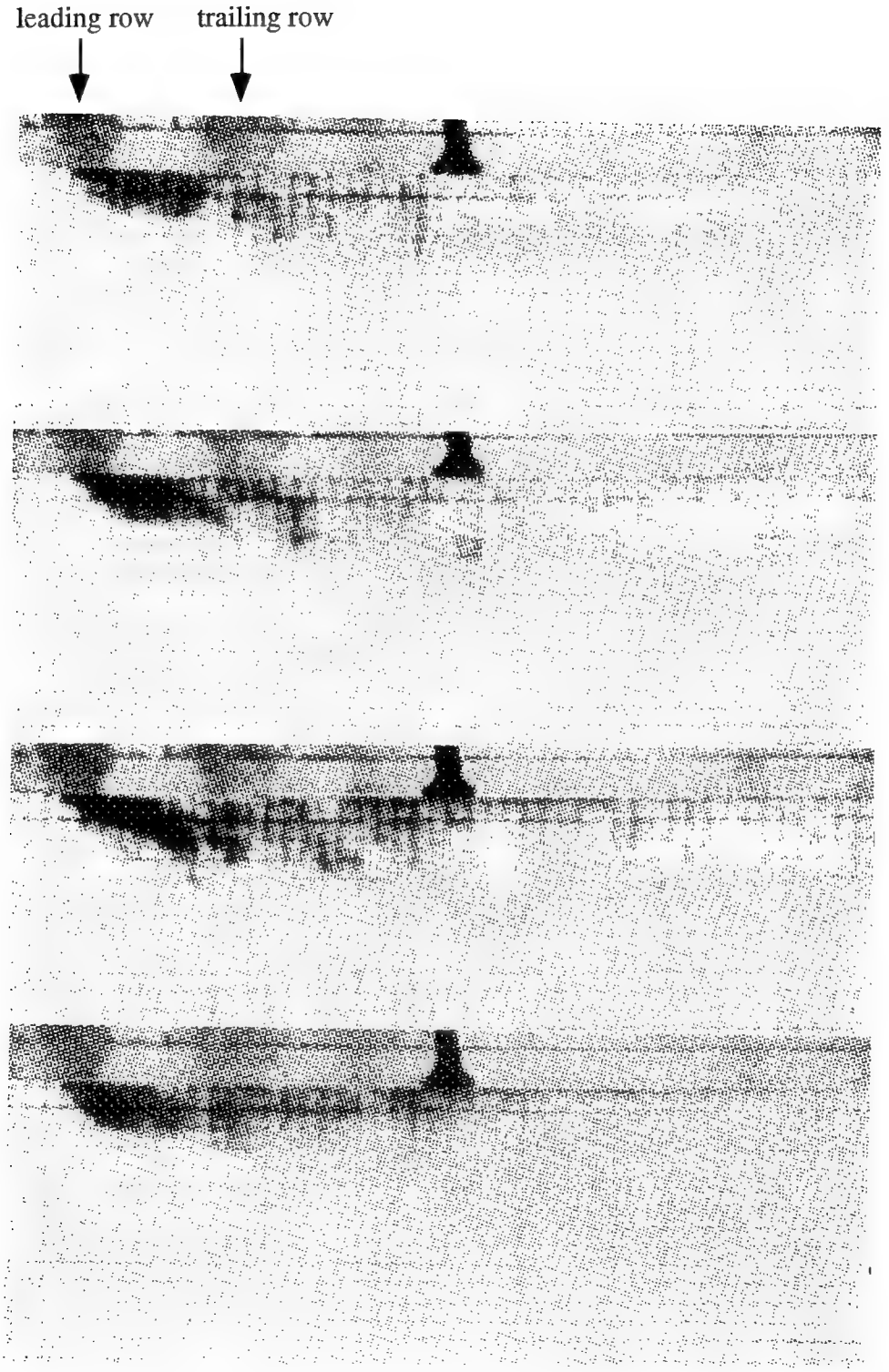

Figure 4-2: Color trajectories of staggered rows with M_L=0.5 and (a) M_T=0.0, (b) M_T=0.5, (c) M_T=1.0, and (d) M_T=2.5.

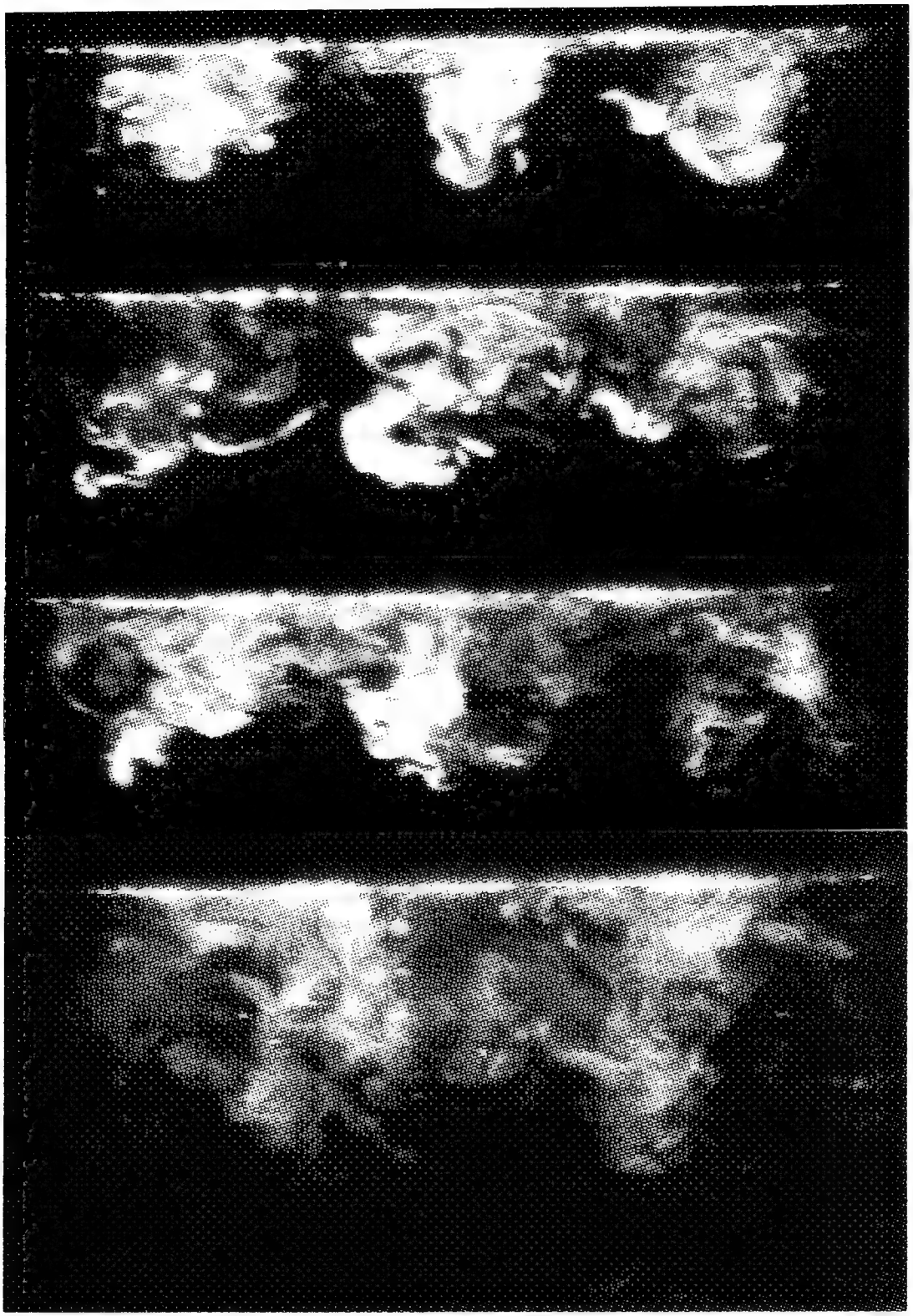

Figure 4-3: Lasersheets of staggered rows with M_L=0.5 and (a) M_T=0.0, (b) M_T=0.5, (c) M_T=1.0, and (d) M_T=2.5.

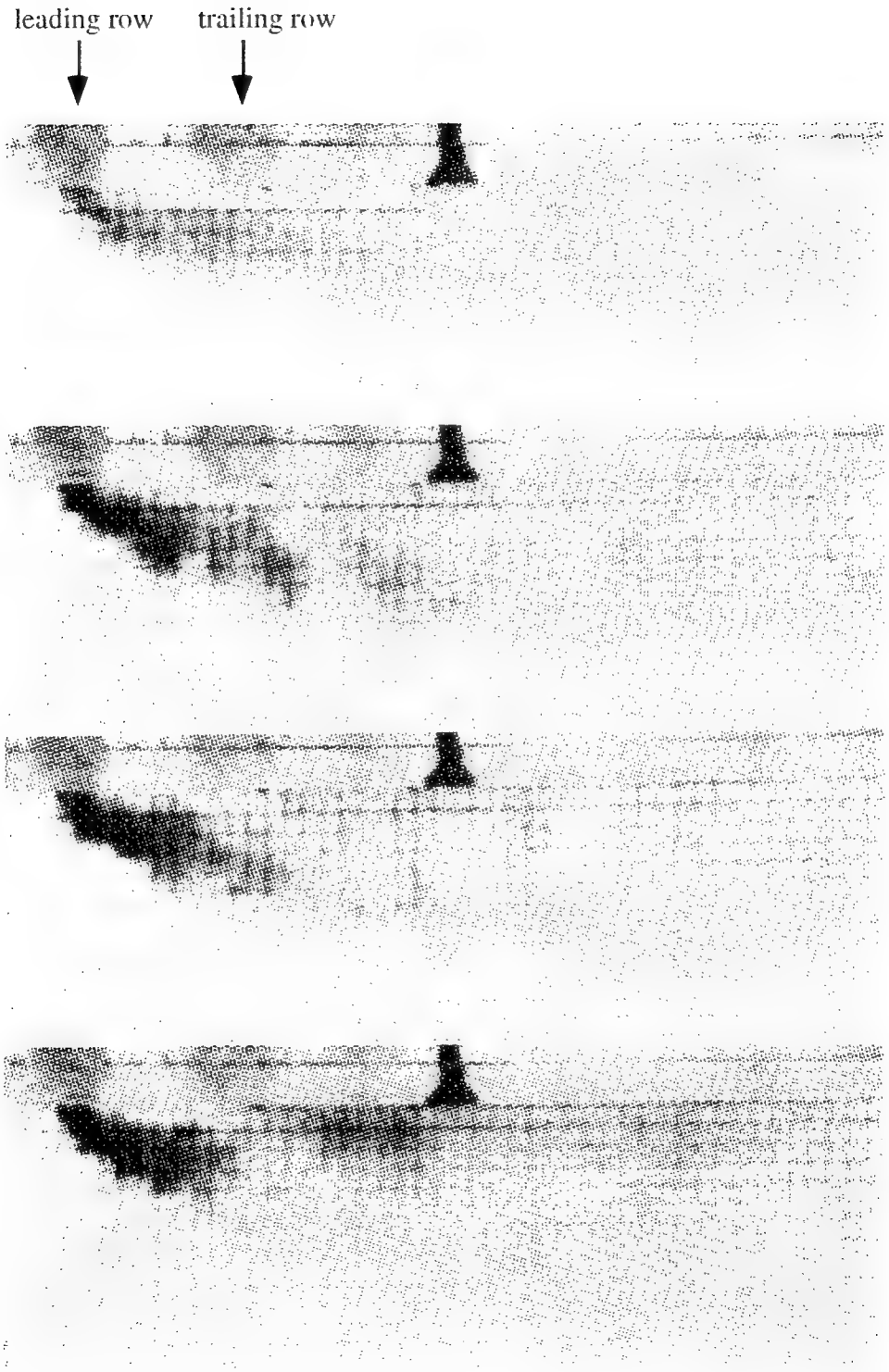

Figure 4-4: Color trajectories of staggered rows with M_L=1.0 and (a) M_T=0.0, (b) M_T=1.0, (c) M_T=1.5, and (d) M_T=2.5.

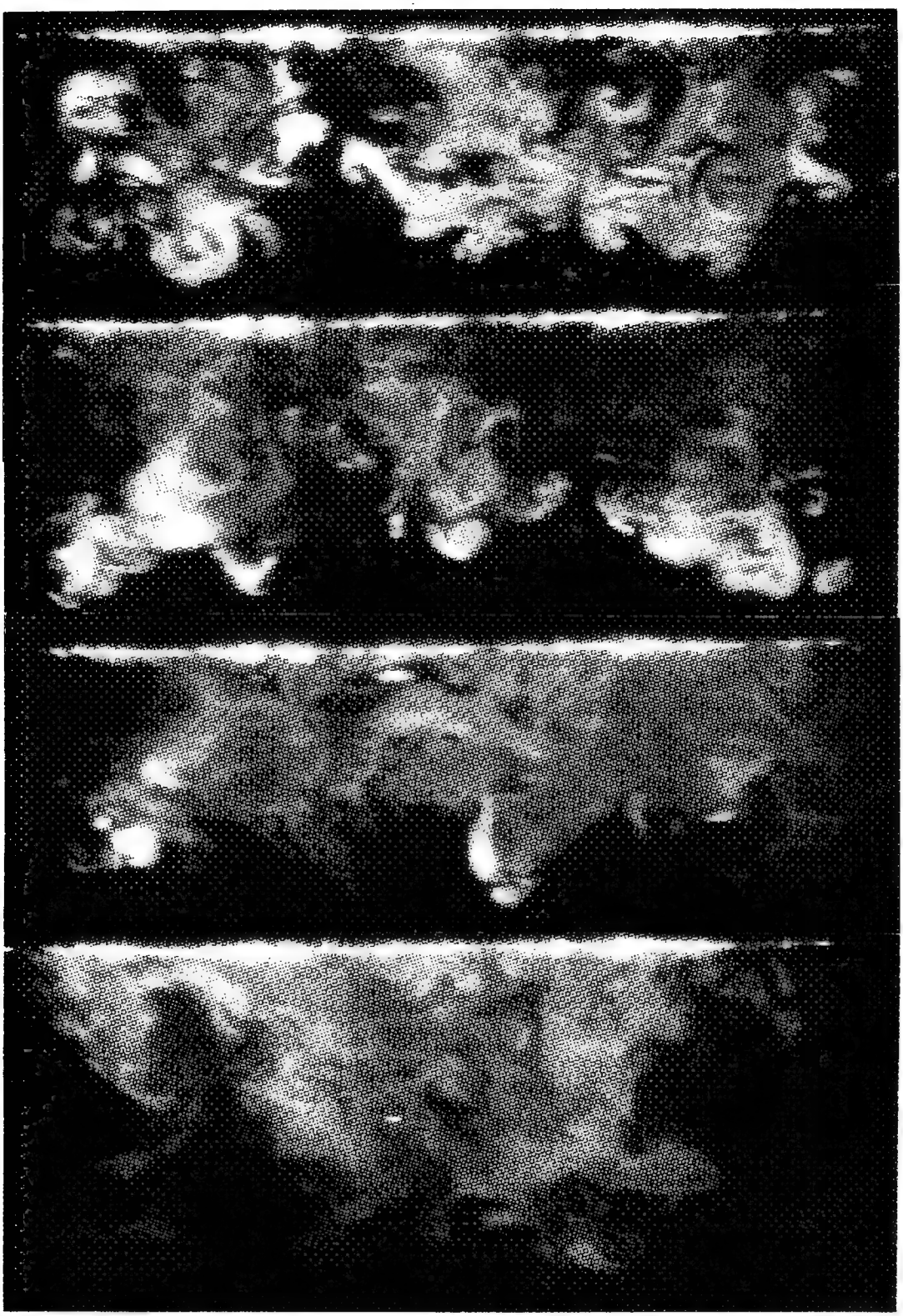

(a)

(b)

(c)

(d)

Figure 4-5: Lasersheets for staggered rows with M_L=1.0 and (a) M_T=0.0, (b) M_T=1.0. (c) M_T=1.5 and (d) M_T=2.5.

tures reappear as was the case for M_L=0.5. At this point, lift-off by mutual induction and entrainment are again detrimental due to the presence of these vortical structures.

The same scalloping of the leading row of jets with increased dye concentration at the wall is noticeable at the higher blowing ratios as may be seen in numerous figures contained in Appendix A, such as figures A-17, A-18, A-24 and A-30. In the same photographs, one may also observe the progression towards smearing of the leading row of jets in the lasersheets. Also, note in the color photograph portions of these figures in Appendix A that as M_L increases, it takes a higher M_T to reattach the flow to the wall and that for a given leading row blowing ratio, increasing M_T reduces the distance downstream at which reattachment occurs.

The theory of vorticity cancellation is supported by the figures contained here and in Appendix A by the successive increases in M_T required to achieve complete smearing. In figure 4-3b with M_L=0.5, complete smearing was accomplished with approximately M_T=1.0. With M_L increased to 1.0, the $|\omega_x|$ of the leading row of jets is increased and a larger $|\omega_x|$ from the downstream row of jets is required for cancellation. Thus, in figure 4-5c complete smearing for M_L=1.0 occurs at M_T=1.5, and, as shown in figure A-18, for M_L=1.5 it occurs at M_T=2.5. This need for ever greater increases in M_T is easily explained. As M_T is increased to produce a larger vorticity vector, $\vec{\omega}$, it also becomes more inclined with respect to the surface. This dictates that M_T should increase not only to account for the difference in $|\omega_x|$ but also for the resulting change in inclination of the trailing jets' vorticity vector.

4.3 Comparison of In-Line Row Results to Single Row Data

Beginning on a similar course to section 4.2, comparing figure 4-6a and figure 4-6b shows little change in the leading row trajectory as indicated by the color dye. However, comparing the related lasersheets of these two figures is again more encouraging. Here, as shown in figures 4-7a and 4-7b, an enhancement of the vortical structure is already evident, where as in the staggered case, a trend toward cancellation was just beginning to establish itself.

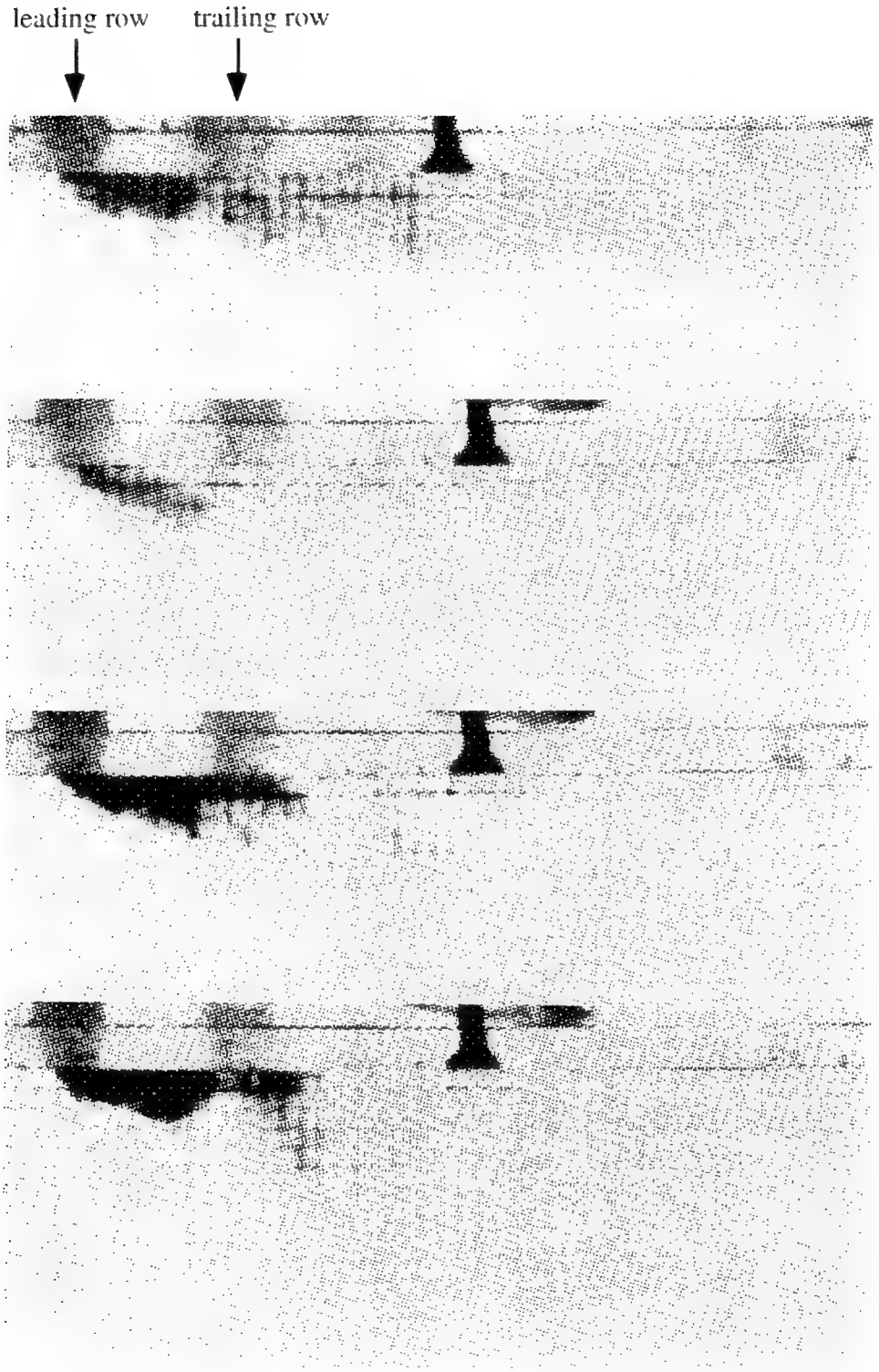

Figure 4-6: Color trajectories of in-line rows with M_L=0.5 and (a) M_T=0.0, (b) M_T=0.5, (c) M_T=1.0, (d) M_T=2.5.

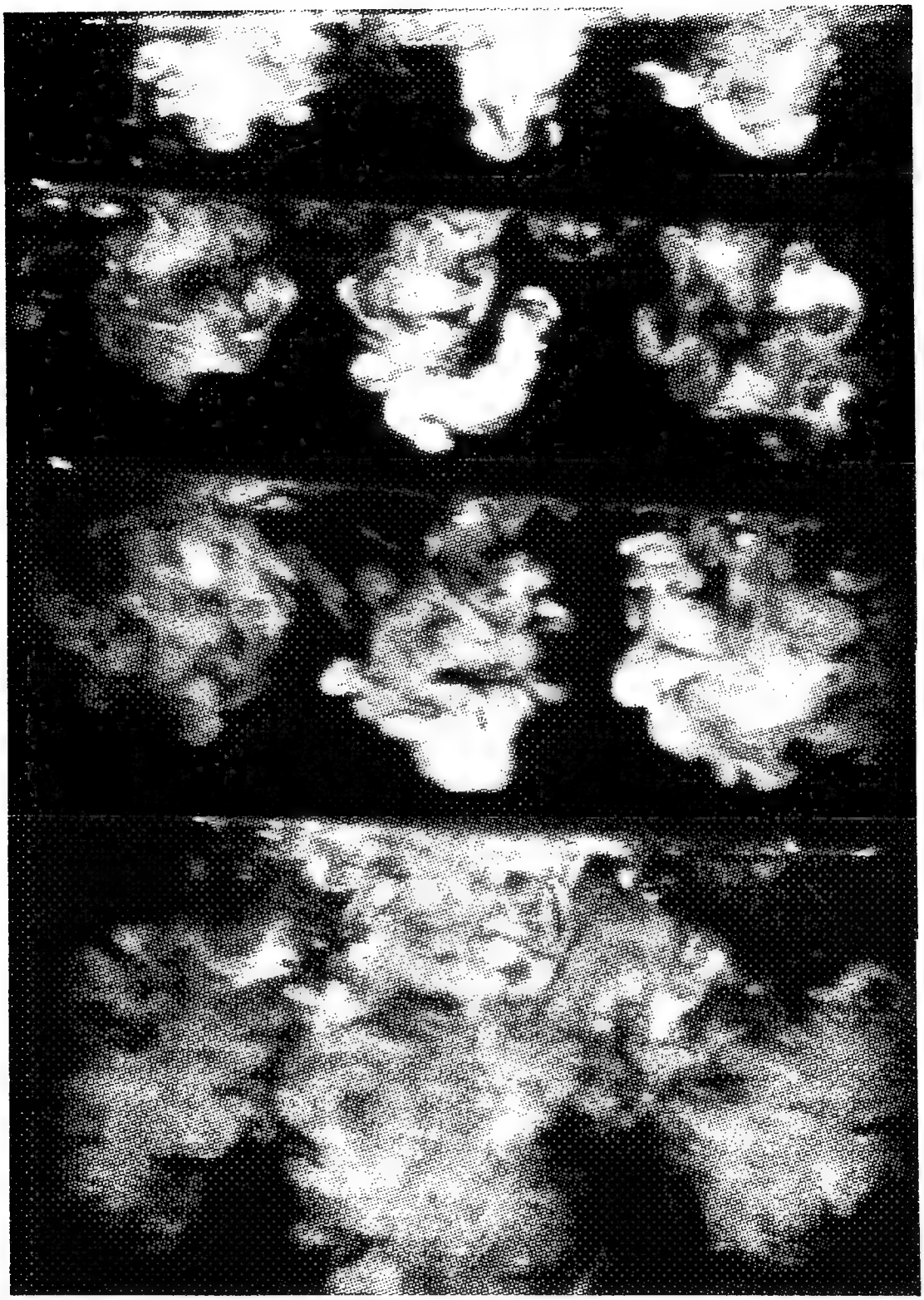

Figure 4-7: Lasersheets of in-line rows with M_L=0.5 and (a) M_T=0.0, (b) M_T=0.5, (c) M_T=1.0, (d) M_T=2.5.

As M_T continues to increase for M_L=0.5, the enhancement of the vortical structure appears to continue increasing as shown in figures 4-7c and 4-7d. Although there is fluorescein dyed fluid near the wall, three distinct vortical structures are evident and the fluid near the wall shows contrasting light and dark regions of varying intensity, which is characteristic of vorticity. Also, in figures 4-6c and 4-6d displacement of the leading row of jets' trajectory is very evident in these color dye photographs.

These trends towards increasing lift-off and increasing vorticity with increased M_T are evident for all M_L's as can be seen in figures 4-8 and 4-9 and in figures A-31 through A-55. It is notable that there does not appear to be an upper limit to the trajectory lift-off and vorticity enhancement in any of these figures. As M_T continues to increase, the vortical structures continue to increase in size and displacement from the wall for the entire range of data taken for this thesis.

4.4 Comparison of Staggered and In-Line Results

The existence of an upper bound for vorticity cancellation in the staggered row case and the apparent lack of an upper bound for vorticity enhancement in the in-line case seems contradictory. Although apparently similar flows, the in-line case has the added consideration of the downstream jets' momentum interaction with the leading row of jets. Thus, even as $|\omega_x|$ is becoming less of an influence with increasing M_T, the increased momentum of the downstream row of jets continues to increase lift-off.

Now, compare figure 4-5c which shows the staggered case for M_L=1.0 and M_T=1.5 from section 4.2, and figure 4-9c which shows the in-line case for the same blowing ratios. As shown by these lasersheets, note that the staggered case shows a near uniform smearing of the leading row of jets, while for the in-line case, coherent vortical structures are still present as evidenced by the areas of light and dark. Also, note that the vertical displacement of the in-line jets in the lasersheets is relatively much larger than that for the staggered case.

It may be supposed that the increased displacement is due to the momentum interaction in the case of the in-line jets. Even if the displacement of either case is due in no part

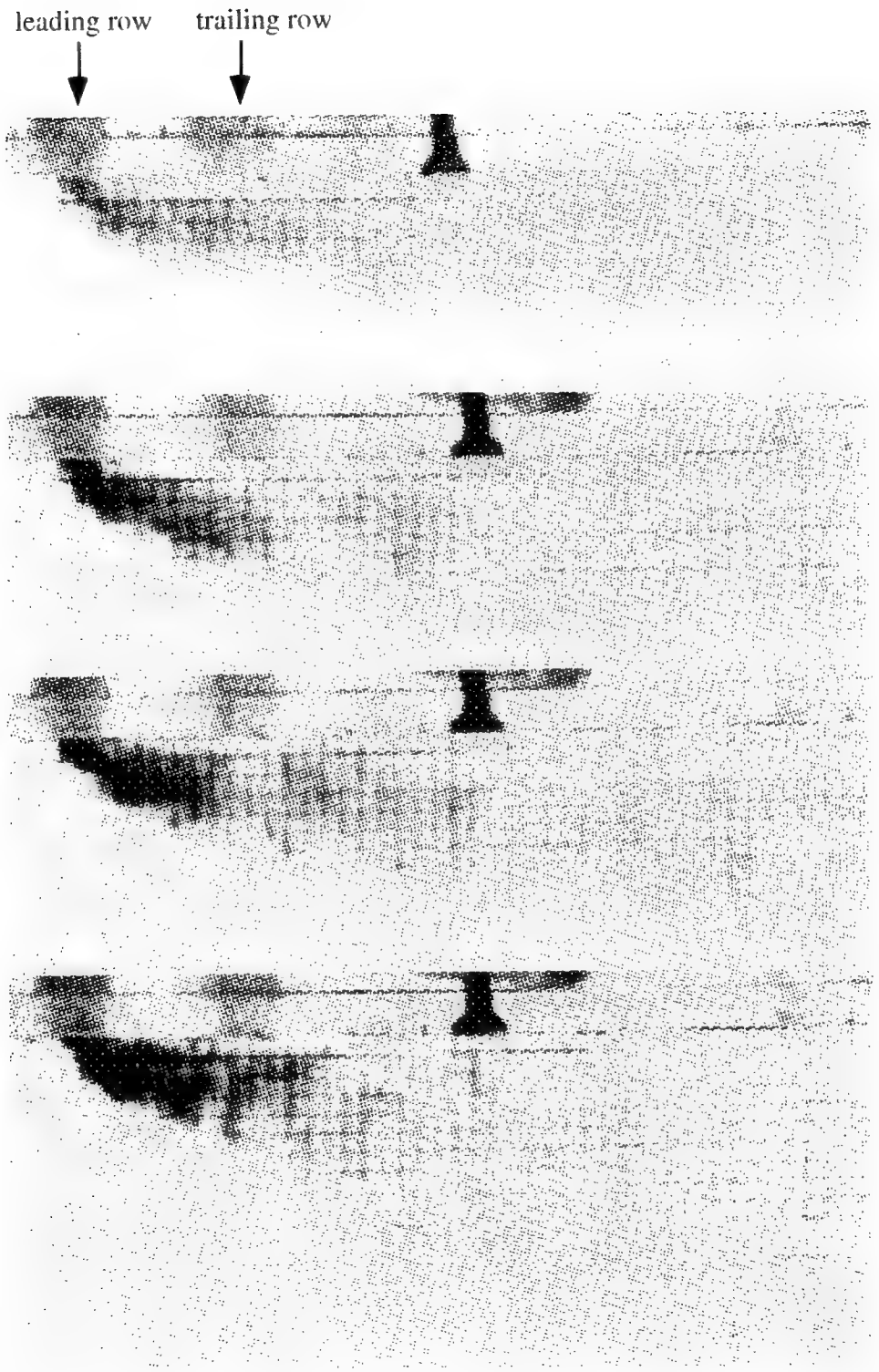

Figure 4-8: Color trajectories of in-line rows with M_L=1.0 and (a) M_T=0.0, (b) M_T=1.0, (c) M_T=1.5, and (d) M_T=2.5.

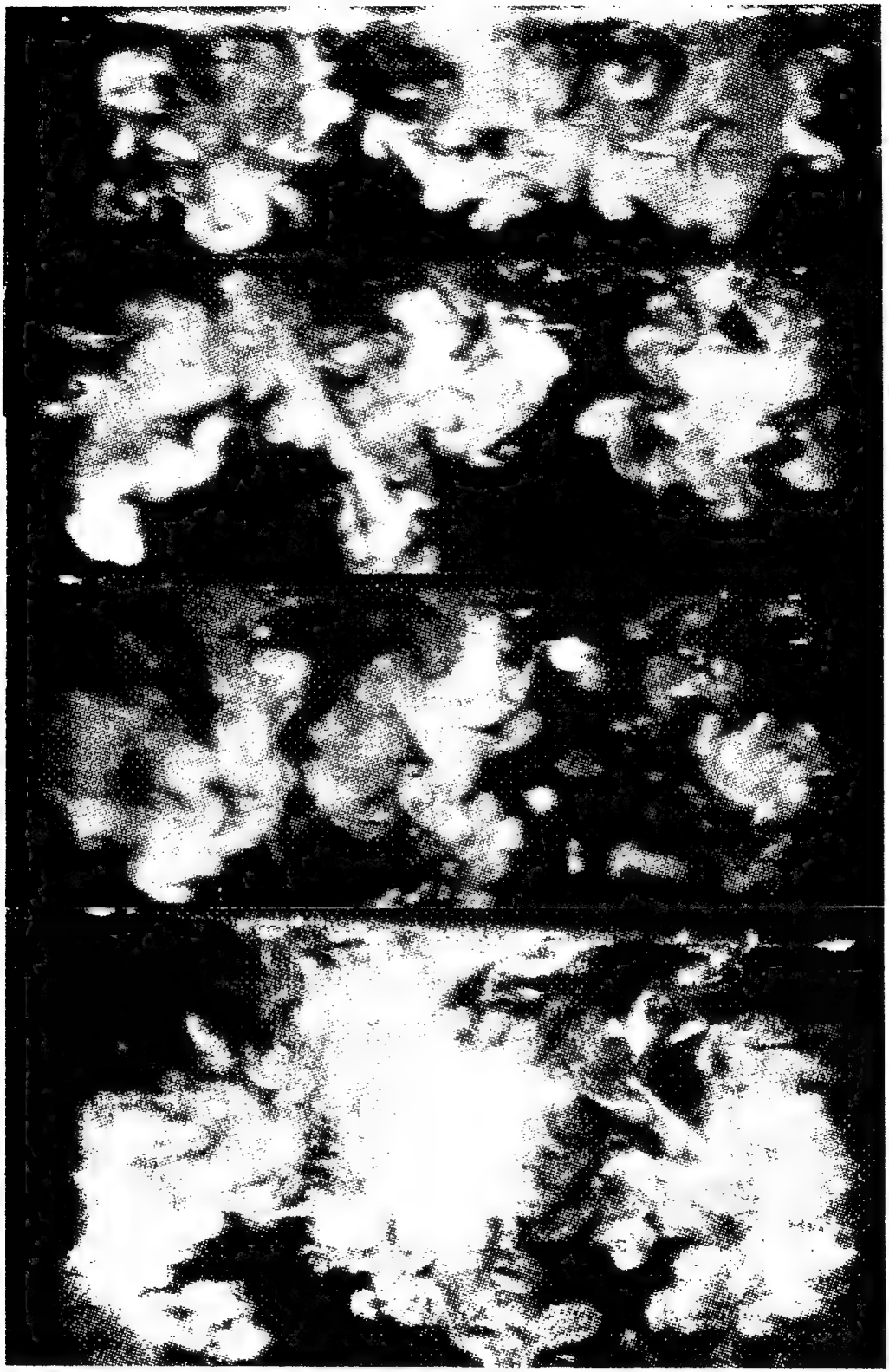

Figure 4-9: Lasersheets for in-line rows with M_L=1.0 and (a) M_T=0.0, (b) M_T=1.0, (c) M_T=1.5, and (d) M_T=2.5. Shown 90%.

to the vorticity, it cannot be denied that the vorticity cancellation in the staggered case is responsible for the elimination of entrainment of the main flow toward the surface and thus improved film cooling in turbine blades.

Finally, consider the oblique photographs shown in figures 4-10 through 4-12. These

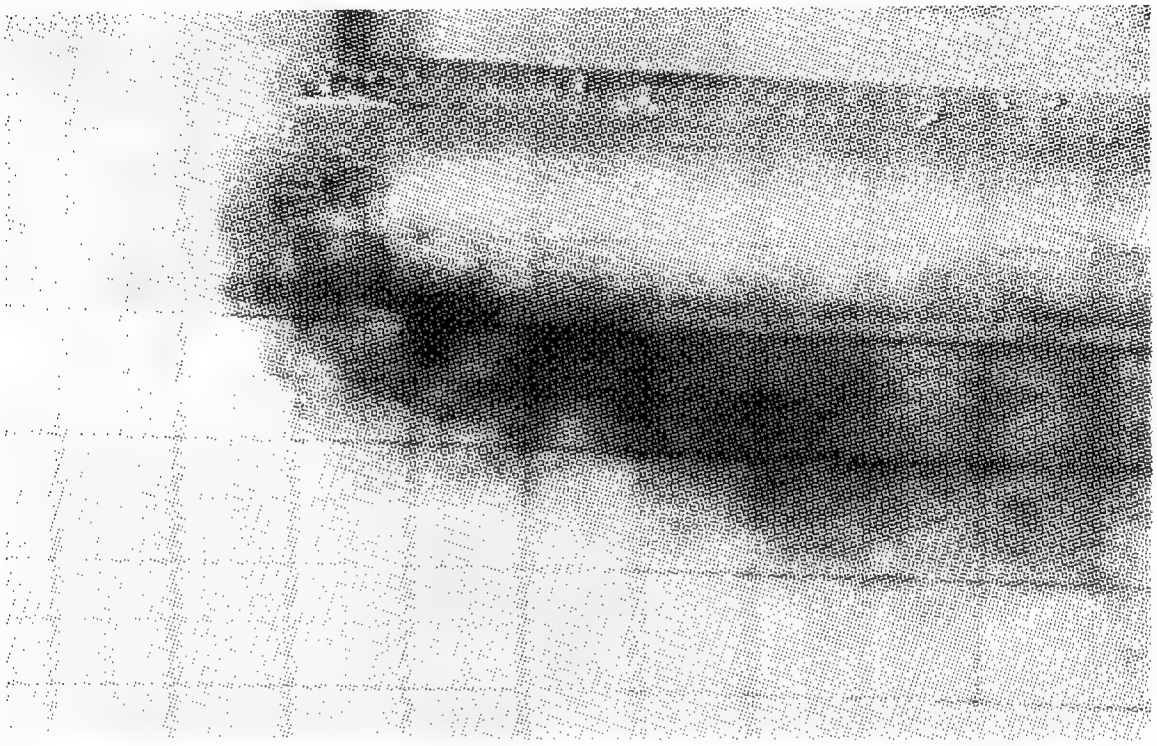

Figure 4-10: Low angle oblique photograph for a single row with M_L=1.0.

figures show low angle oblique photographs taken for M_L=1.0. For the staggered and in-line photographs, M_T=2.0. Included for clarity, these figures show distinctly several items of interest. Comparing figure 4-10 and figure 4-11, the in-line photograph of figure 4-11 shows clearly a trajectory which is further displaced from the wall. Finally, comparing figures 4-10 and 4-12, the scalloping and reattachment of the leading row of jets is evident for the staggered case shown in figure 4-12.

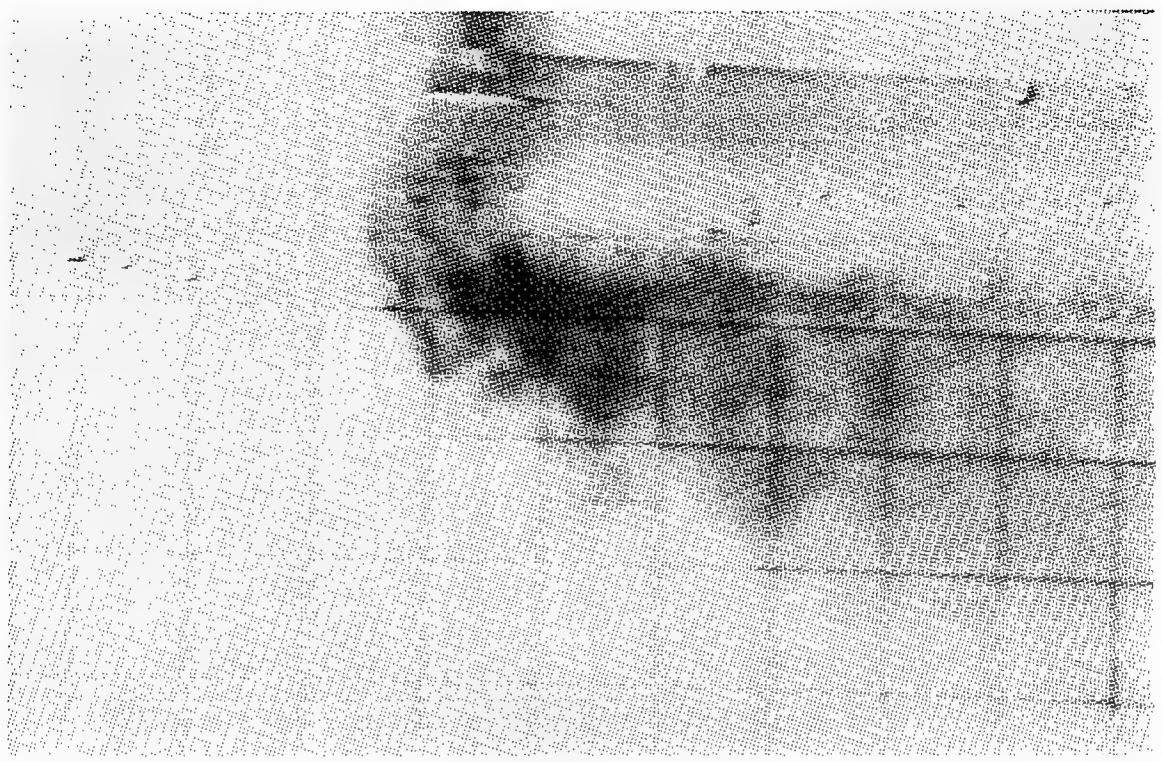

Figure 4-11: Low angle oblique photograph for in-line rows with M_L=1.0 and M_T=2.0.

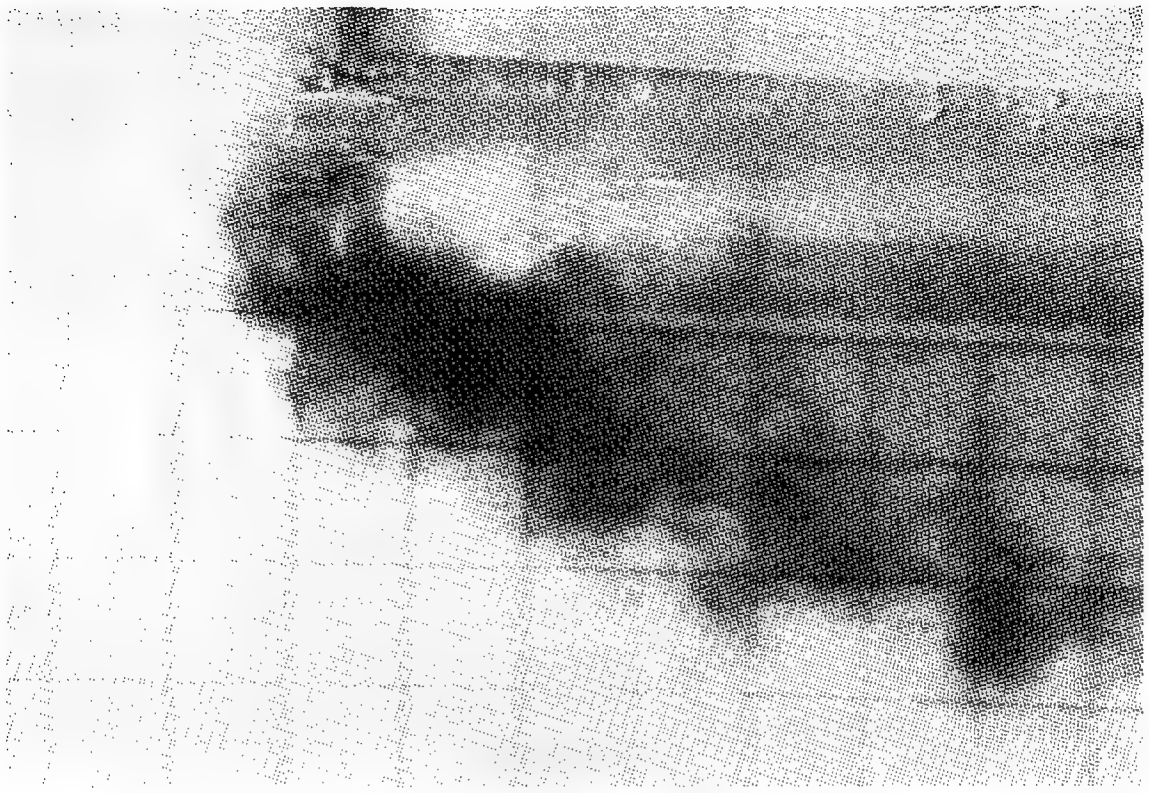

Figure 4-12: Low angle oblique photograph for staggered rows with M_L=1.0 and M_T=2.0.

Chapter 5: Recommendations and Summary

This chapter provides recommendations for areas of future research. These areas of future research are recommended where the present data is inconclusive or does not sufficiently support the proposed phenomenon. Finally, a summary of the research conducted and the conclusions reached is given.

5.1 Recommendations for Future Research efforts

5.1.1 Edge Effects

In examining figures such as Figures A-15, A-23, A-30, A-52 and A-53, one noticeable difference between the staggered and in-line lasersheets of these cases is apparent. In the case of staggered rows, the middle jet appears to be displaced relatively less than its adjacent jets. This may be explained by the lack of an infinite array of jets within the row. The jets on the outside of the row do not have the benefit of an equal number of vortex pairs on both sides. Thus, they see a relatively smaller reduction in lift-off.

Conversely, in Figures A-52 and A-53 which show in-line rows of jets, the opposite effect appears to occur. The middle jet is the furthest displaced of the three. This is expected from the discussion in chapter 3 for a single row based on the lift-off by mutual induction principle and the proximity of other vortices. The occurrences described are the predicted results. They were not included in the actual results because many of the figures in Appendix A do not share this trend.

The establishment of this position and configuration dependent lift-off relationship will certainly serve to reconfirm the conclusion that vorticity cancellation and enhance-

ment is critical in film cooling. This dependence will easily be established by the construction of inserts for the apparatus used which vary intra-row spacing and the number of jets per row. Lasersheets will then be accomplished as for this thesis for single row cases. As intra-row spacing is increased, the variation in jet lift-off between jets should decrease until, effectively, an isolated kidney vortex case is reached. Next, as the number of jets within the row is increased, a decrease in displacement related to distance from the row centerline should present itself. Finally, it must be recommended for future experiments where the isolation of effects is of interest that a greater number of jets be used within each row to eliminate these edge effects.

5.1.2 Expanded Research

Obviously, the intent of this entire research effort is to better understand the physical phenomena that govern the flow field of jets in crossflow. For that reason, expansion of the data obtained here is essential to answer the following questions:

- 1. What are the effects of variation of inter-row and intra-row spacing?
- 2. What effect does a reduction in the injection angle have on vorticity interaction and lift-off?

It has already been suggested that a 'best case' intra-row spacing exists where the vortices are equally separated and lift-off is eliminated, but the dependence on inter-row spacing is less clear. Over time and distance, the vorticity of a jet is turned, diffused and dissipated. Perhaps a reduction in the inter-row distance will allow for better cancellation.

The last supposition leads to the second question. Physically, it seems likely that reducing the injection angle would not only reduce the jets vertical momentum but also increase the axial component of the vorticity, $|\omega_x|$. Increasing $|\omega_x|$ for an isolated jet would be detrimental by virtue of increasing lift-off and entrainment of main flow fluid. This may prove beneficial, however, if it improves vorticity cancellation for multiple jets and thus eliminates lift-off and entrainment.

5.1.3 Quantitative Flow Field Measurements

Ideally, a quantitative result is desirable. For that reason, reaccomplishment of these

experiments with a vorticity measurement system is recommended. In this way, the physically apparent smearing could be correlated to an actual absence of vorticity. Additionally, such systems use time averaging which could be used to dismiss time dependence in an initial consideration.

5.2 Summary

The flow visualization research conducted for this thesis supports several important conclusions. First, vorticity interaction within and between jets in cross-flow is a major influence on jet trajectory and entrainment. Second, the proximity and strength of the jets' vortices determine whether lift-off and entrainment can be altered and thus film cooling effectiveness improved. Finally, vorticity and flow field measurements are essential if a quantitative understanding of the phenomena is to be established.

List of References

Eroglu, Adnan. "An Experimental Investigation of Entrainment and Mixing in Pulsed and Exponential Transverse Jets." diss. University of Washington, 1991.

Fric, T.F. "Structure in the Near Field of the Transverse Jet." diss. California Institute of Technology, 1990.

Haven, Brenda A. and M. Kurosaka. "Contoured 'Shaped' Holes: Improving Cooling Effectiveness & Aero Performance" White Paper Briefing to the A.F.O.S.R., 1994.

Kerrebrock, Jack L. *Aircraft Engines and Gas Turbines.* 2nd ed. Cambridge: MIT Press, 1992.

Kurosaka, M. "Contoured Holes for Film Cooling: the Effect of Kidney Shaped Vortices." Proposal for the A.F.O.S.R., 1994.

Norton, R.J.G. et.al. *Turbine Cooling System Design: Volume I - Technical Report.* Washington: GPO, 1990.

United States. *Integrated High Performance Turbine Engine Technology Initiative.* Ed. William Koop. N.p: n.p., [c. 1990].

Appendix A : Experimental Results

This chapter contains the complete set of color and lasersheet photographs for the experiments conducted. Figures A-1, A-7, A-13, A-19, and A-25 are the single row injection cases for leading blowing ratios, M_L, from 0.5 to 2.5. Figures A-2 through A-6 are the corresponding set of staggered row figures to figure A-1 that have trailing blowing ratios, M_T, from 0.5 to 2.5. The other sets are similar up to A-30.

Figures A-31 through A-55 were obtained for the in-line row cases. Figures A-31 through A-35 have M_L=0.5 with M_T ranging from 0.5 to 2.5. Each successive set of five is similar with M_L increasing by 0.5 correspondingly.

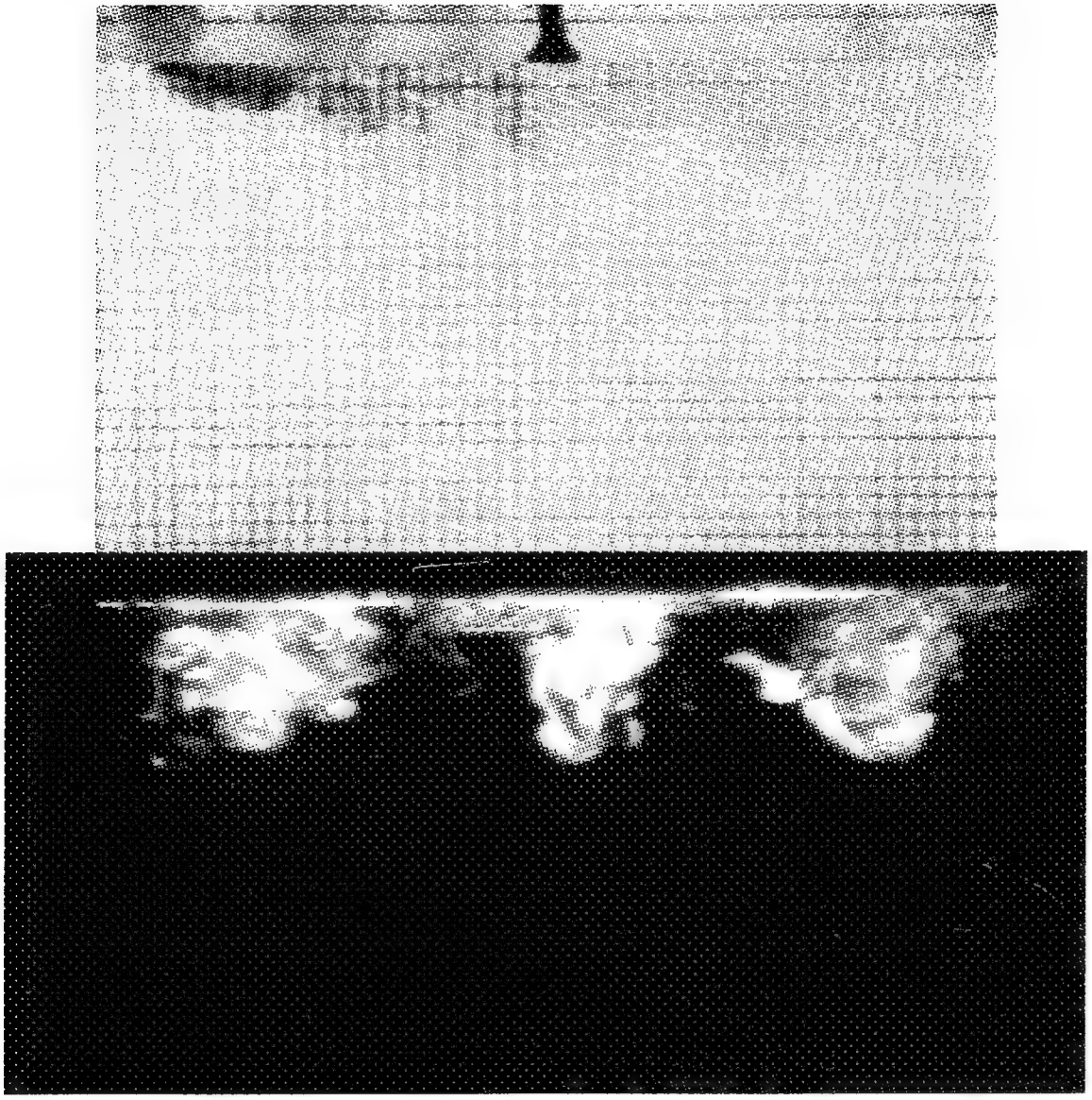

Figure A-1: Single row with M_L=0.5.

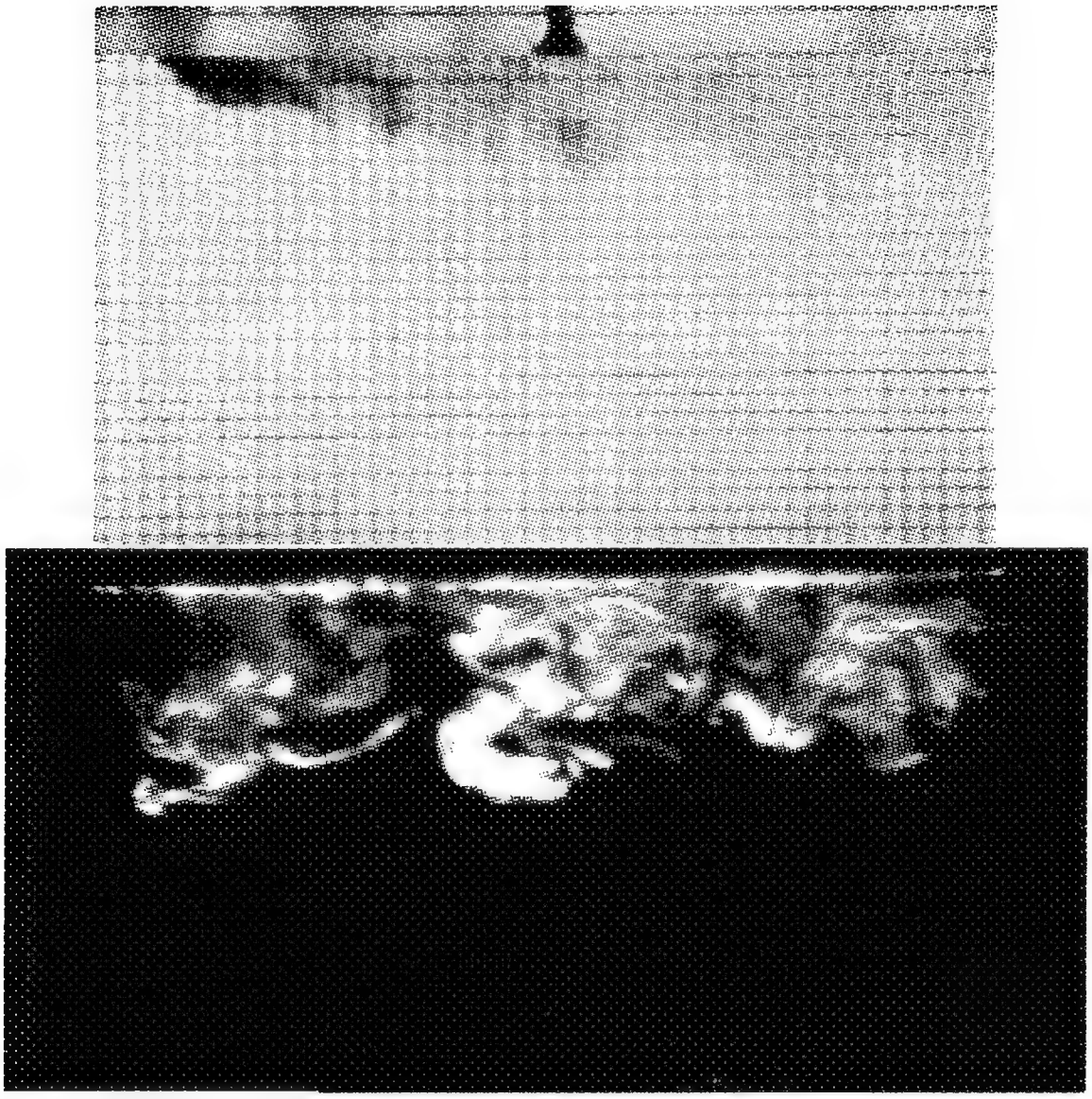

Figure A-2: Staggered row injection with M_L=0.5 and M_T=0.5.

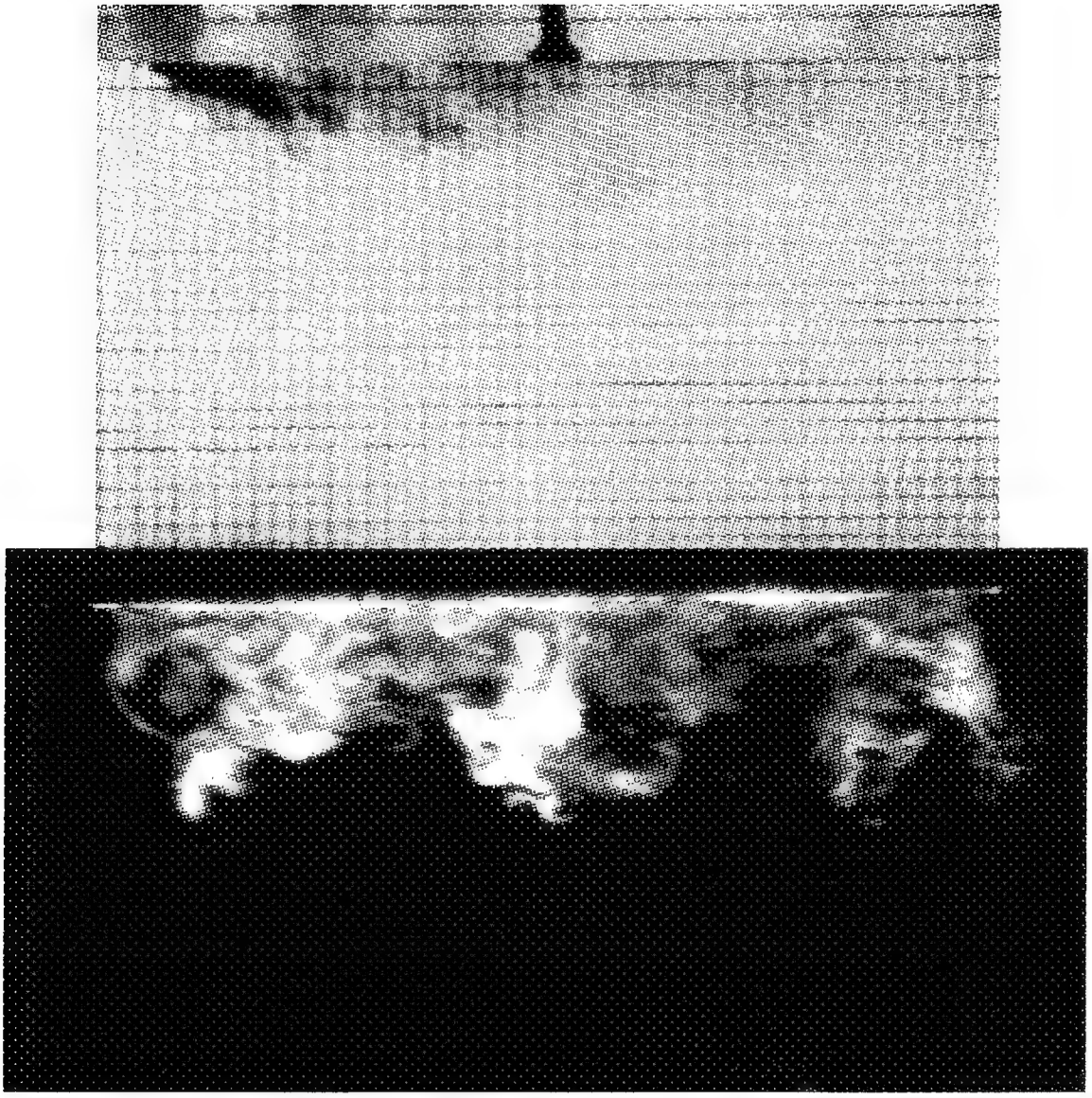

Figure A-3: Staggered row injection with M_L=0.5 and M_T=1.0.

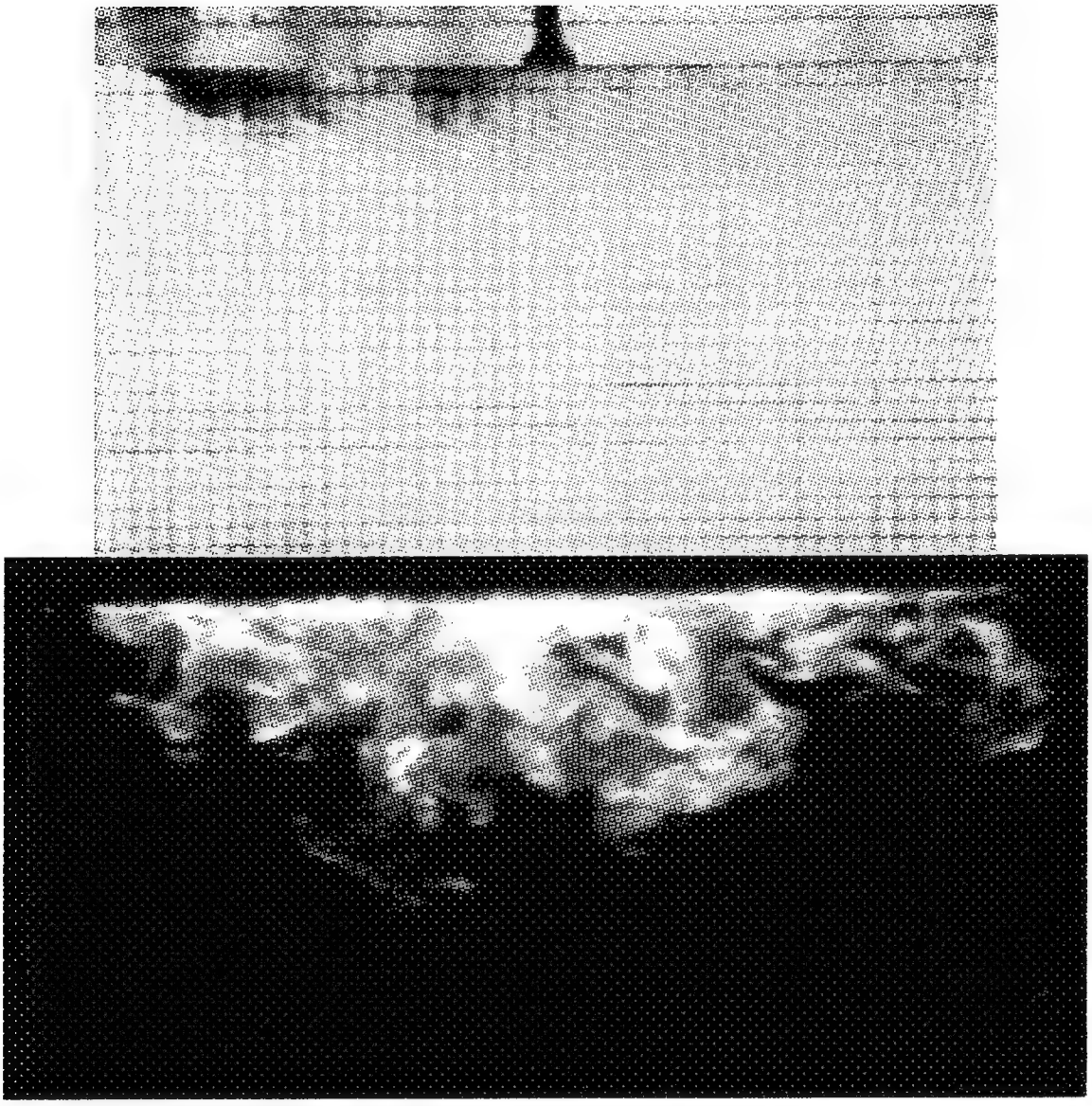

Figure A-4: Staggered row injection with M_L=0.5 and M_T=1.5.

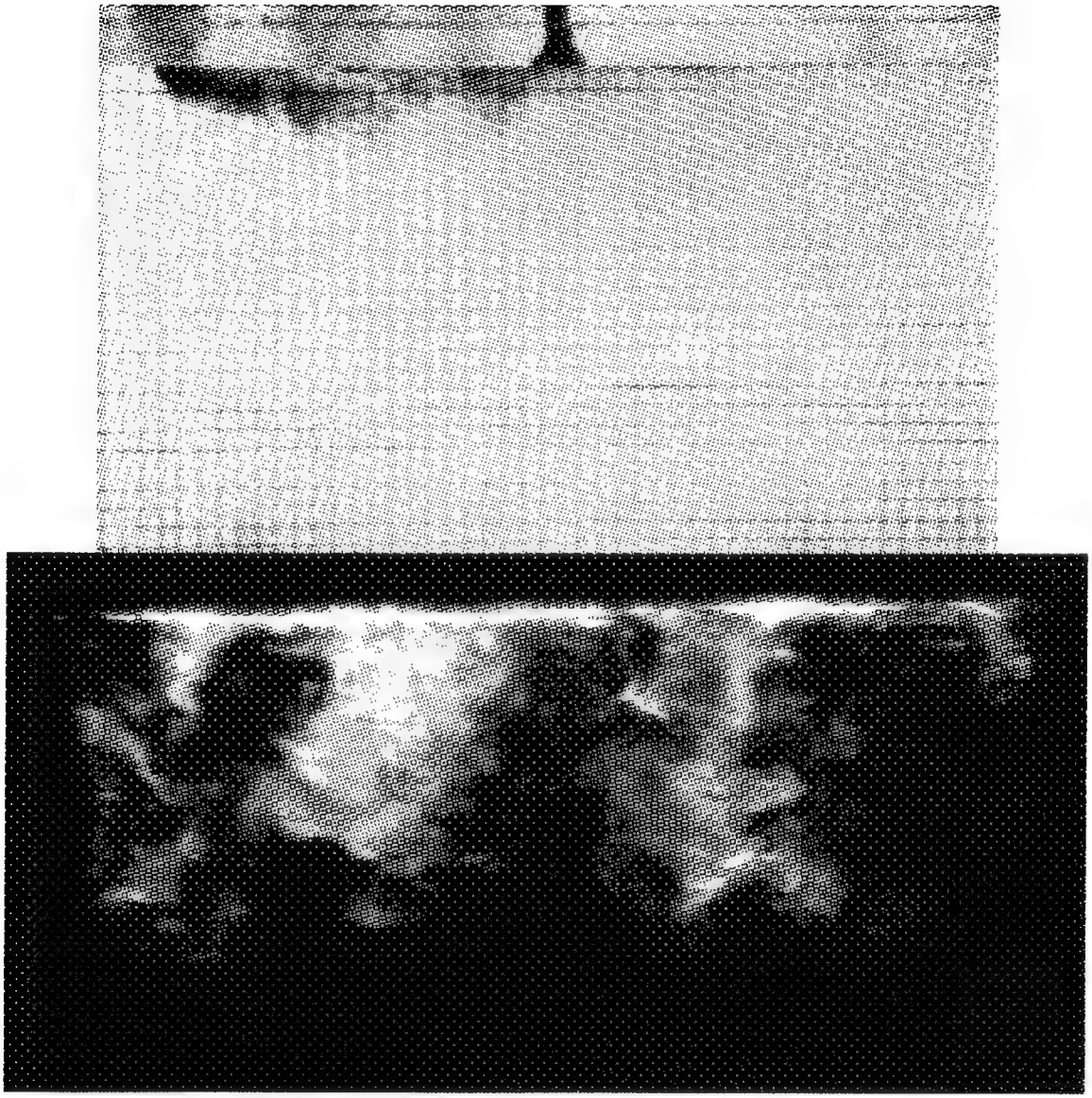

Figure A-5: Staggered row injection with M_L=0.5 and M_T=2.0.

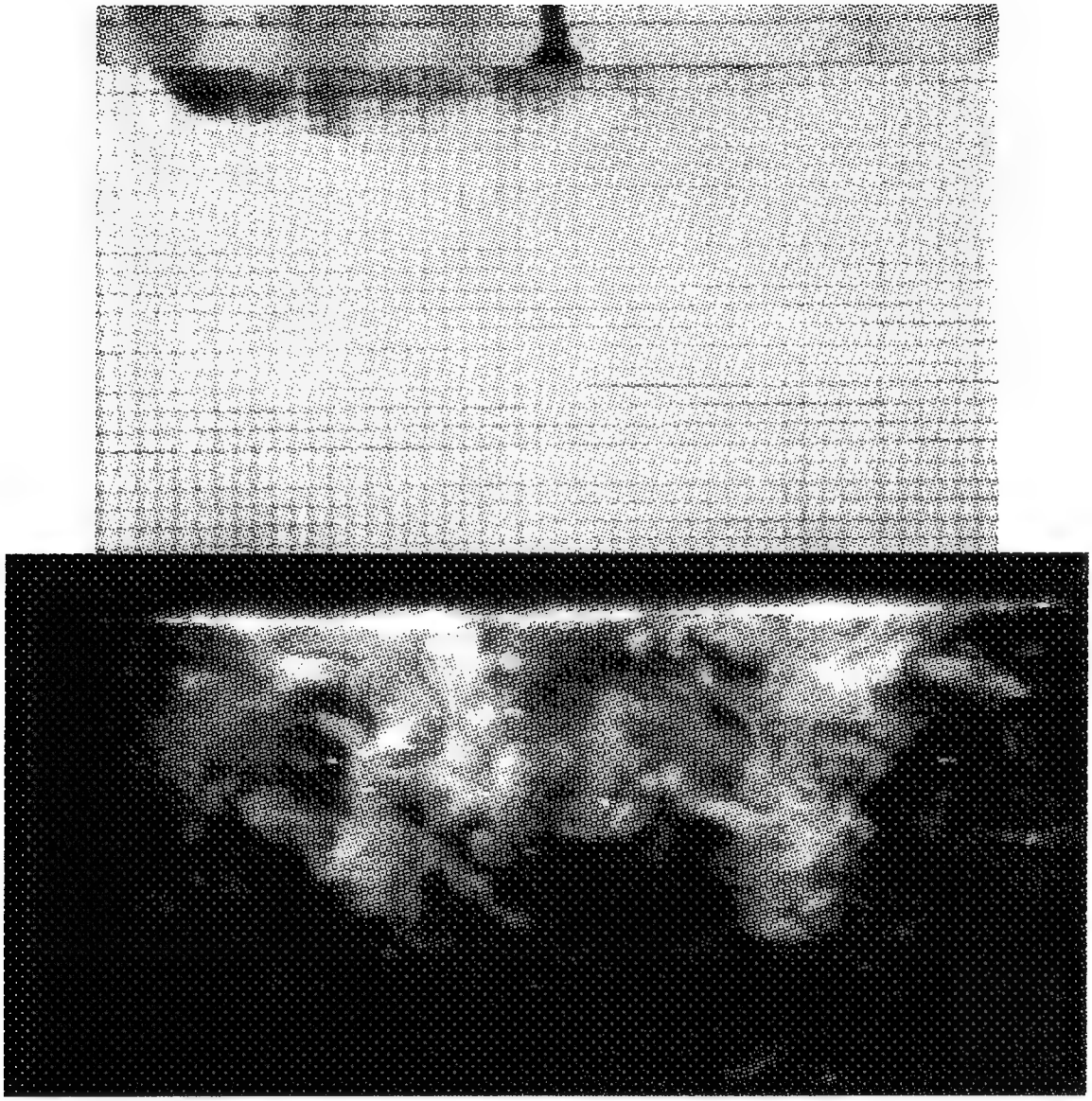

Figure A-6: Staggered row injection with M_L=0.5 and M_T=2.5.

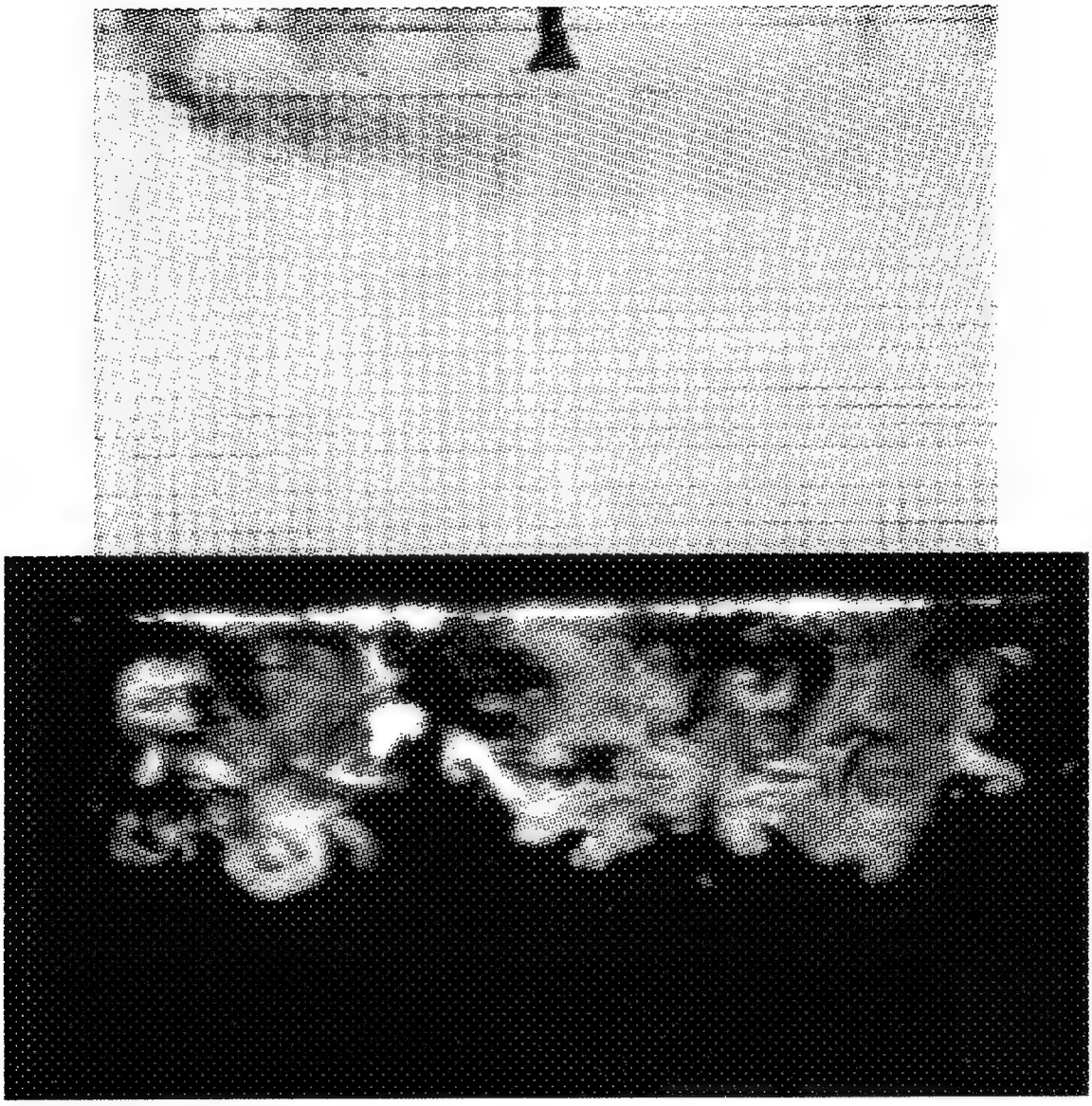

Figure A-7: Single row injection with M_L=1.0.

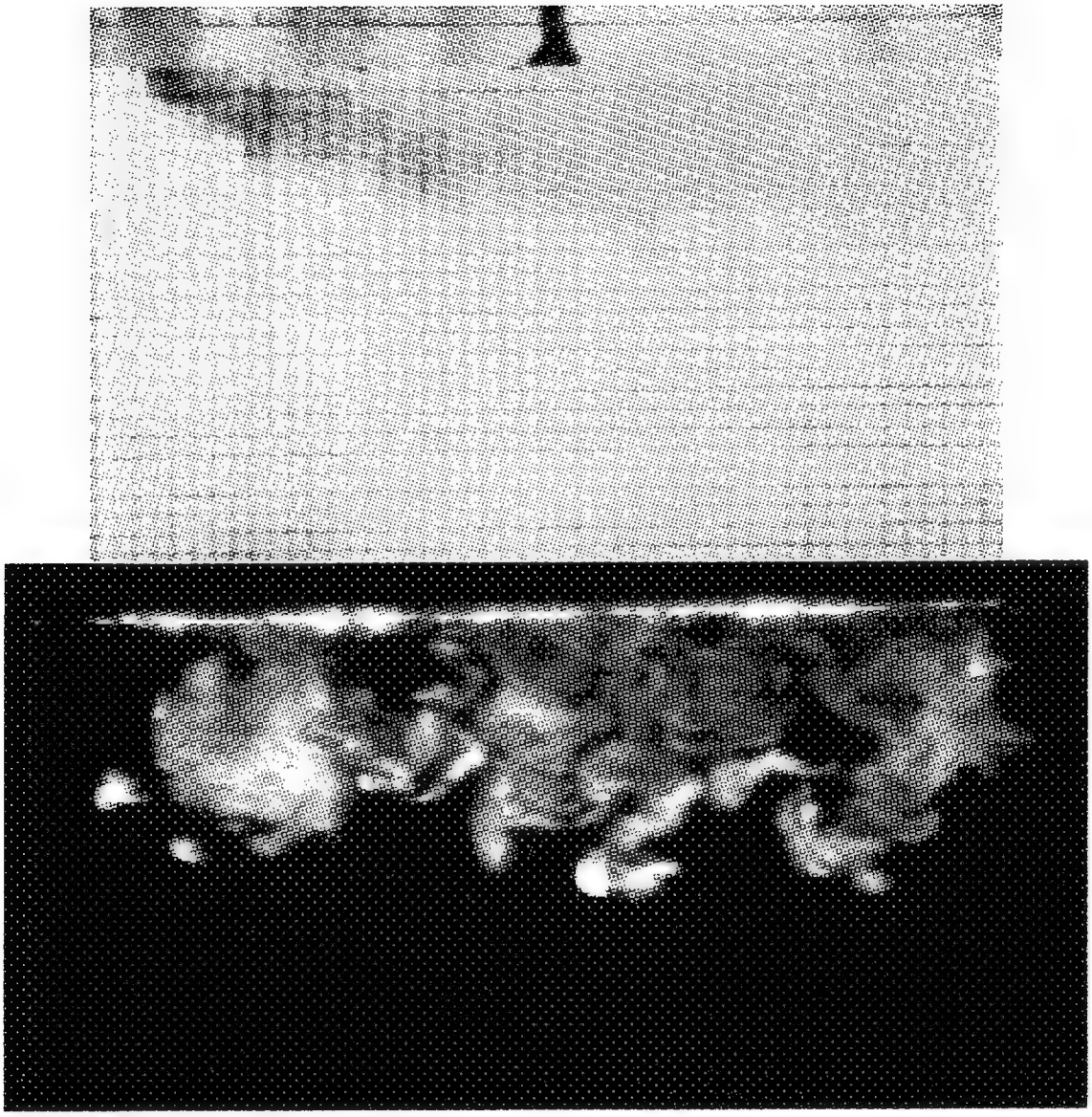

Figure A-8: Staggered row injection with M_L=1.0 and M_T=0.5.

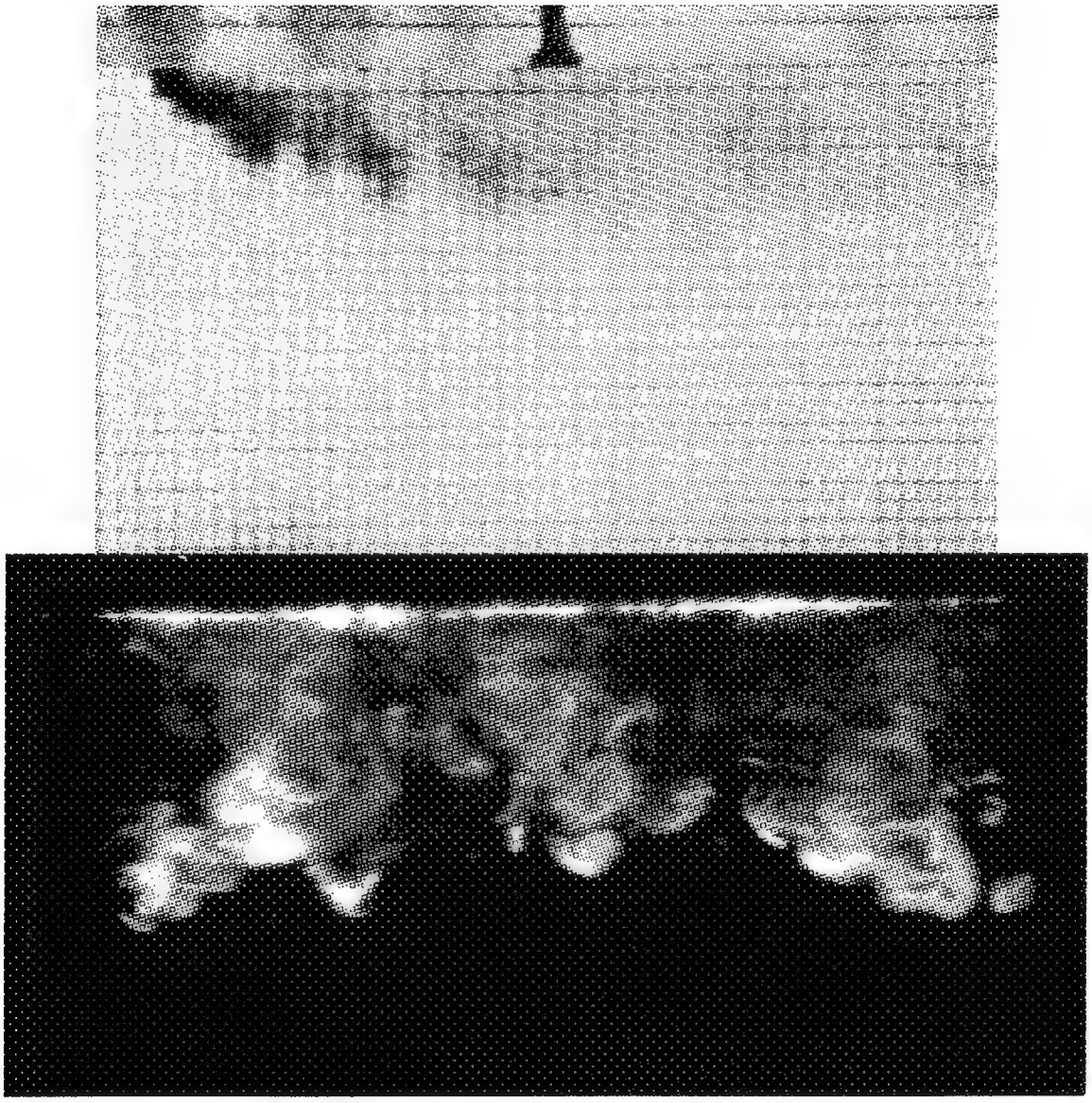

Figure A-9: Staggered row injection with M_L=1.0 and M_T=1.0.

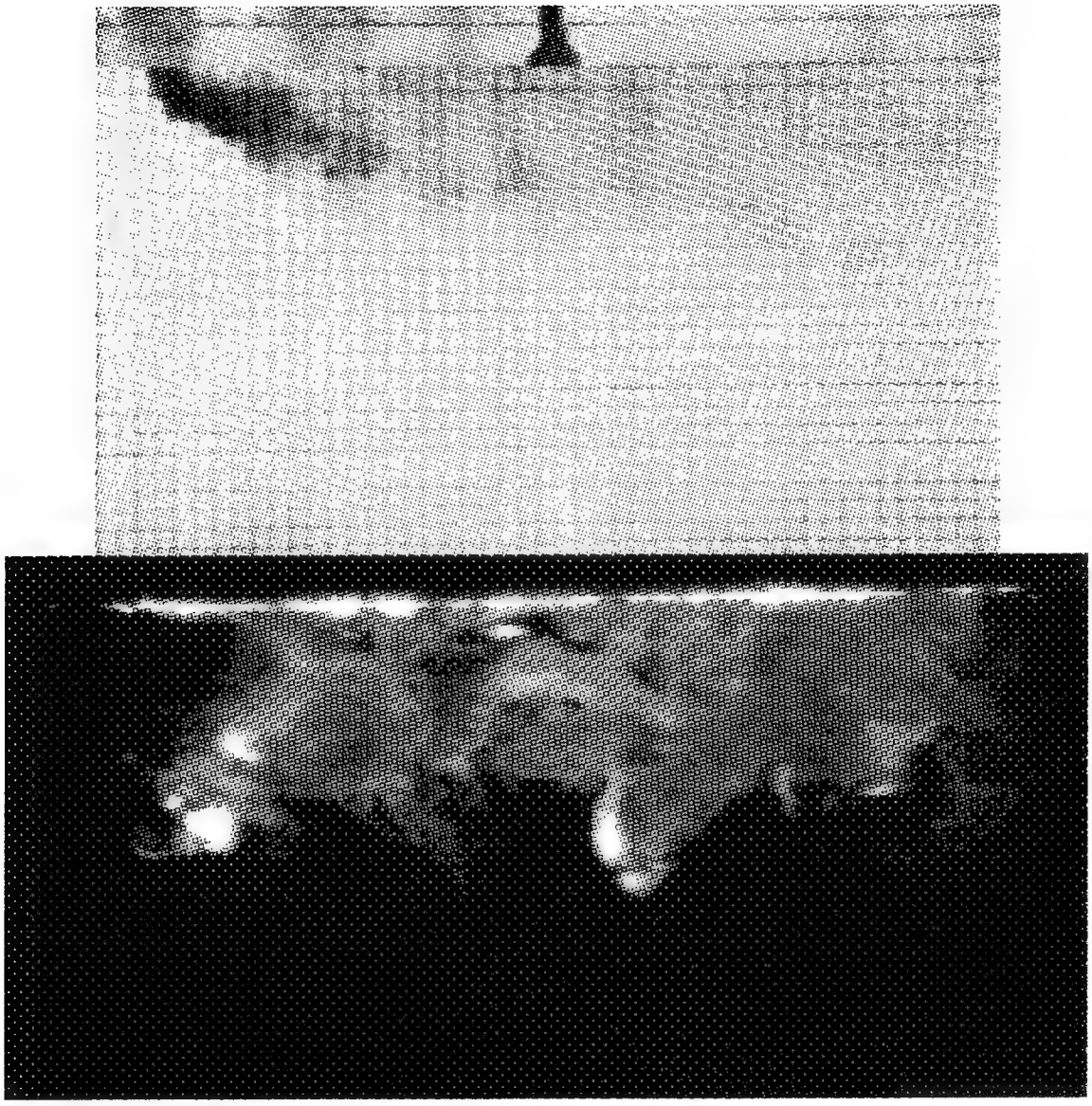

Figure A-10: Staggered row injection with M_L=1.0 and M_T=1.5.

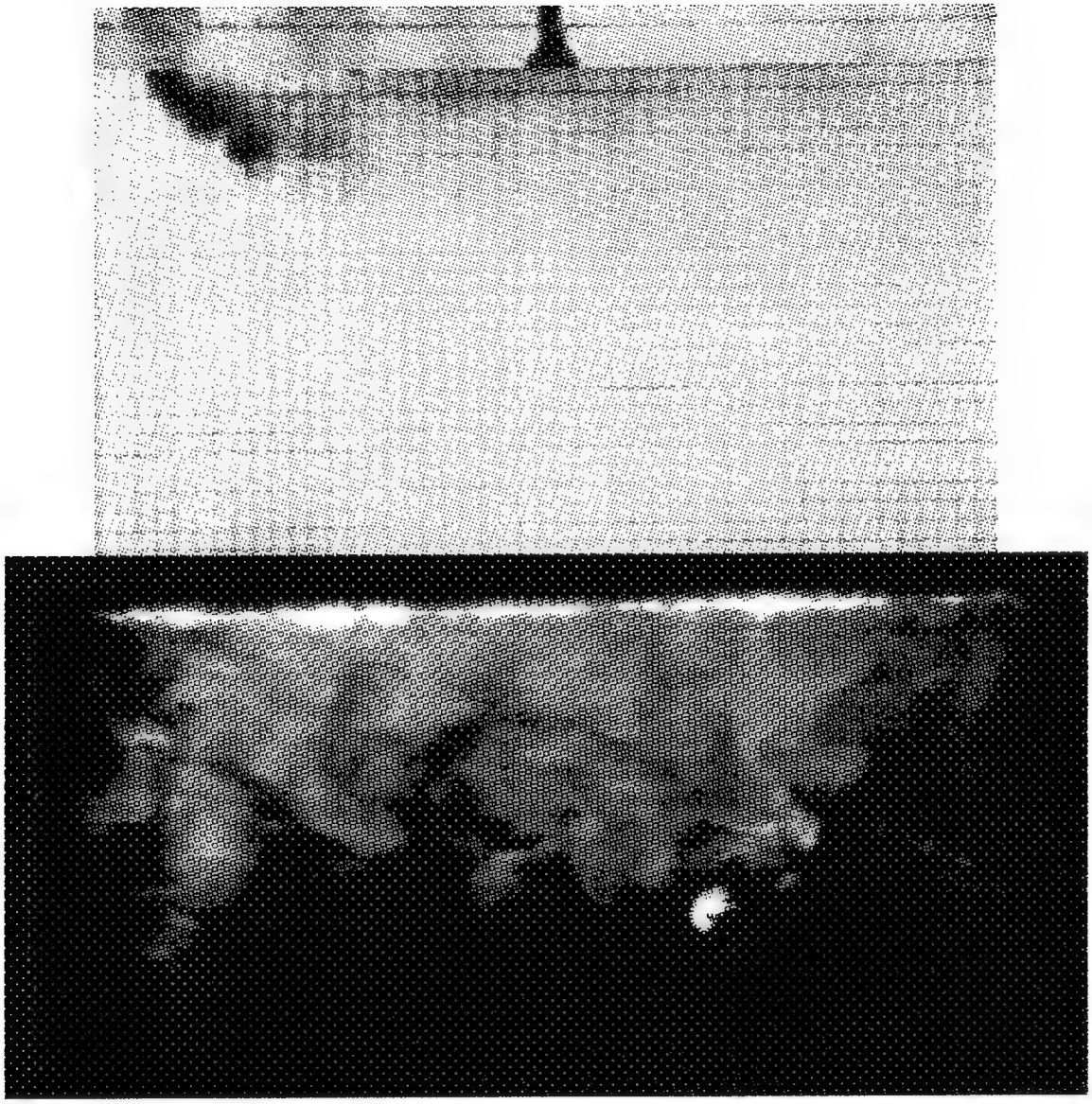

Figure A-11: Staggered row injection with M_L=1.0 and M_T=2.0.

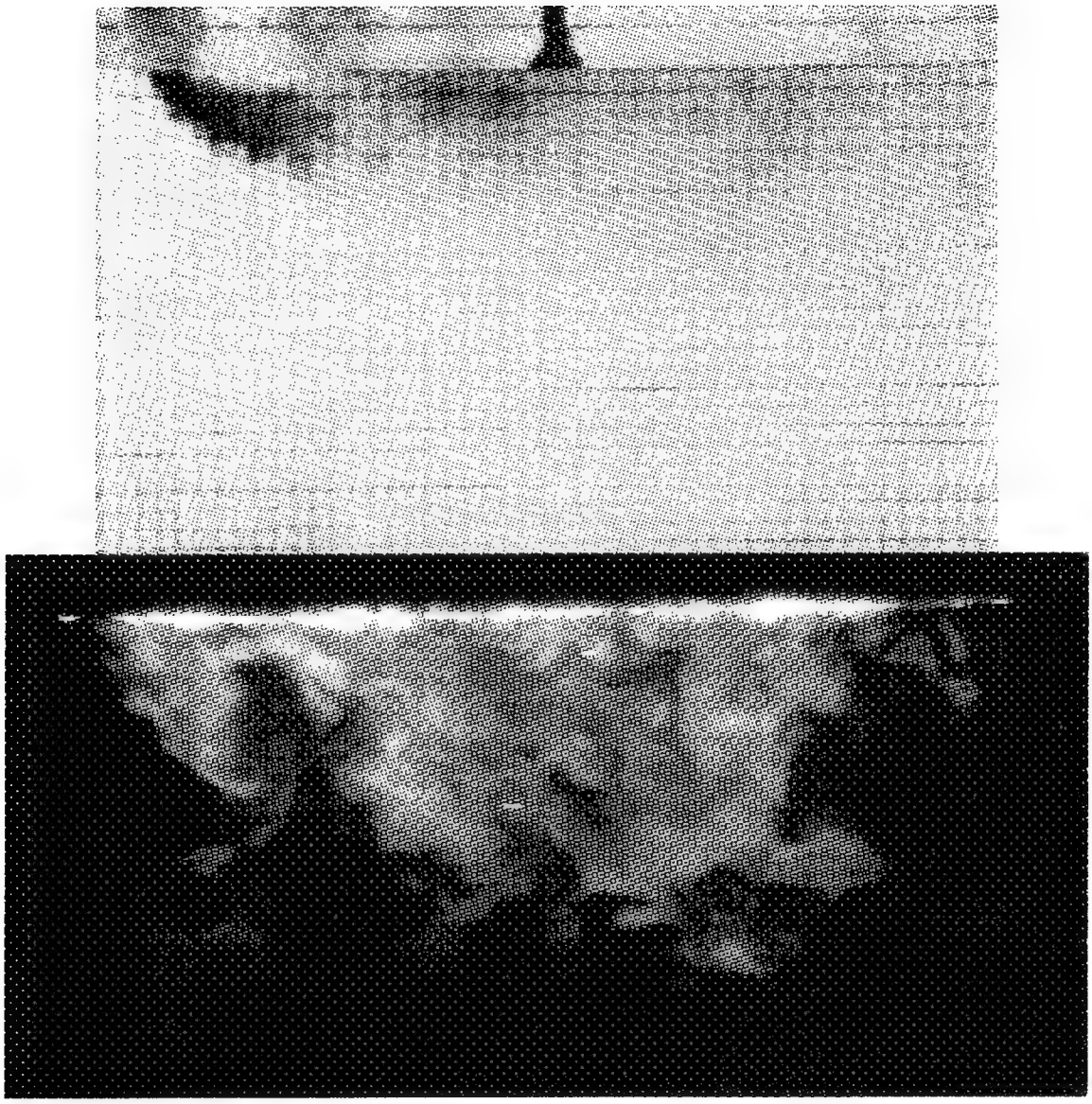

Figure A-12: Staggered row injection with M_L=1.0 and M_T=2.5

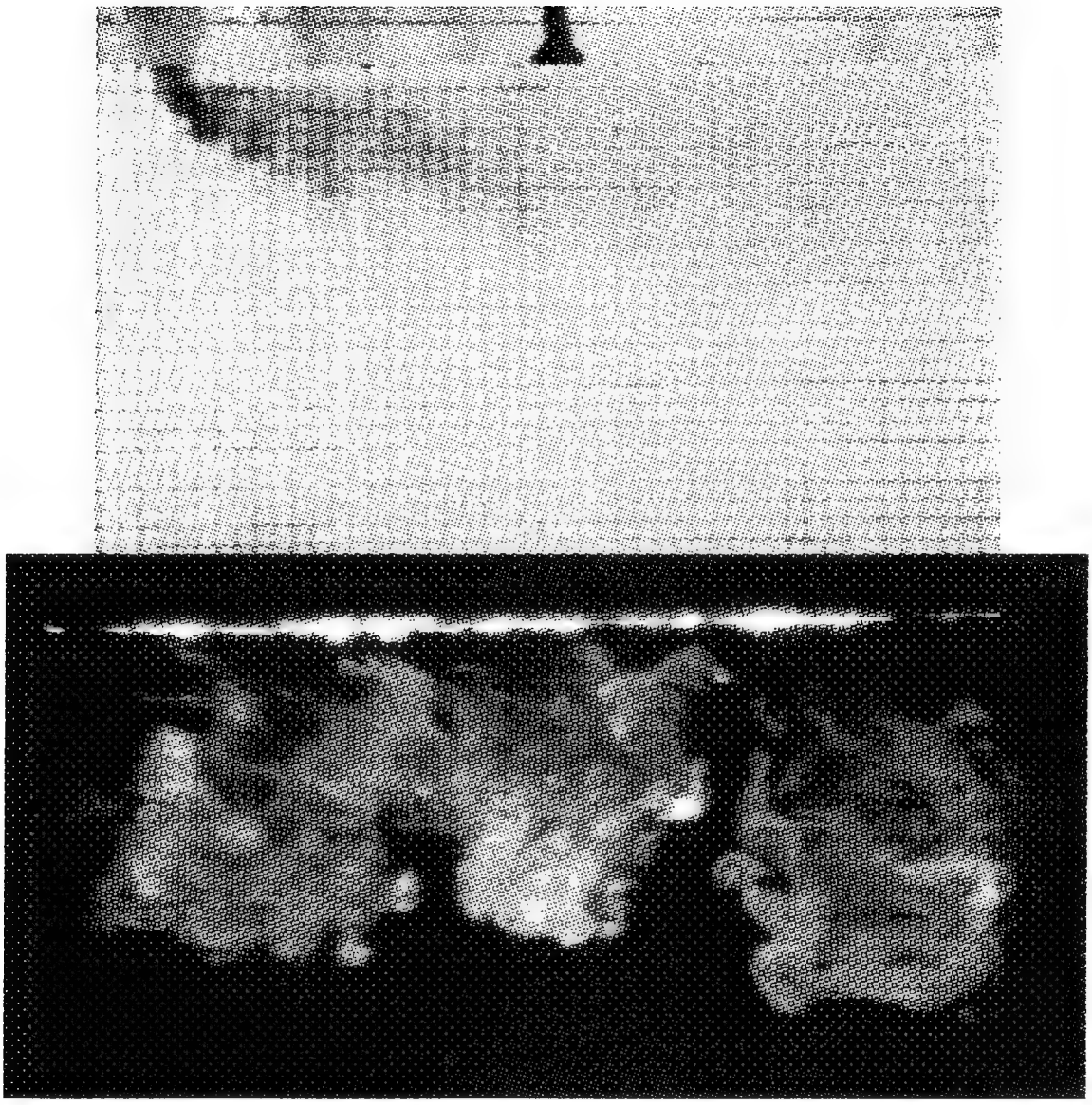

Figure A-13: Single row injection with M_L=1.5.

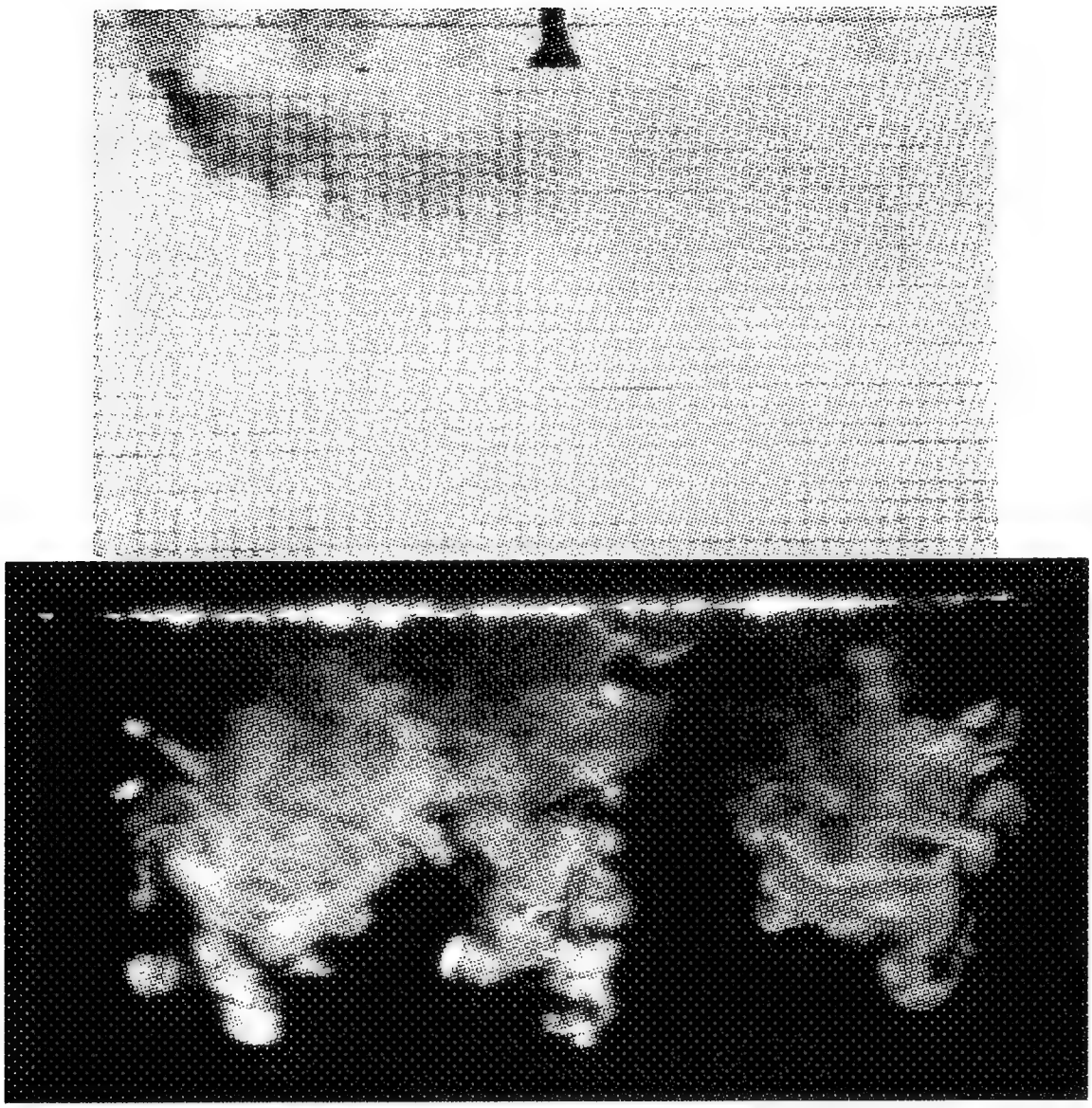

Figure A-14: Staggered row injection with M_L=1.5 and M_T=0.5.

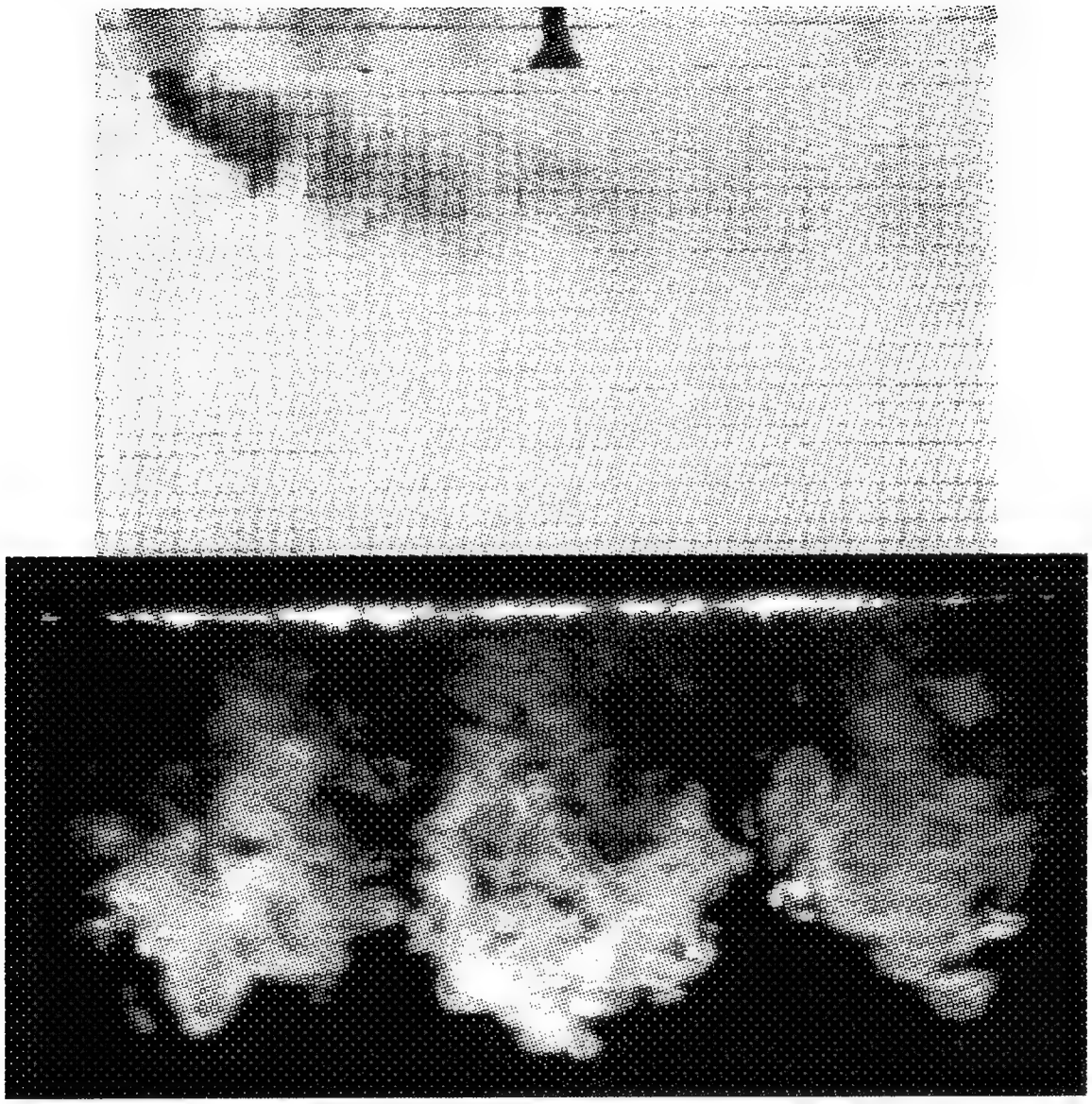

Figure A-15: Staggered row injection with M_L=1.5 and M_T=1.0.

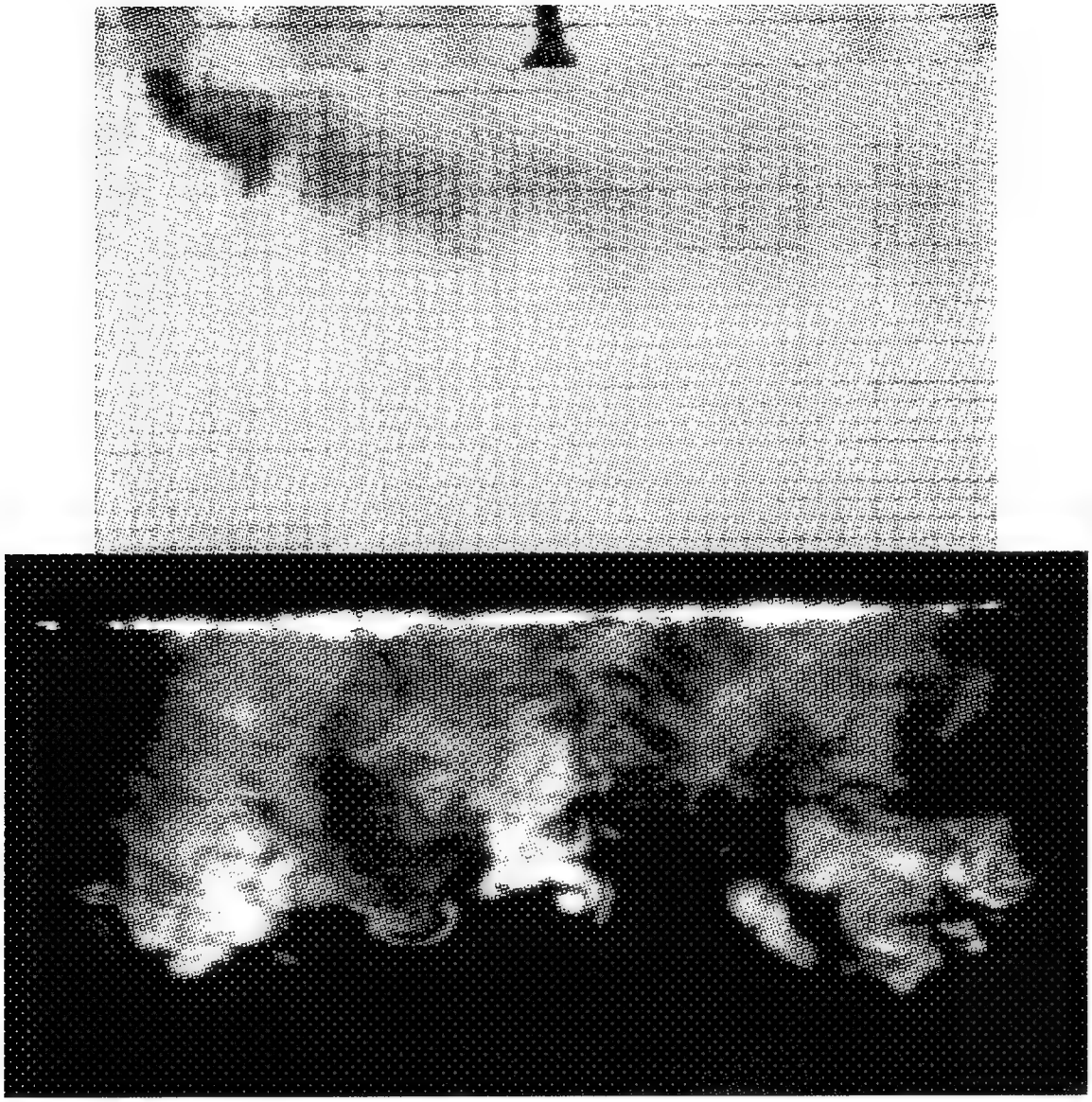

Figure A-16: Staggered row injection with M_L=1.5 and M_T=1.5.

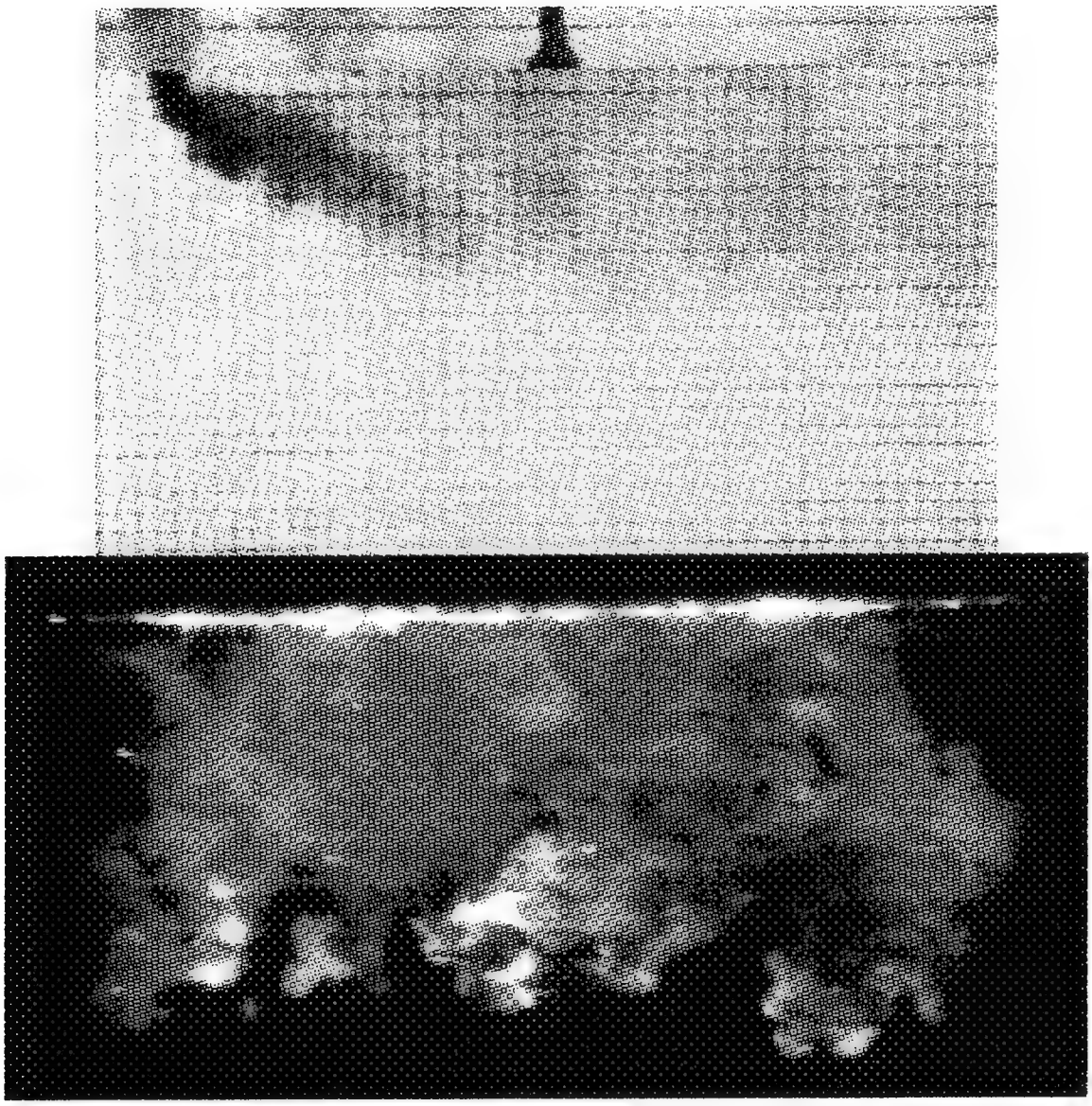

Figure A-17: Staggered row injection with M_L=1.5 and M_T=2.0.

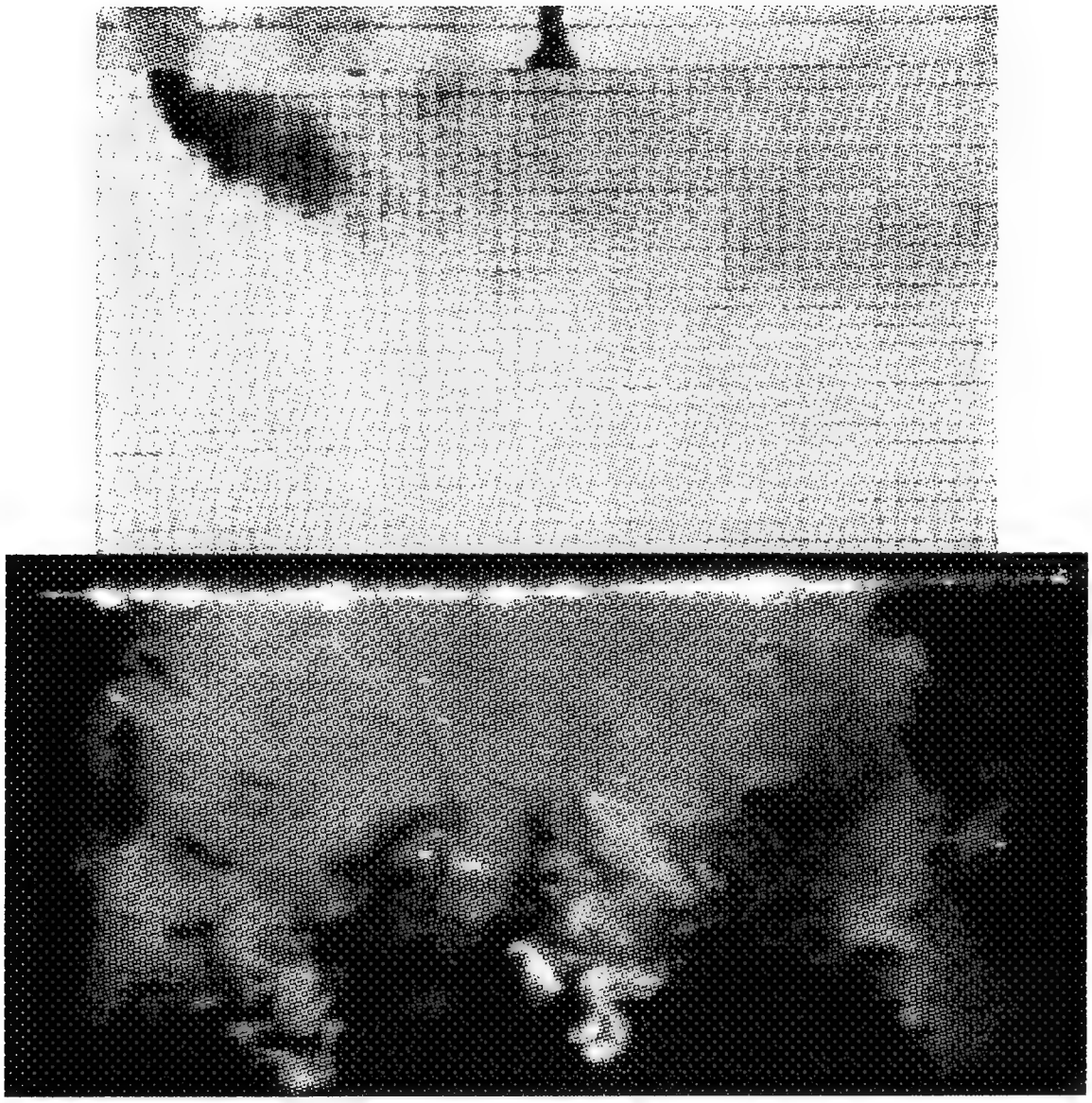

Figure A-18: Staggered row injection with M_L=1.5 and M_T=2.5.

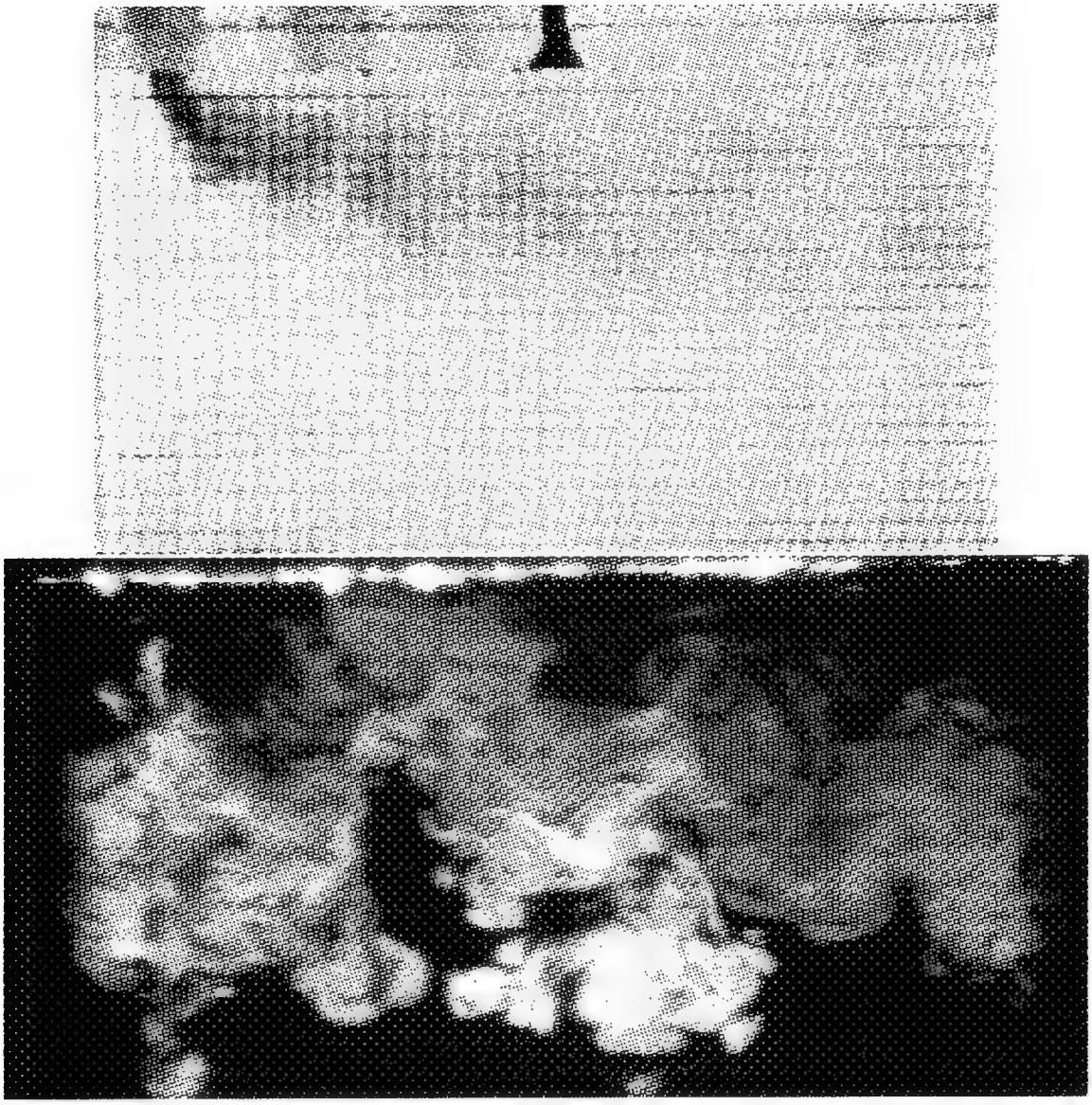

Figure A-19: Single row injection with M_L=2.0.

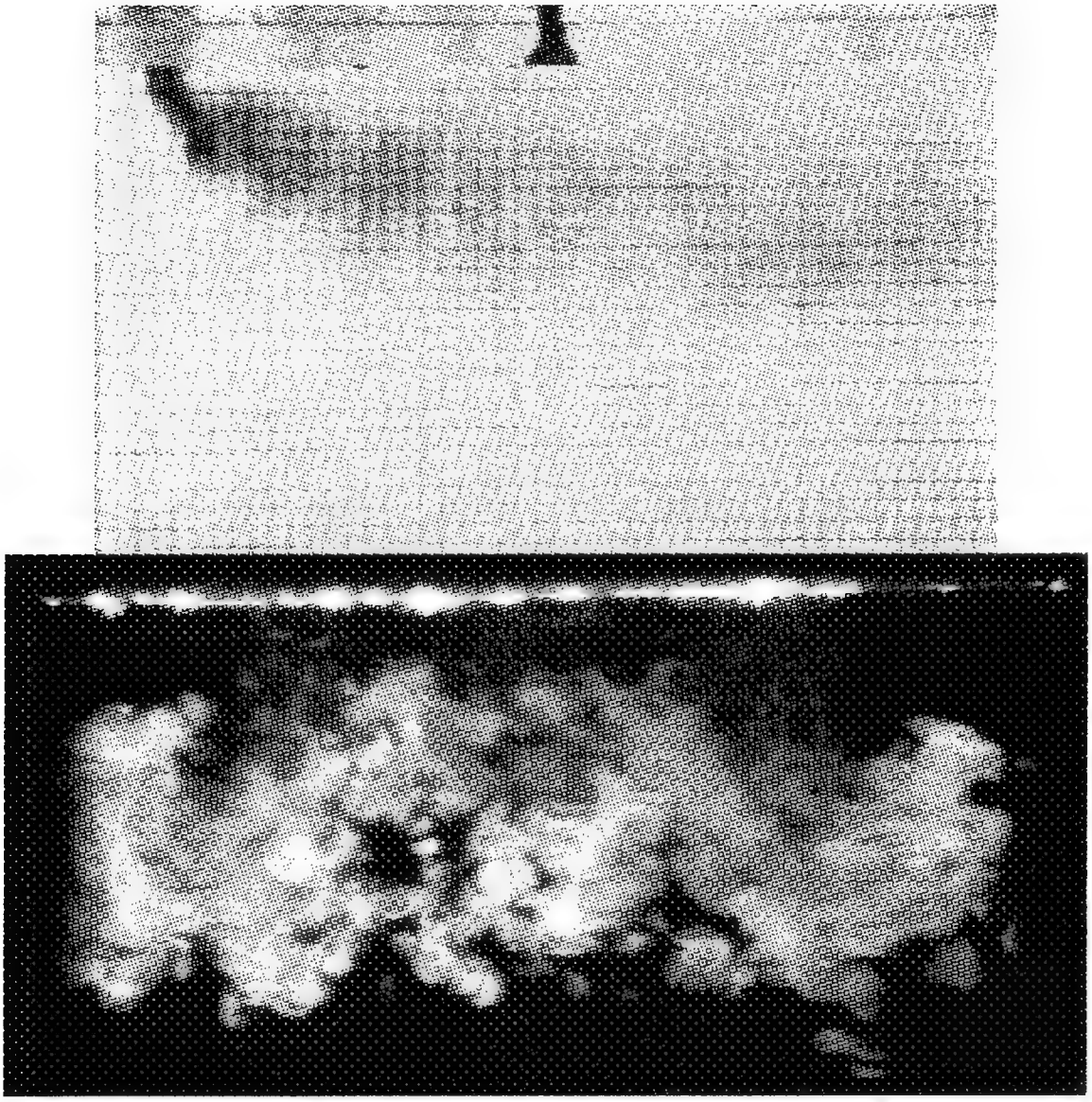

Figure A-20: Staggered row injection with M_L=2.0 and M_T=0.5.

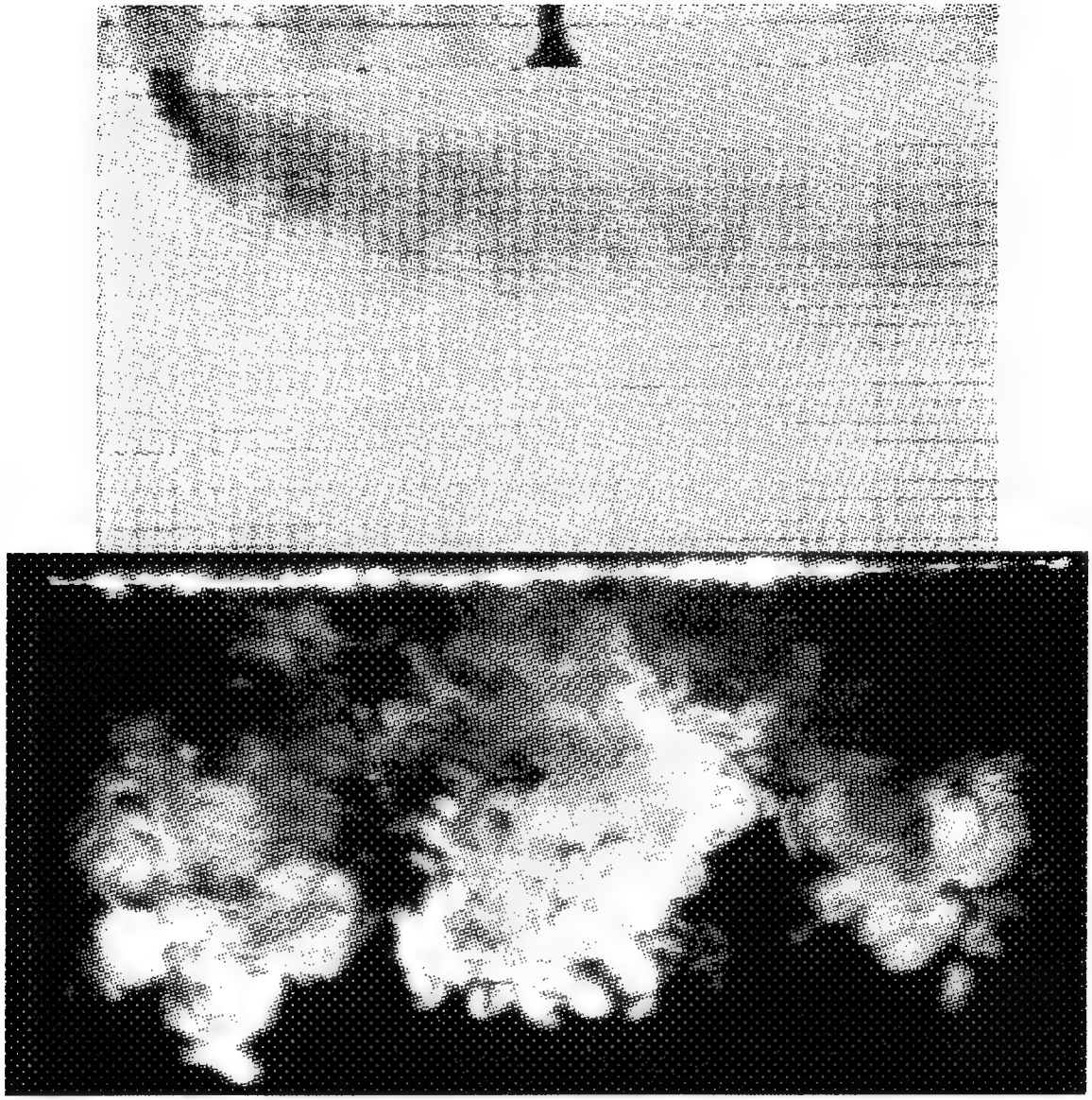

Figure A-21: Staggered row injection with M_L=2.0 and M_T=1.0.

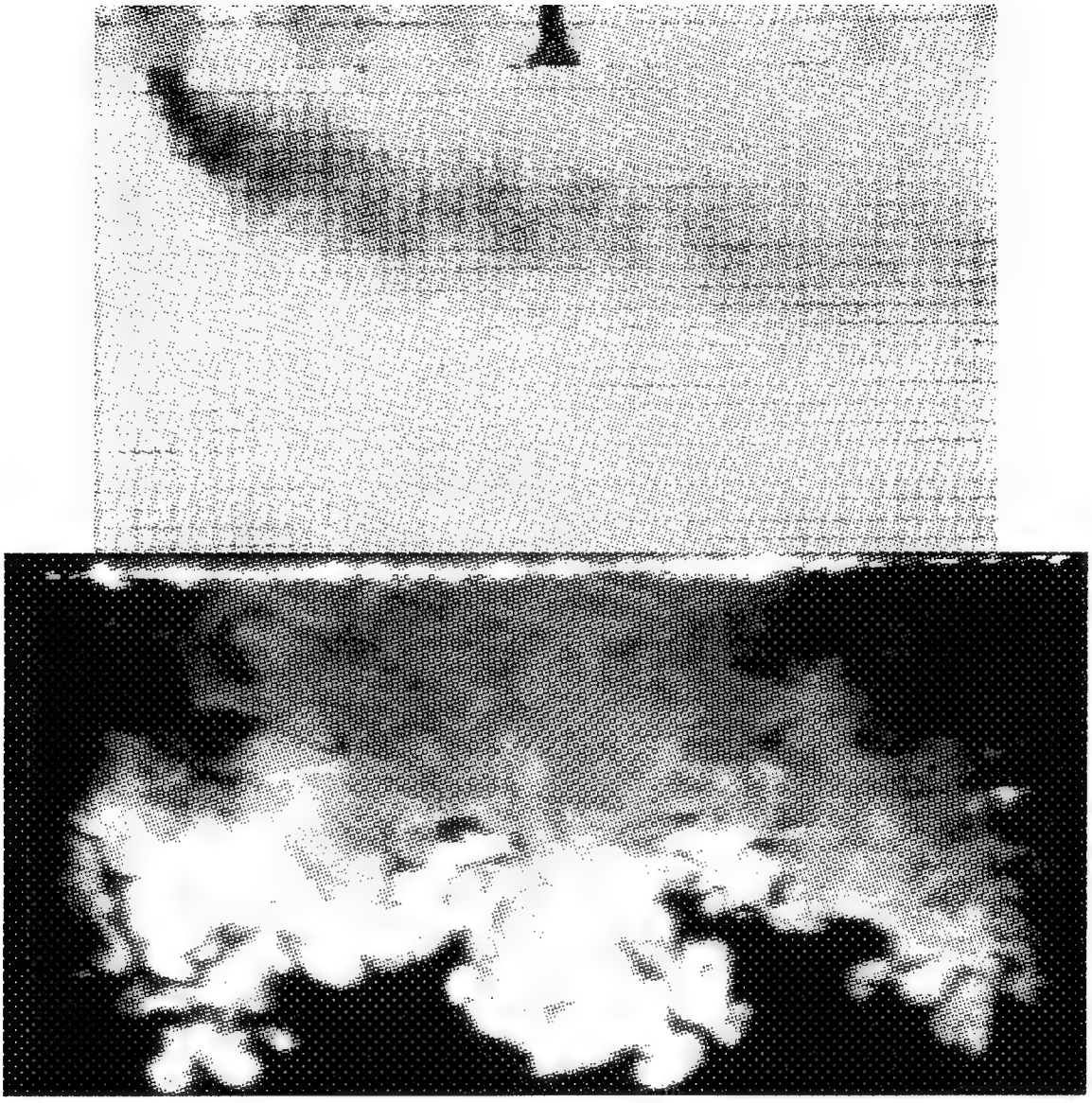

Figure A-22: Staggered row injection with M_L=2.0 and M_T=1.5.

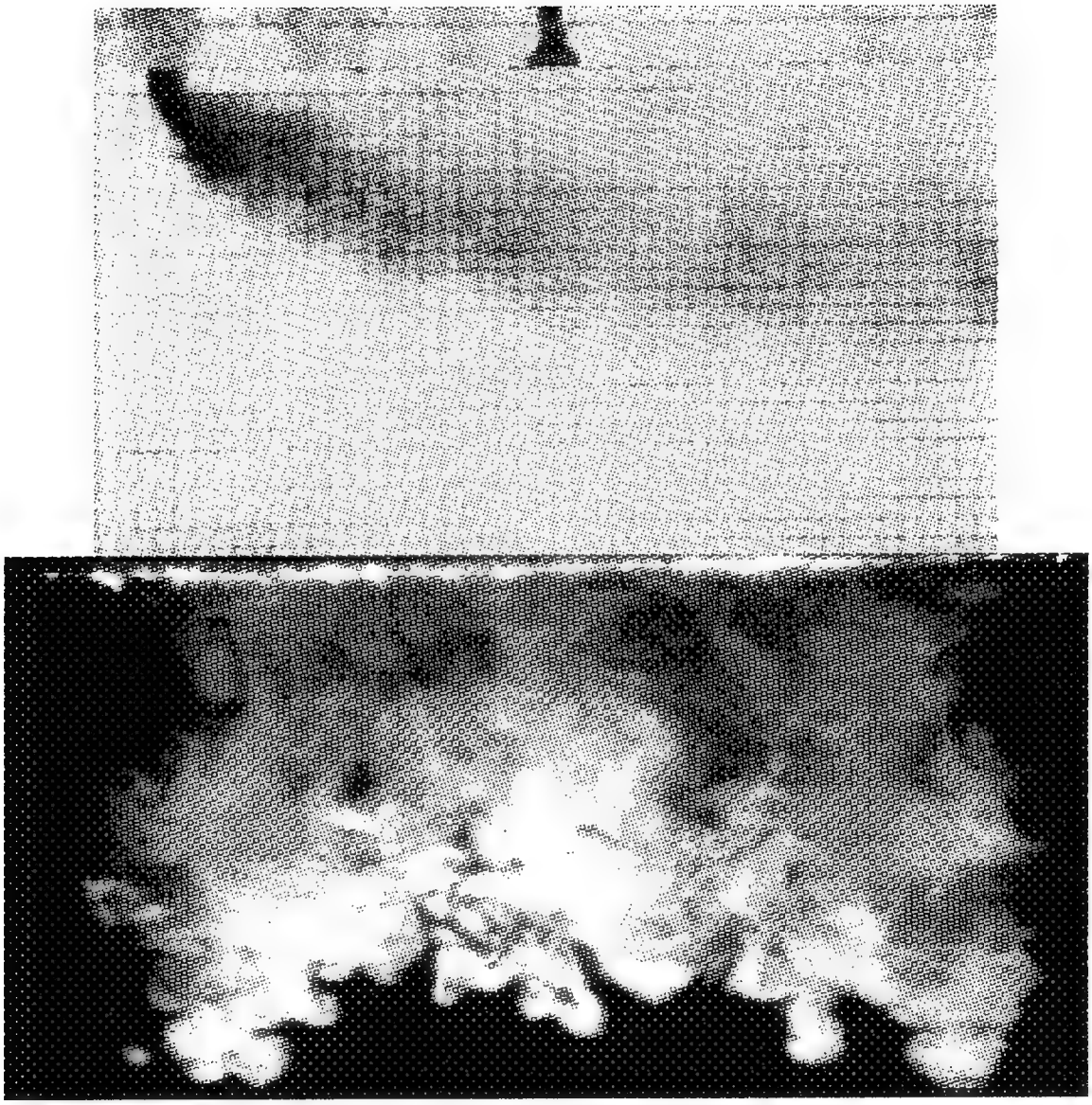

Figure A-23: Staggered row injection with M_L=2.0 and M_T=2.0.

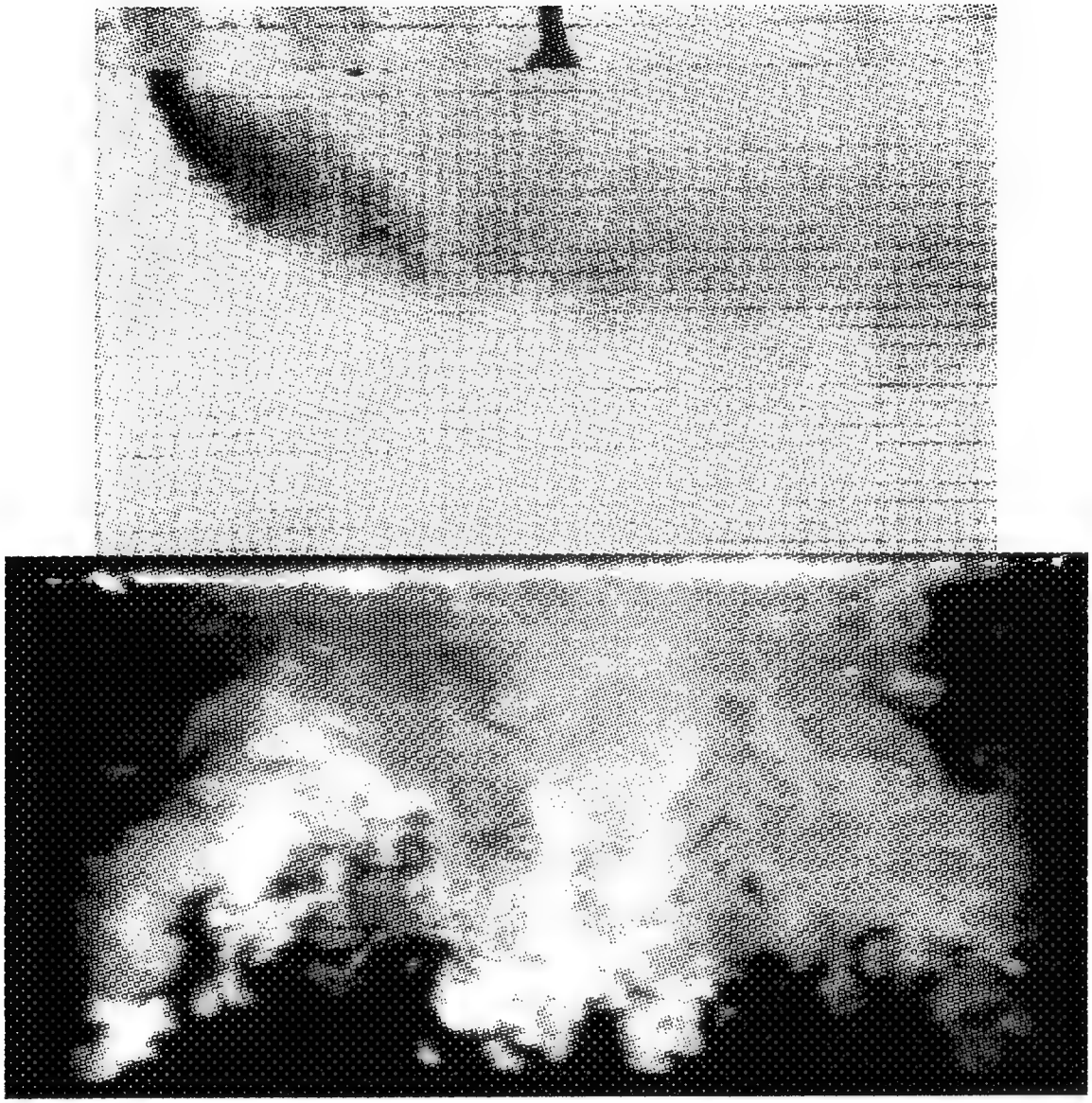

Figure A-24: Staggered row injection with M_L=2.0 and M_T=2.5.

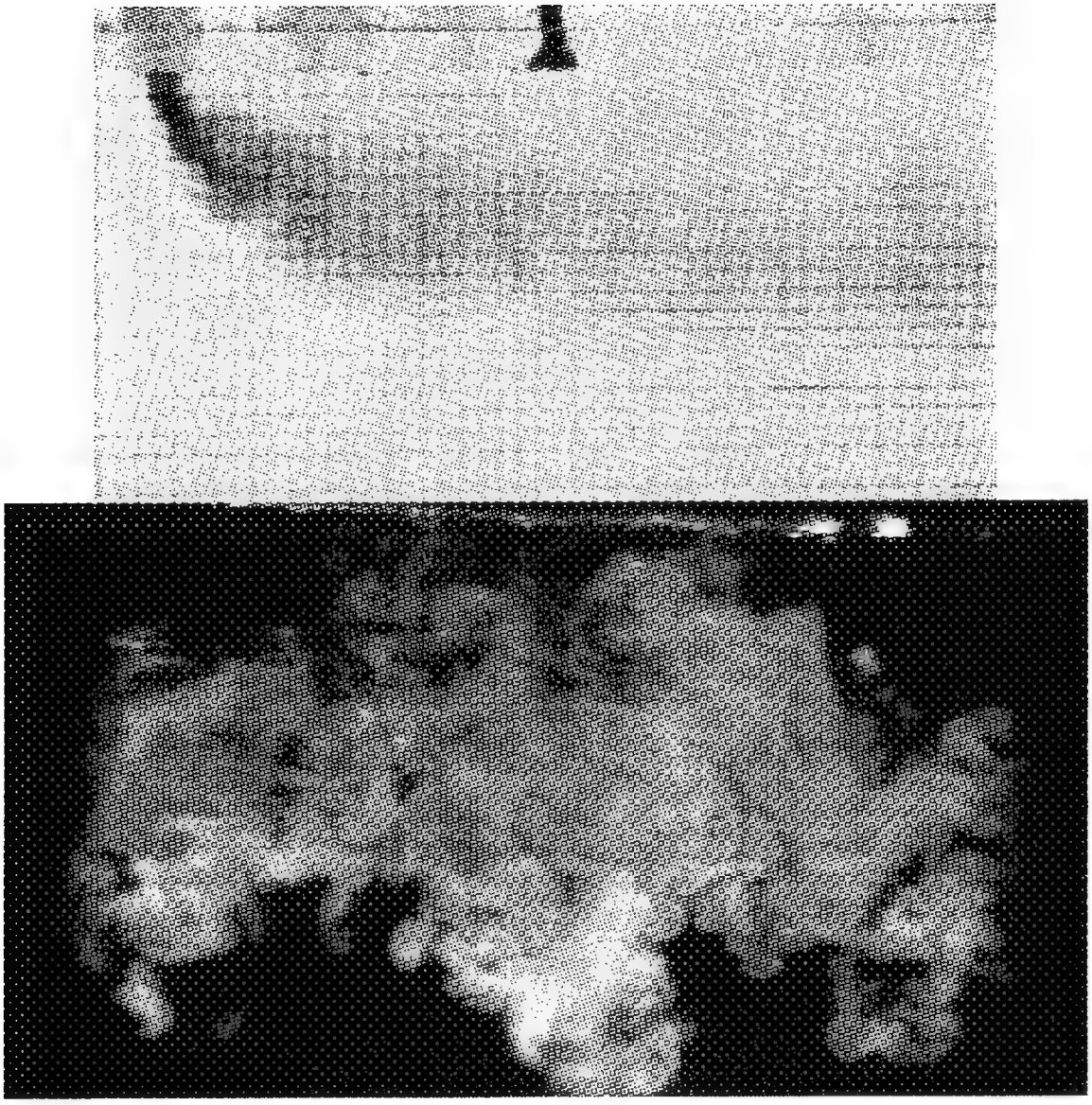

Figure A-25: Single row injection with M_L=2.5.

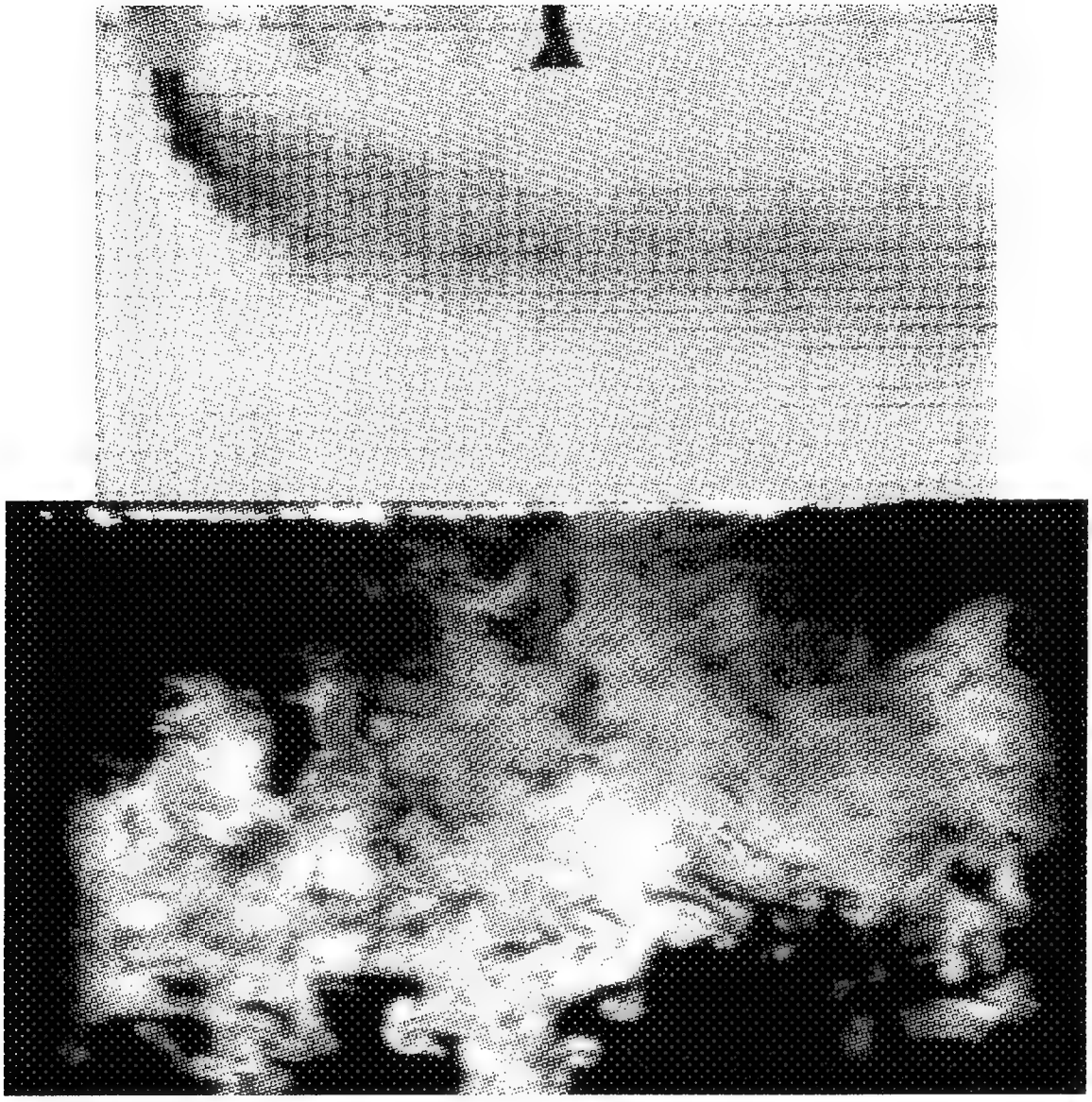

Figure A-26: Staggered row injection with M_L=2.5 and M_T=0.5.

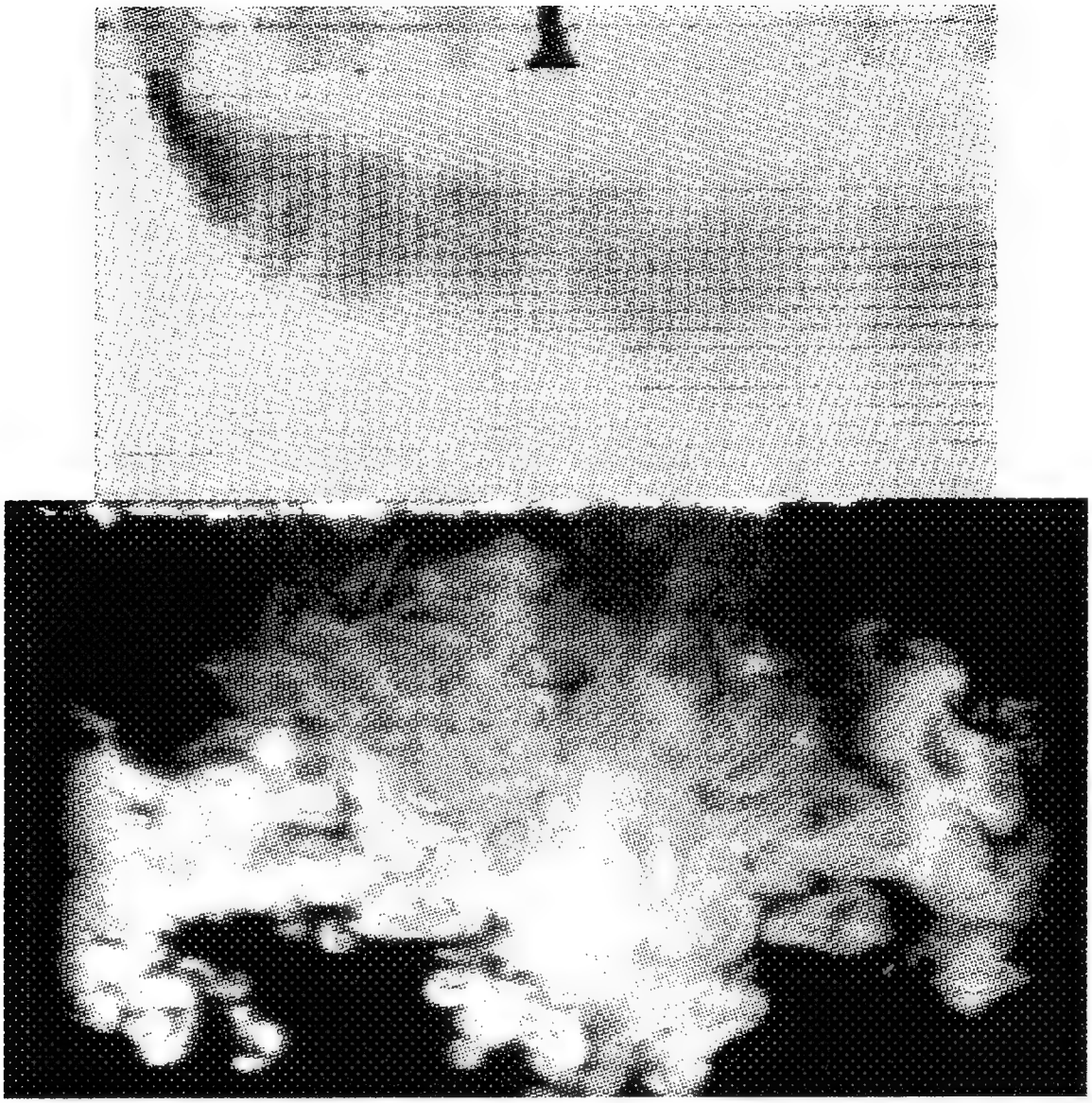

Figure A-27: Staggered row injection with M_L=2.5 and M_T=1.0.

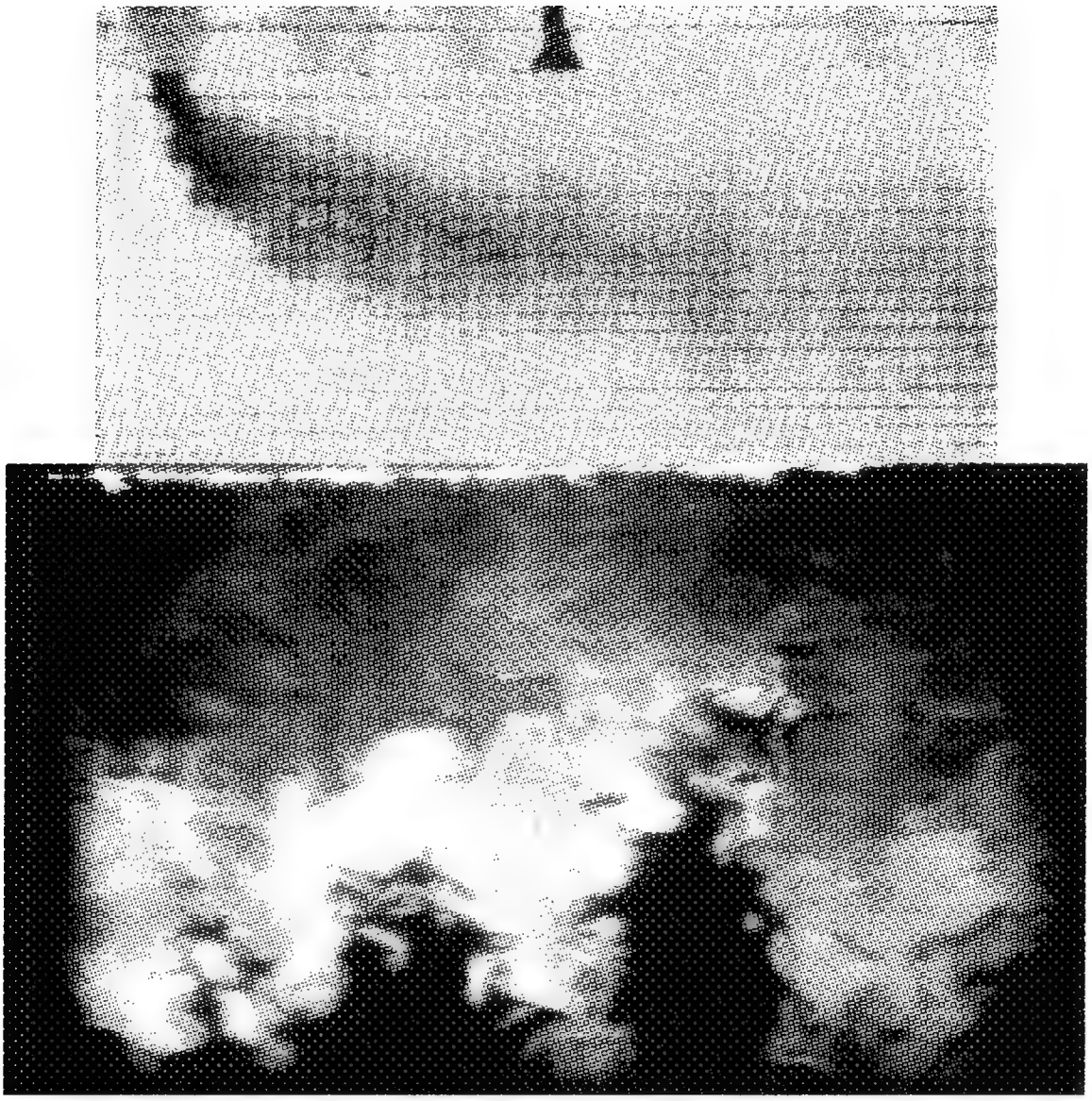

Figure A-28: Staggered row injection with M_L=2.5 and M_T=1.5.

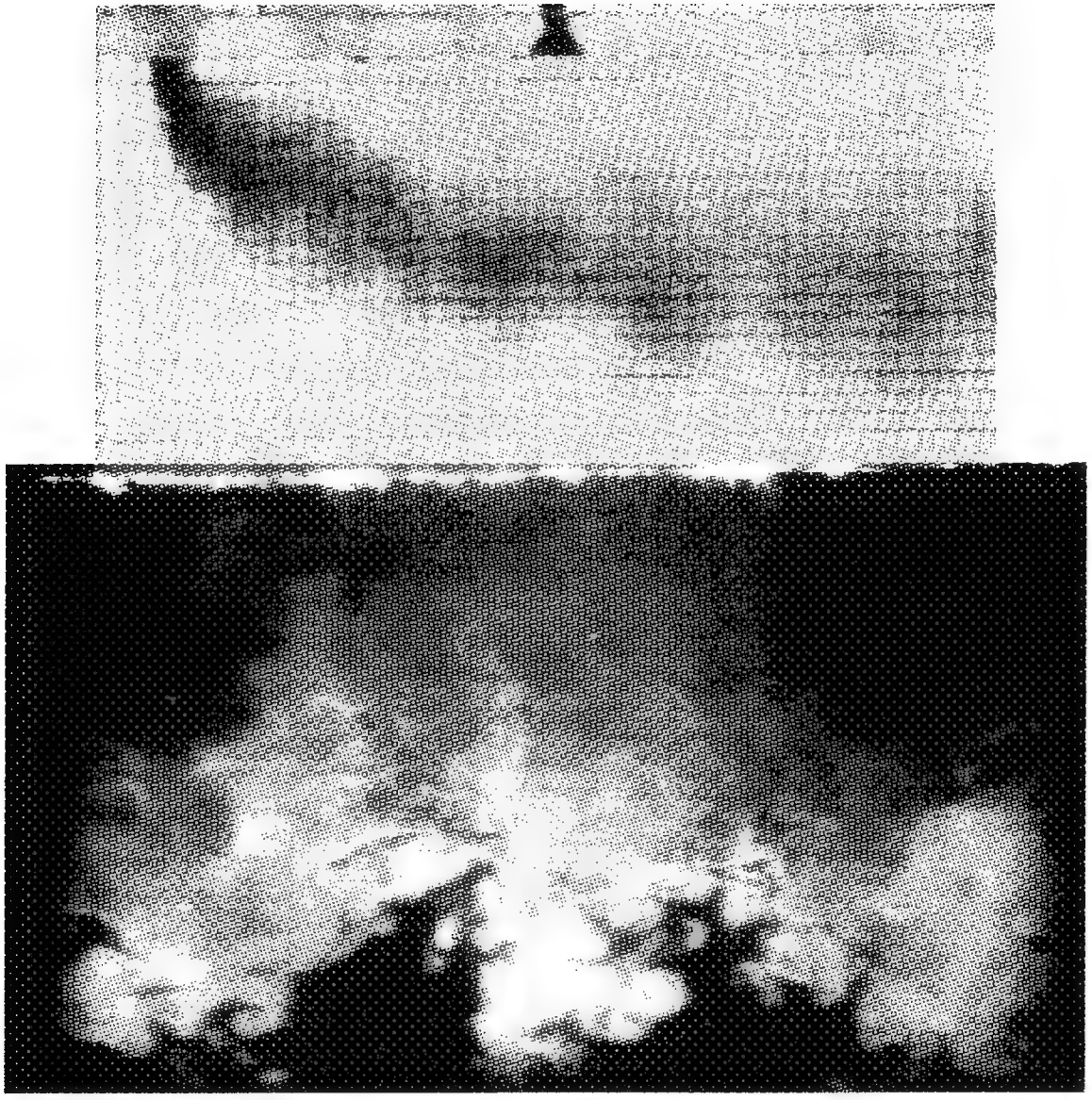

Figure A-29: Staggered row injection with M_L=2.5 and M_T=2.0.

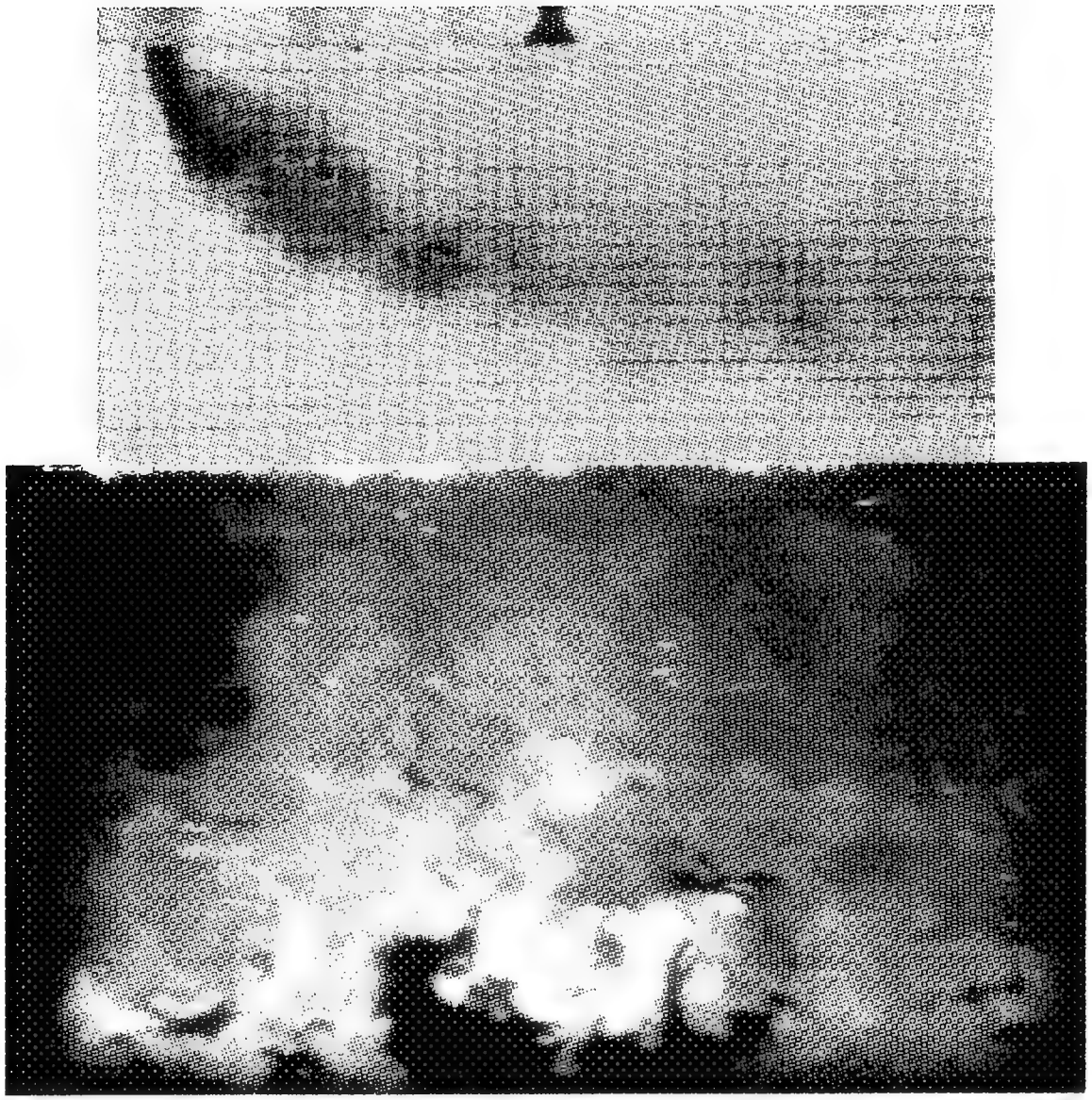

Figure A-30: Staggered row injection with M_L=2.5 and M_T=2.5.

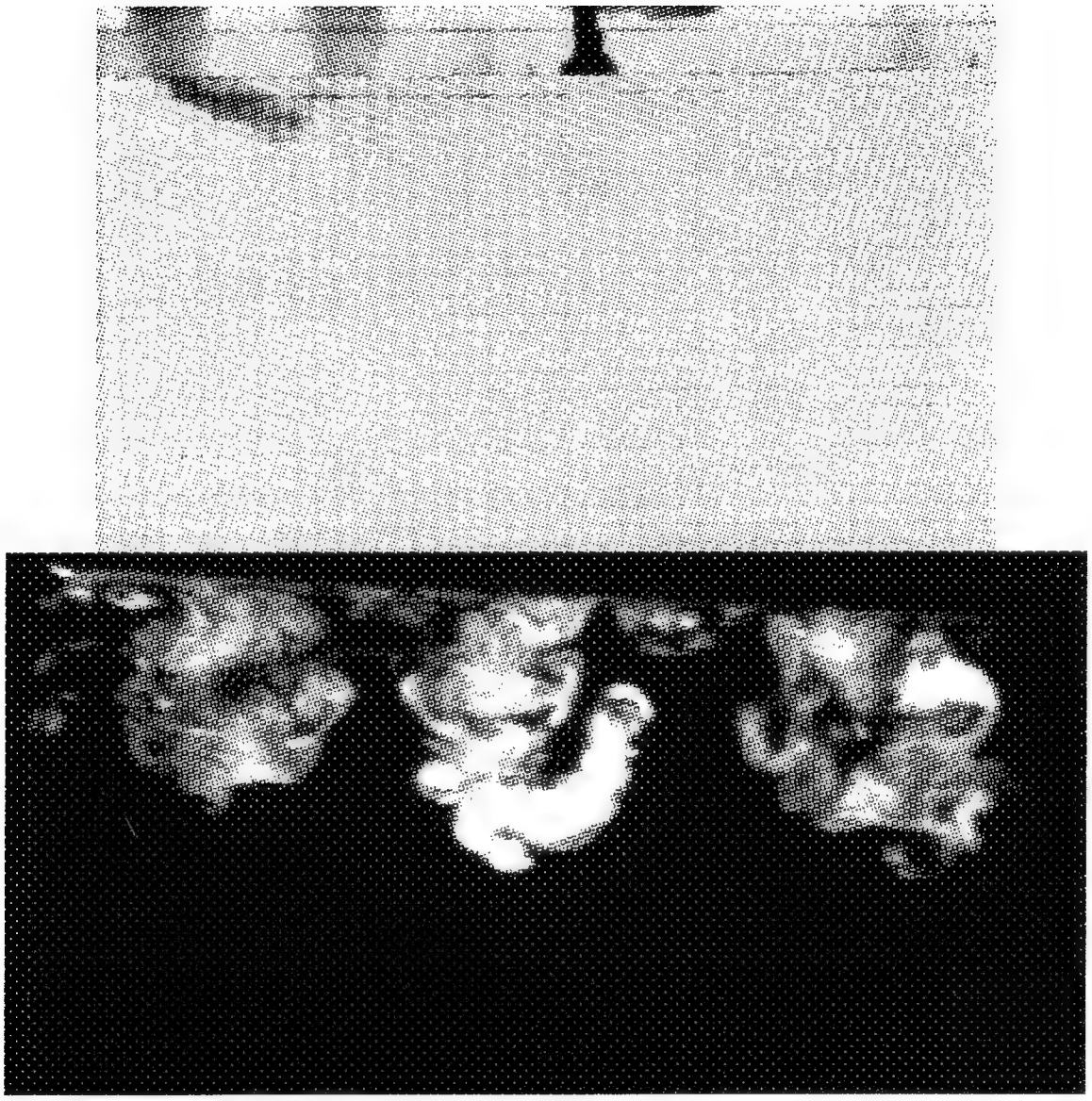

Figure A-31: In-line row injection with M_L=0.5 and M_T=0.5.

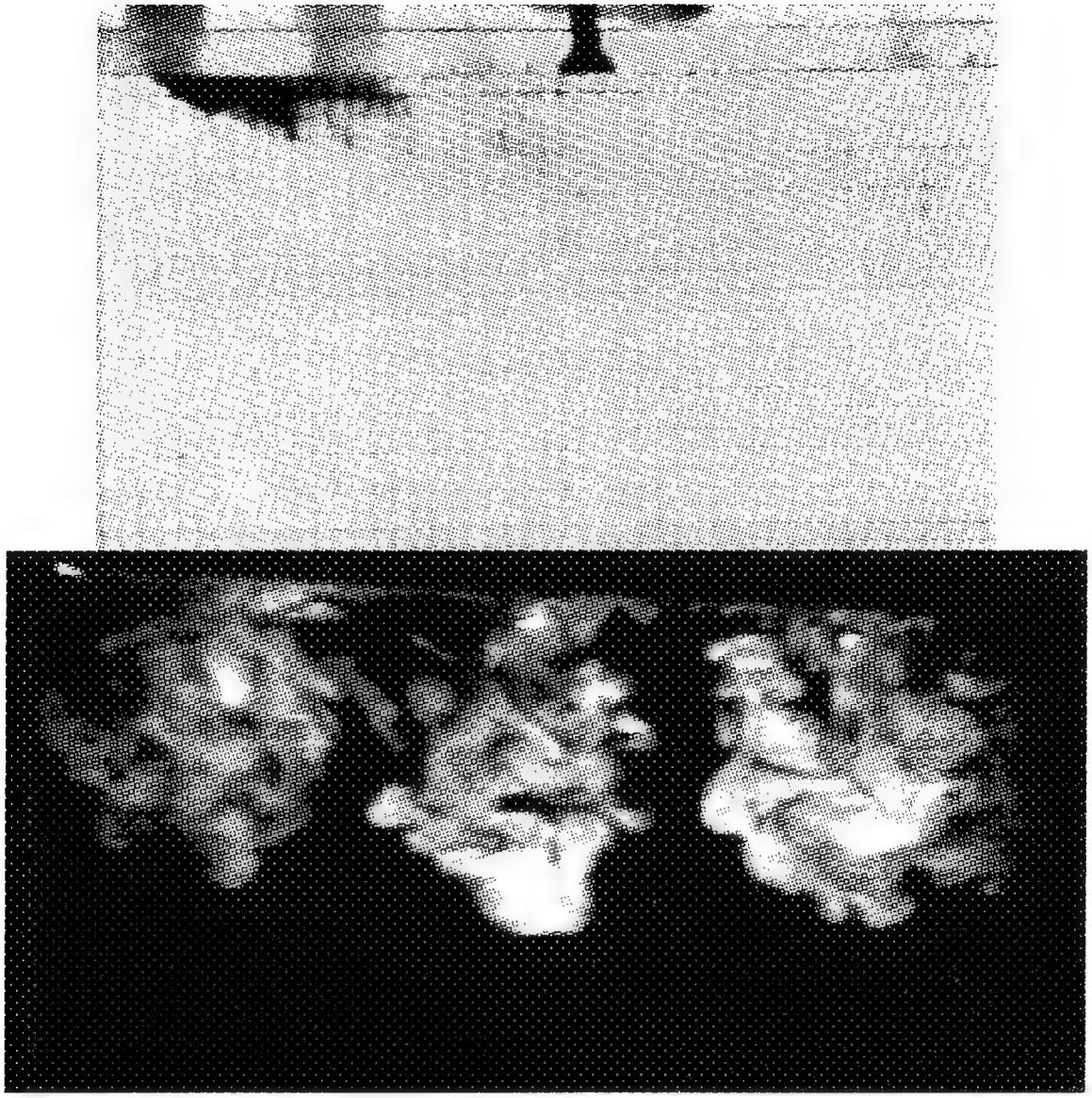

Figure A-32: In-line row injection with M_L=0.5 and M_T=1.0.

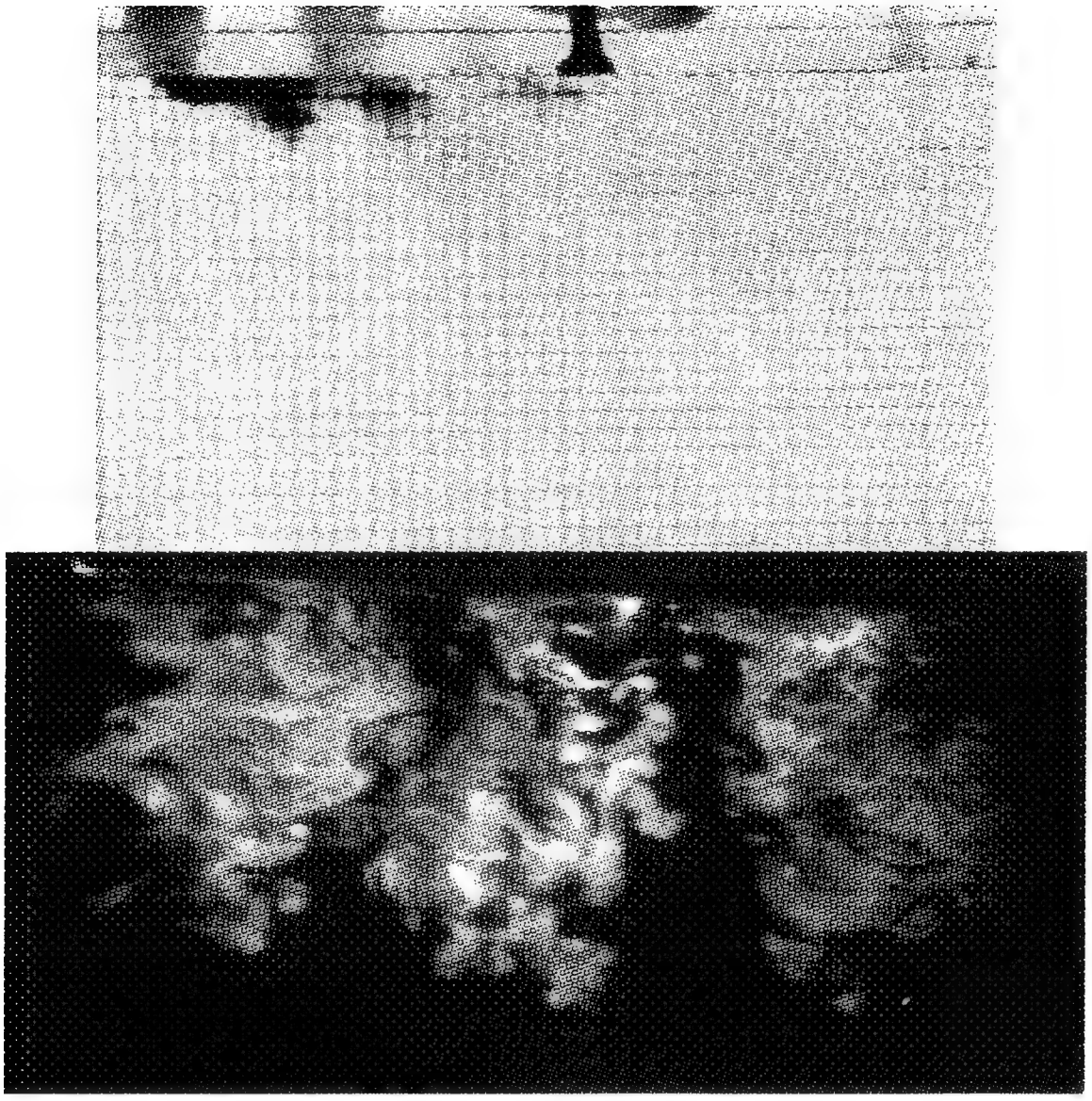

Figure A-33: In-line row injection with M_L=0.5 and M_T=1.5.

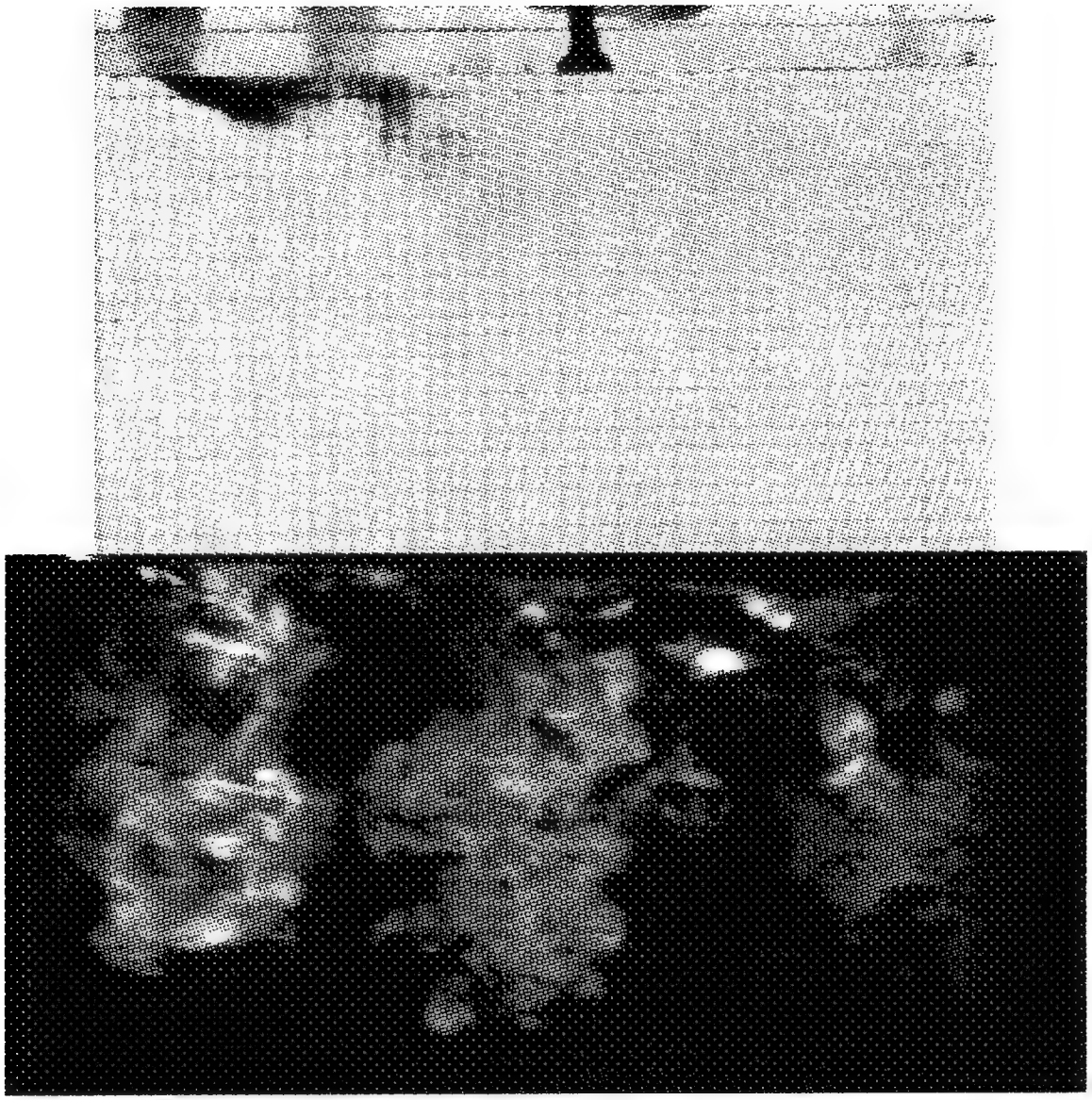

Figure A-34: In-line row injection with M_L=0.5 and M_T=2.0.

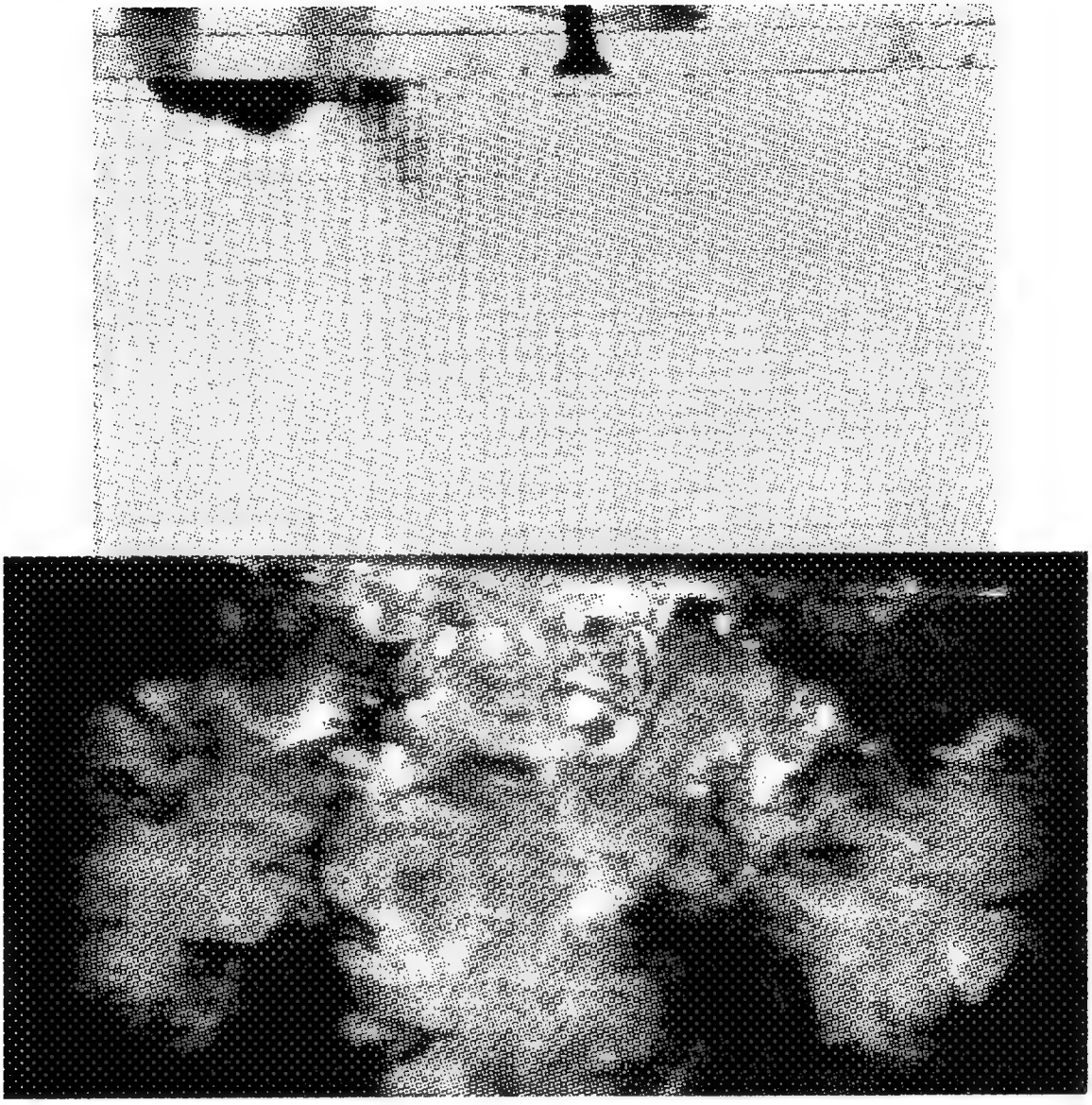

Figure A-35: In-line row injection with M_L=0.5 and M_T=2.5.

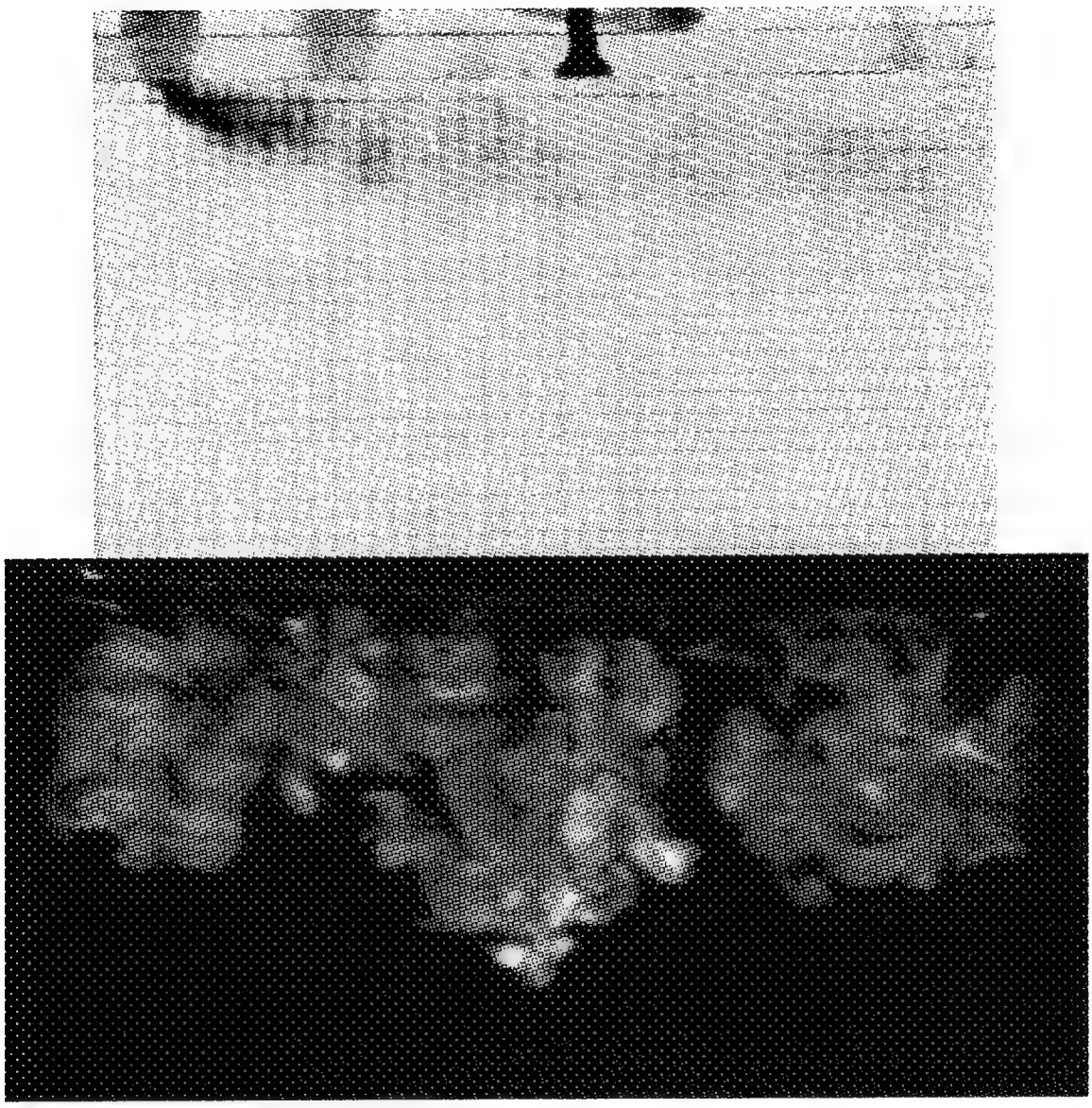

Figure A-36: In-line row injection with M_L=1.0 and M_T=0.5.

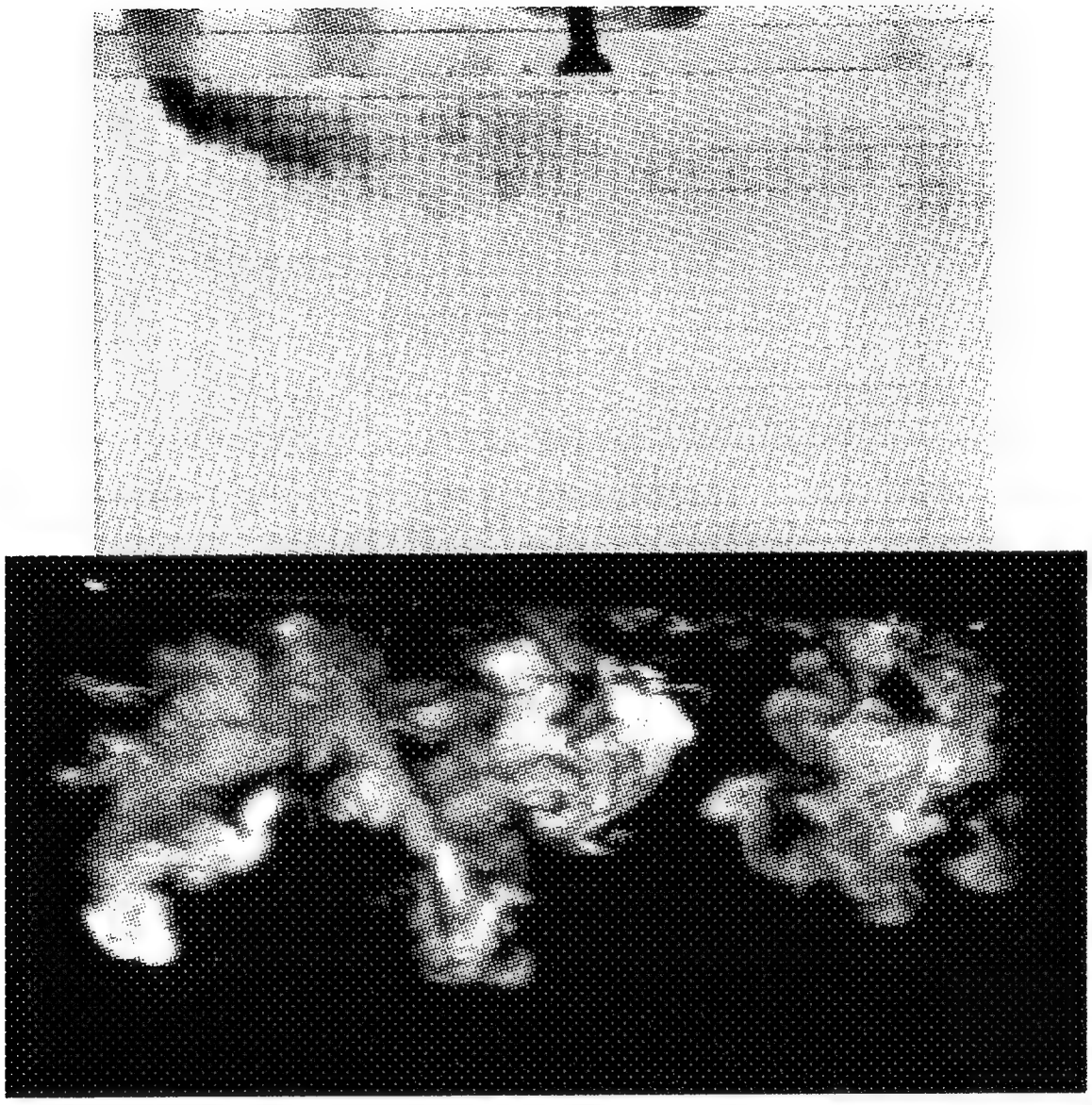

Figure A-37: In-line row injection with M_L=1.0 and M_T=1.0.

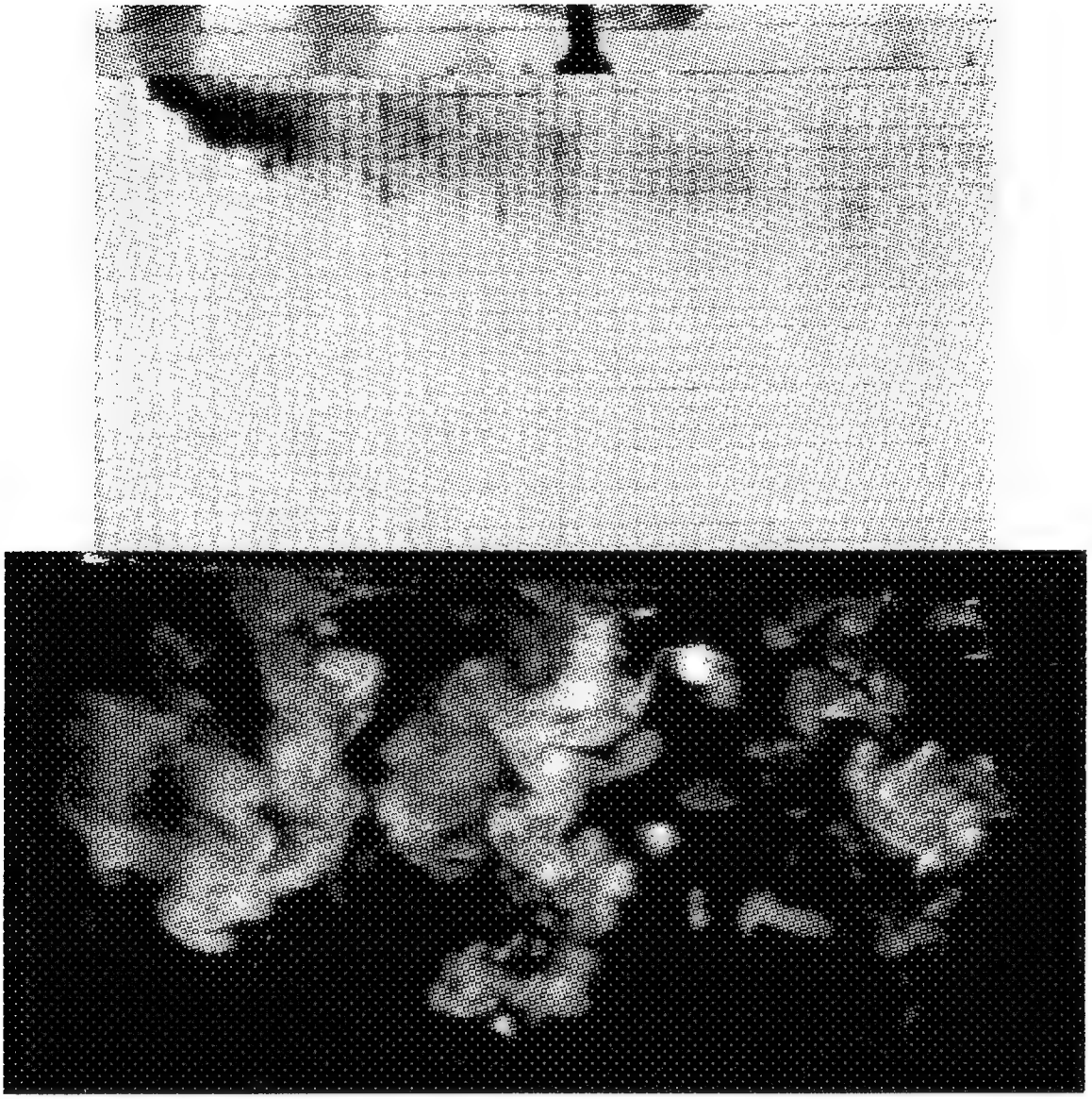

Figure A-38: In-line row injection with M_L=1.0 and M_T=1.5.

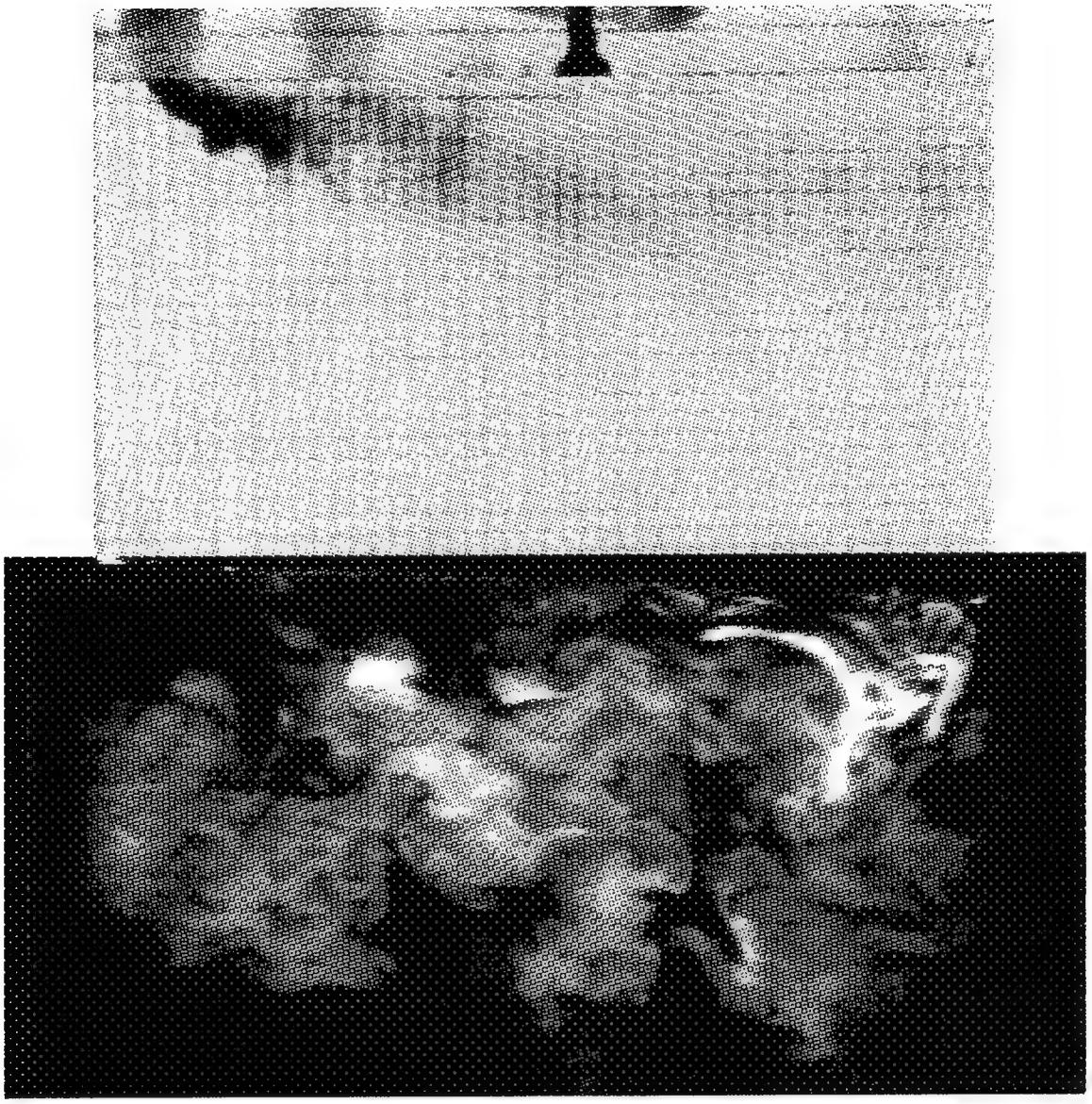

Figure A-39: In-line row injection with M_L=1.0 and M_T=2.0.

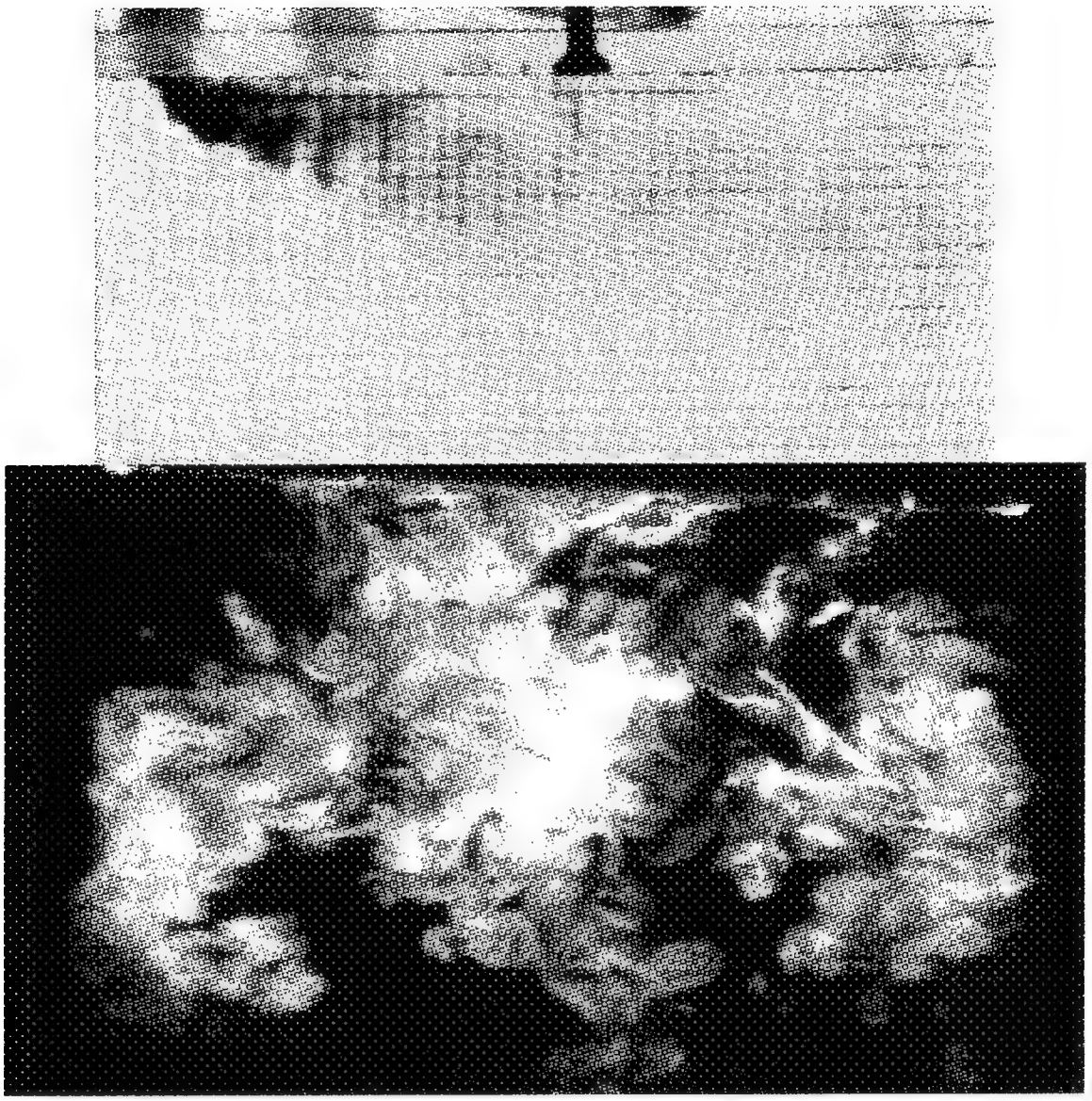

Figure A-40: In-line row injection with M_L=1.0 and M_T=2.5.

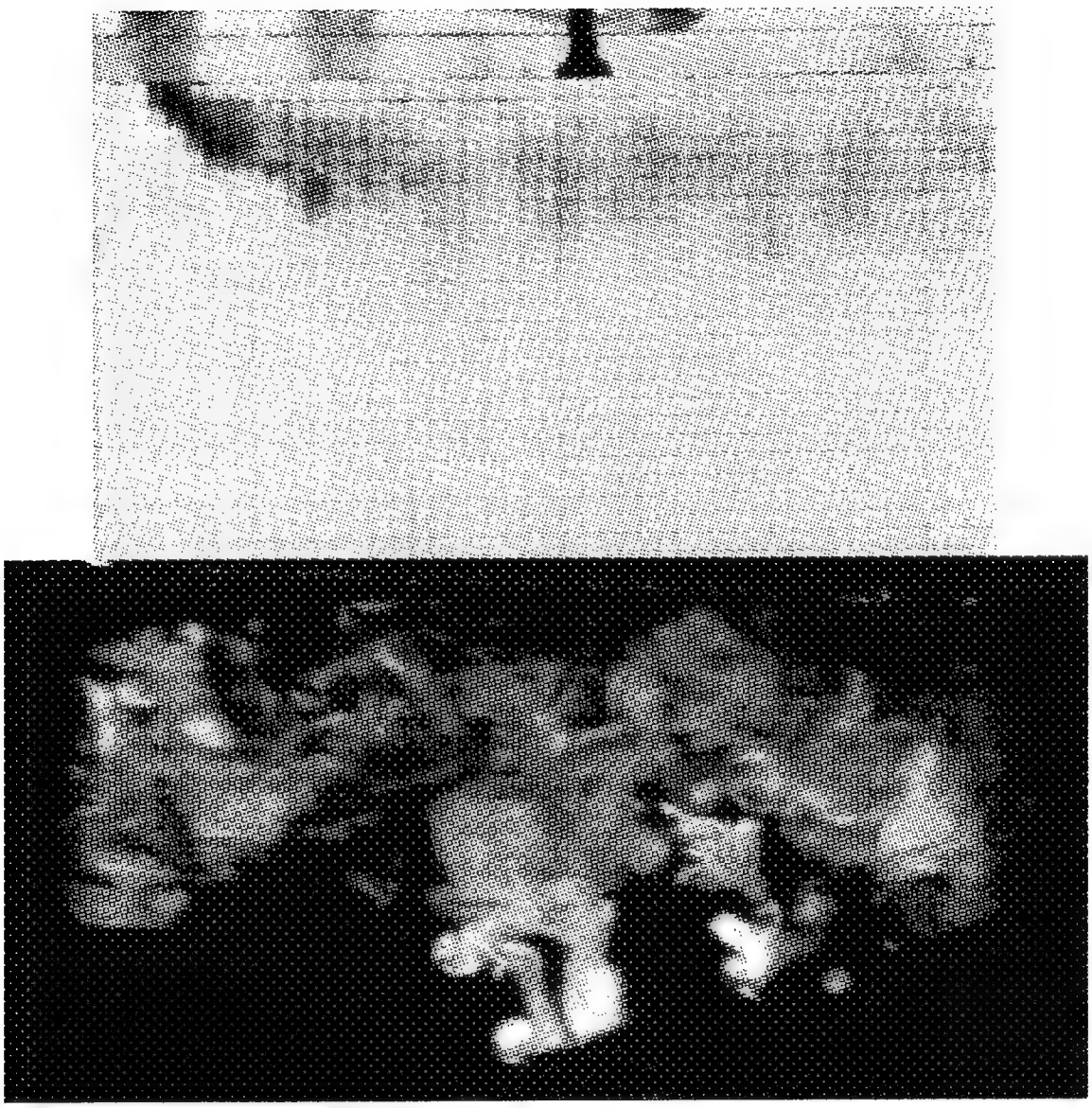

Figure A-41: In-line row injection with M_L=1.5 and M_T=0.5.

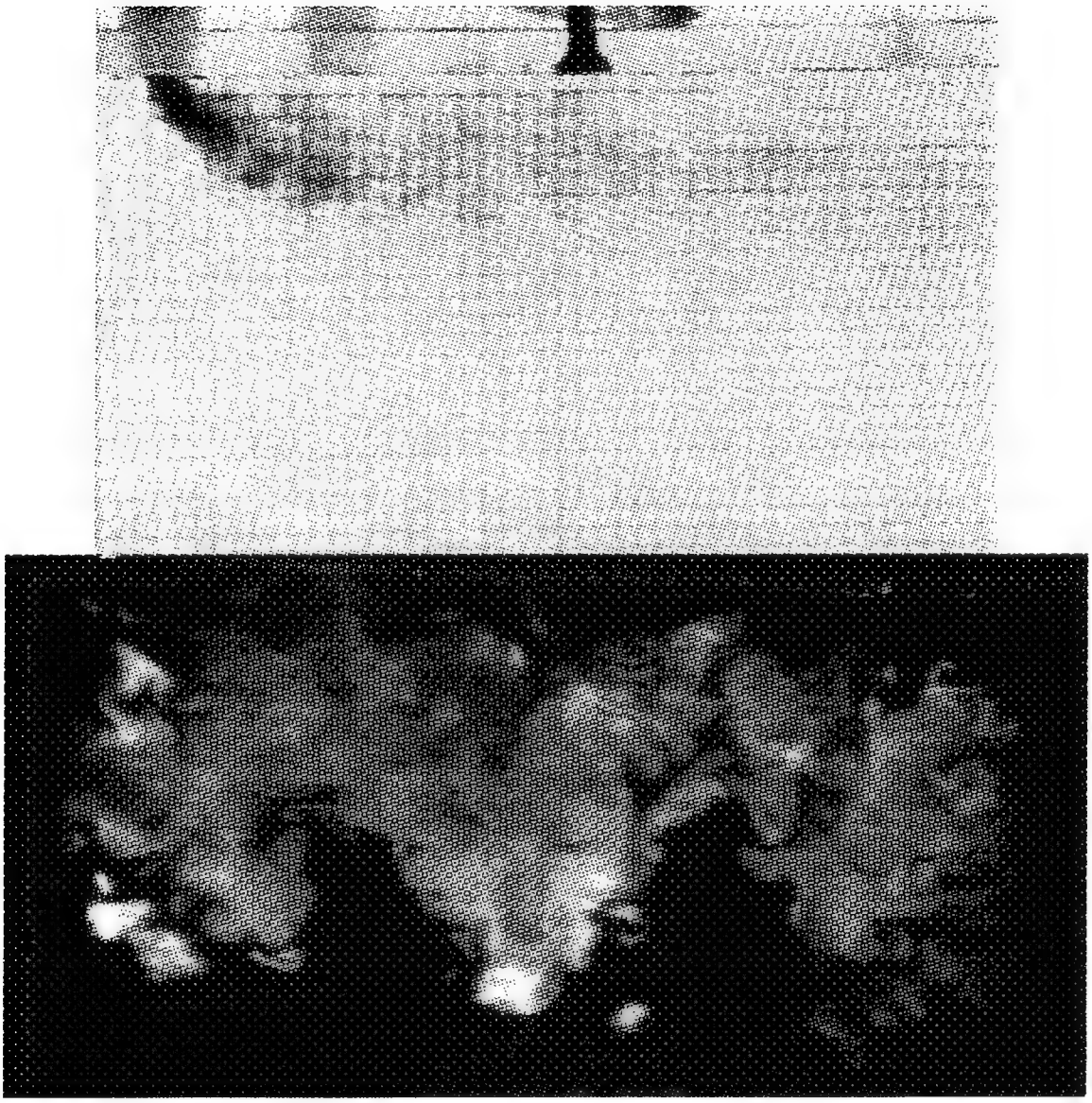

Figure A-42: In-line row injection with M_L=1.5 and M_T=1.0.

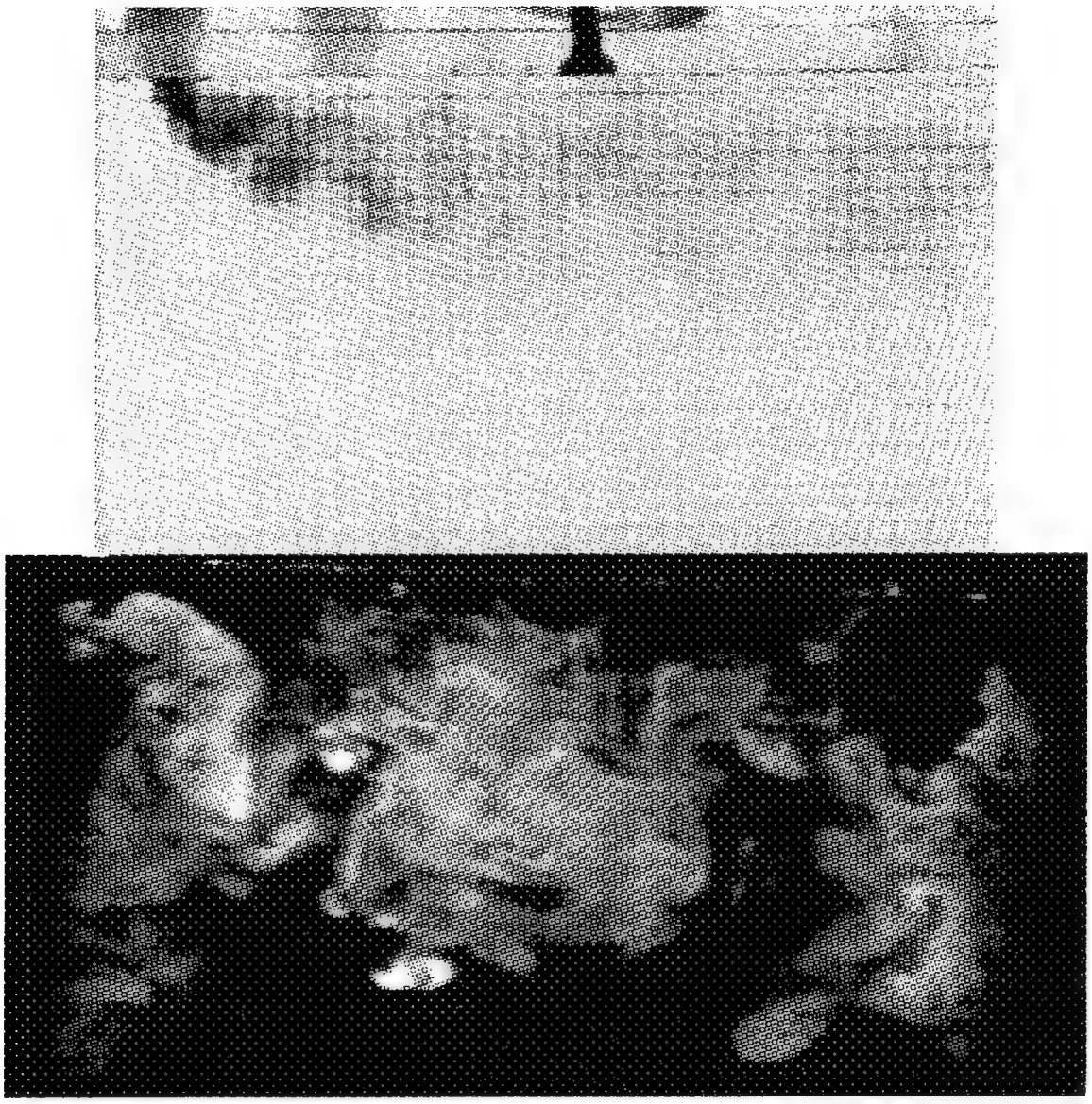

Figure A-43: In-line row injection with M_L=1.5 and M_T=1.5.

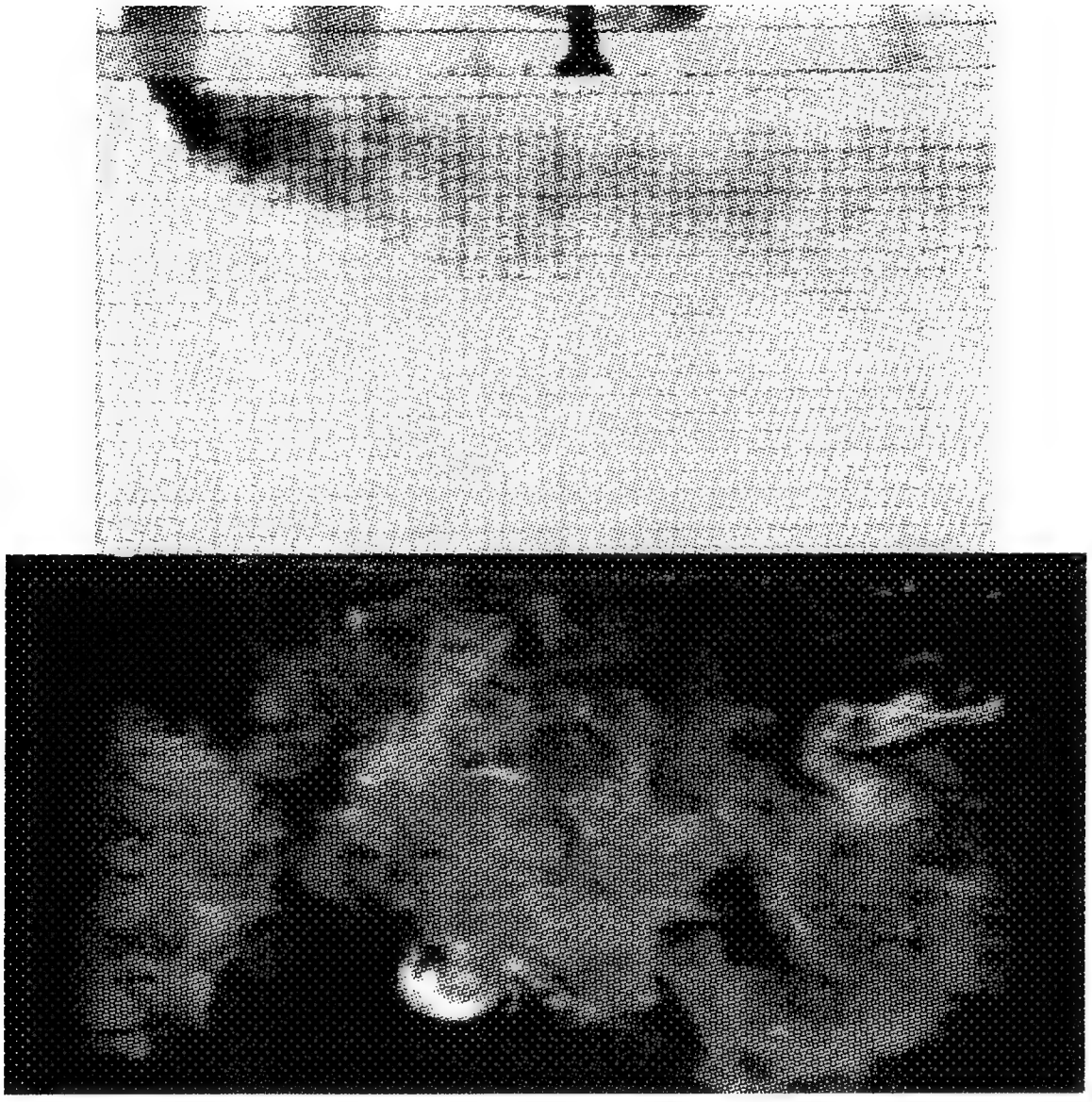

Figure A-44: In-line row injection with M_L=1.5 and M_T=2.0.

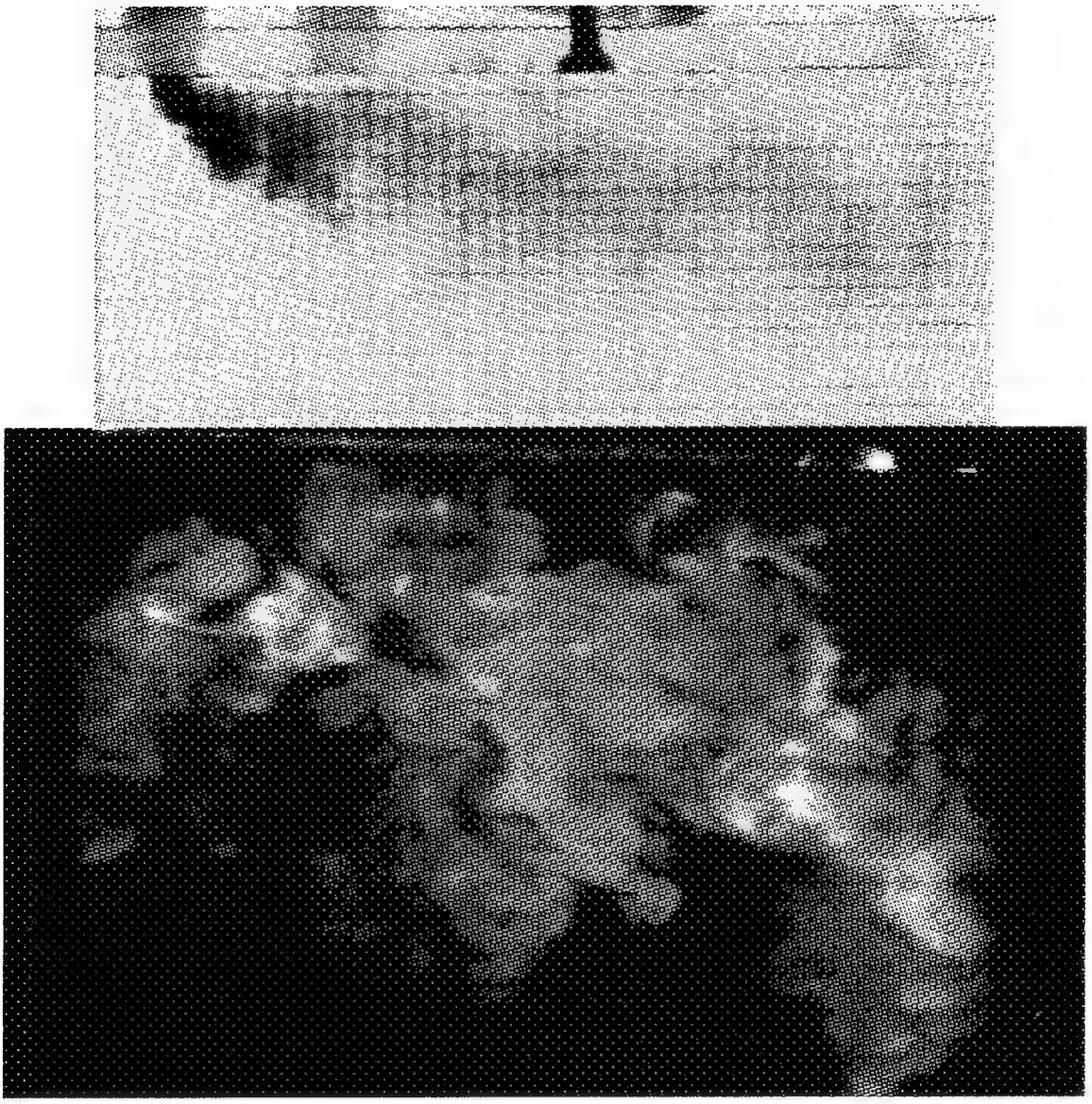

Figure A-45: In-line row injection with M_L=1.5 and M_T=2.5.

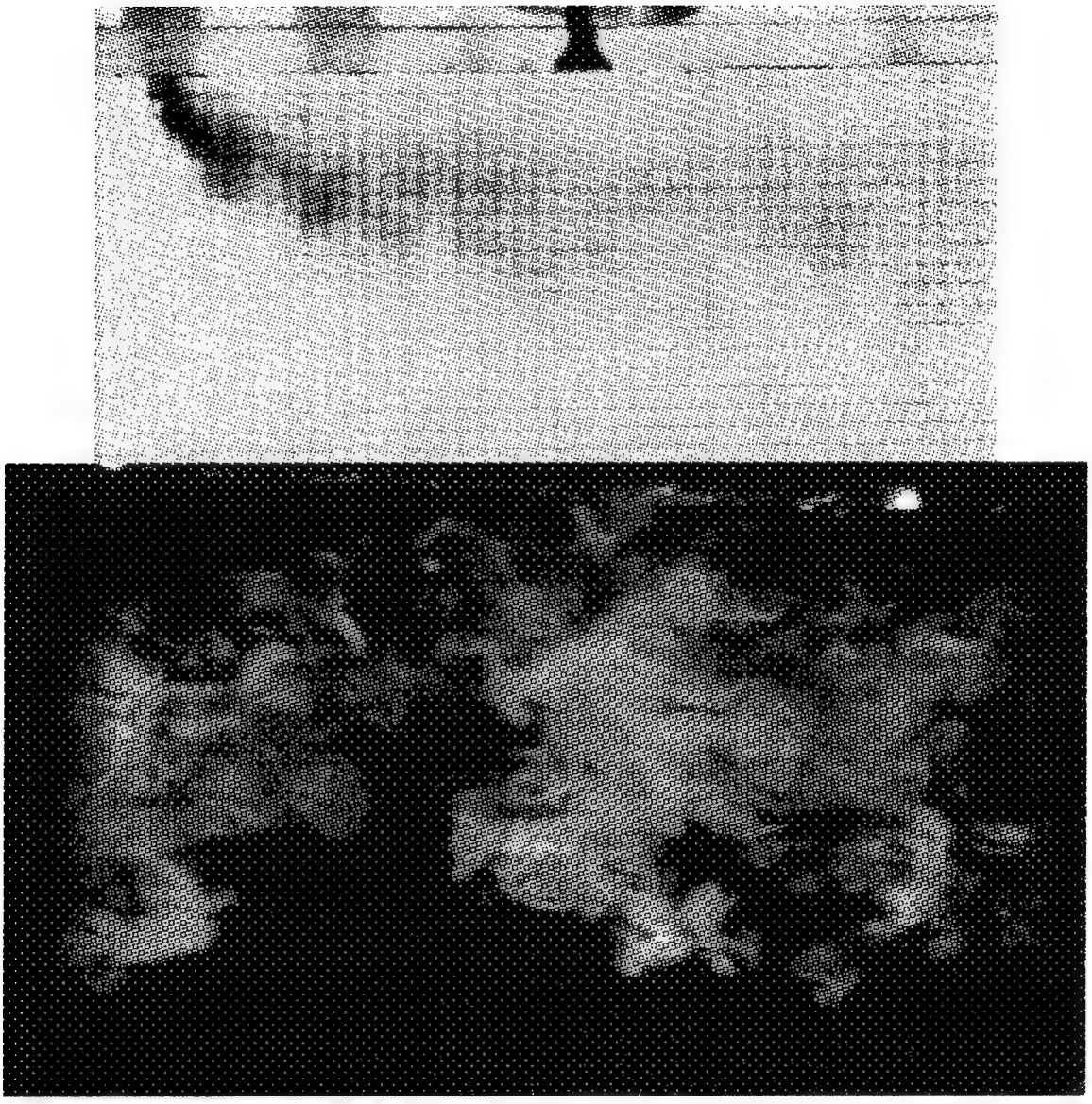

Figure A-46: In-line row injection with M_L=2.0 and M_T=0.5.

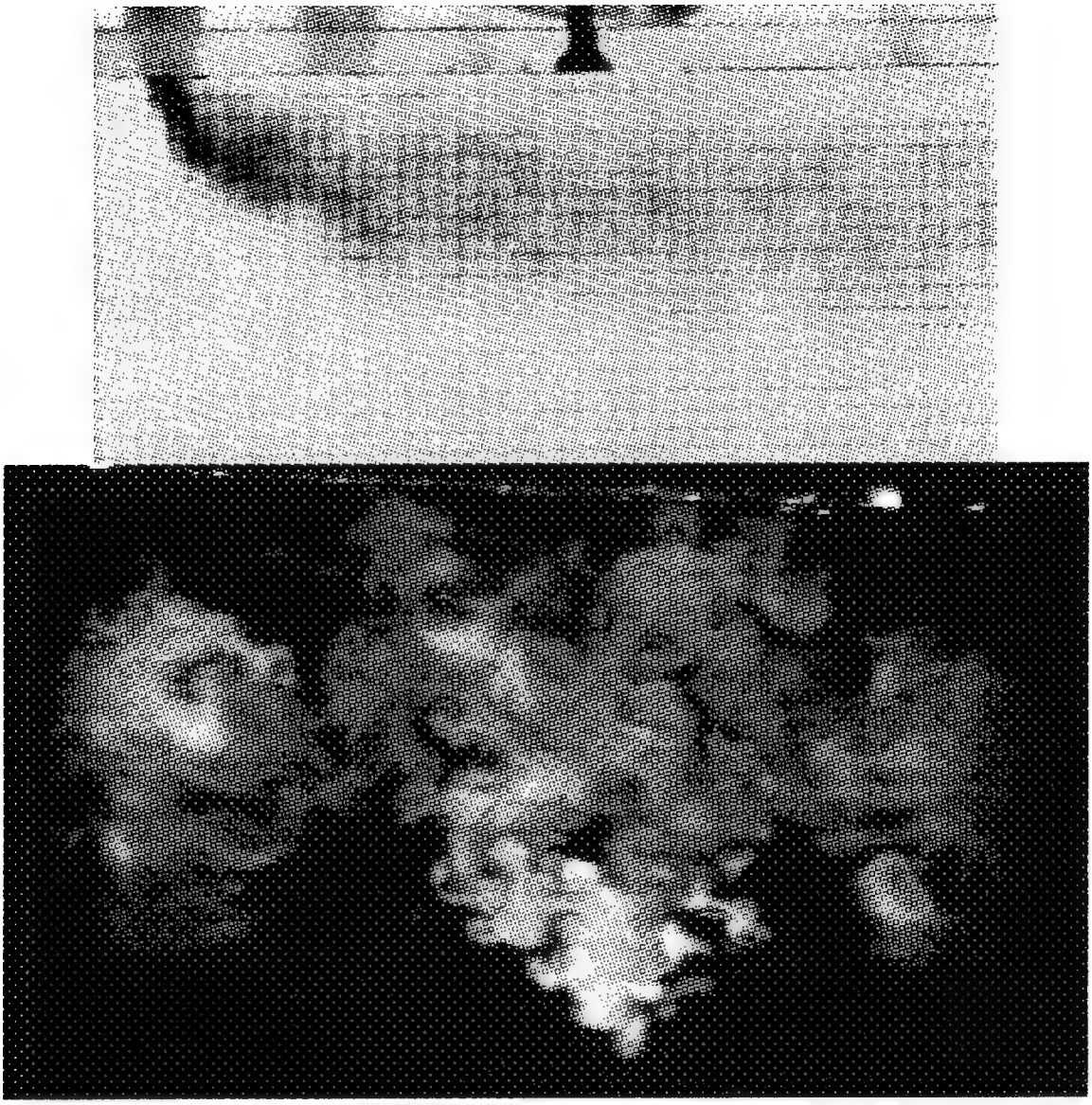

Figure A-47: In-line row injection with M_L=2.0 and M_T=1.0.

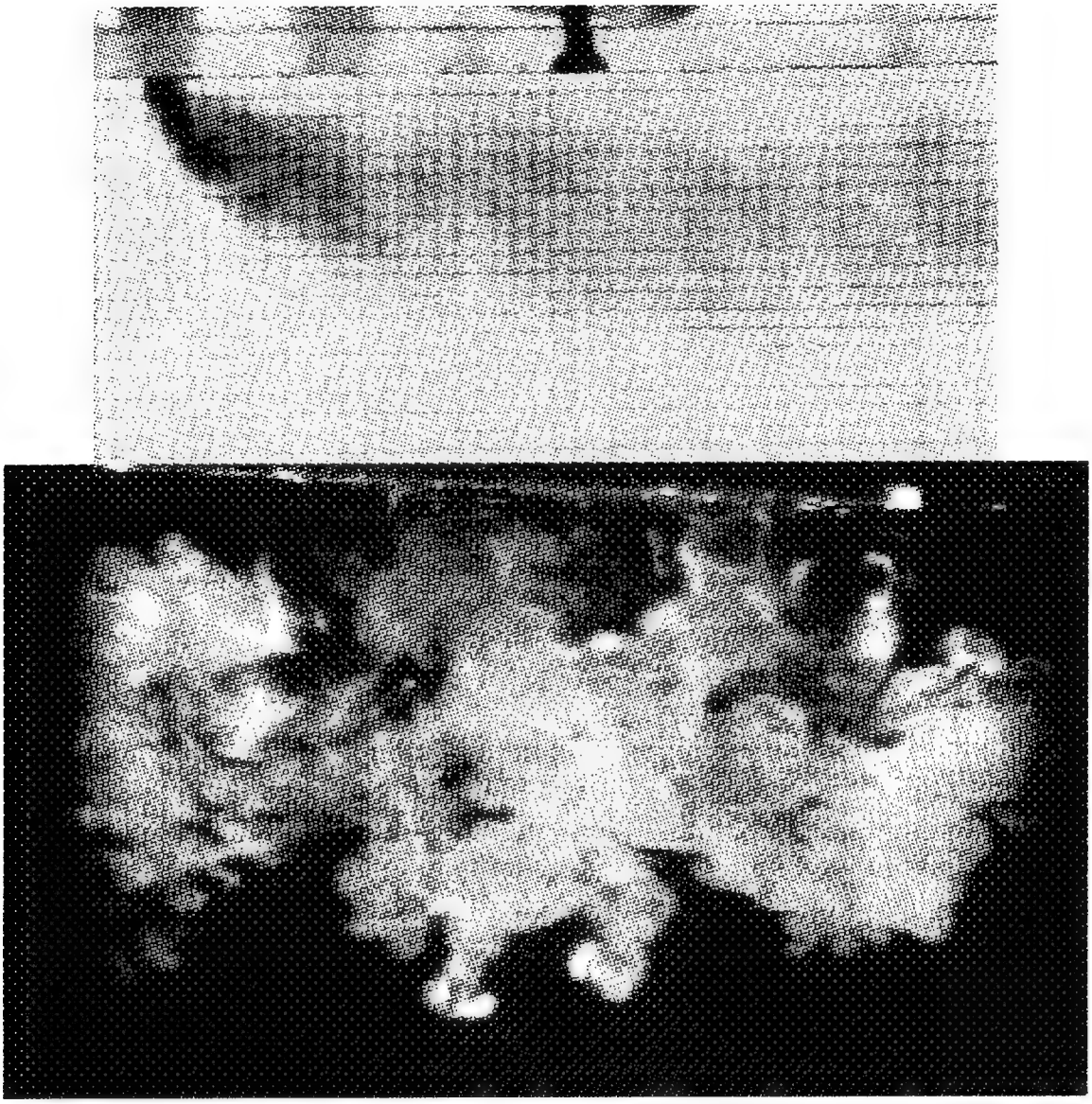

Figure A-48: In-line row injection with M_L=2.0 and M_T=1.5.

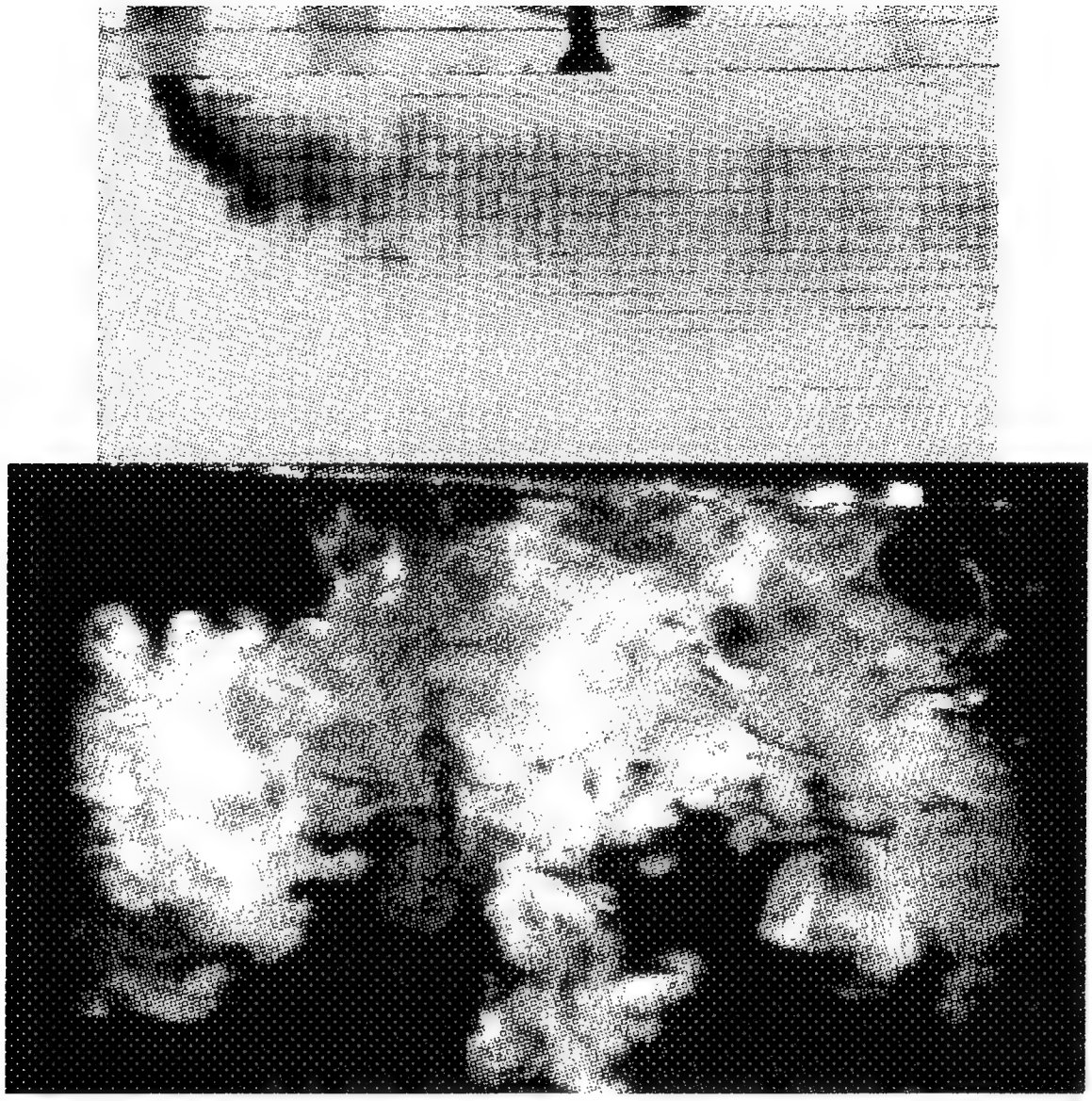

Figure A-49: In-line row injection with M_L=2.0 and M_T=2.0.

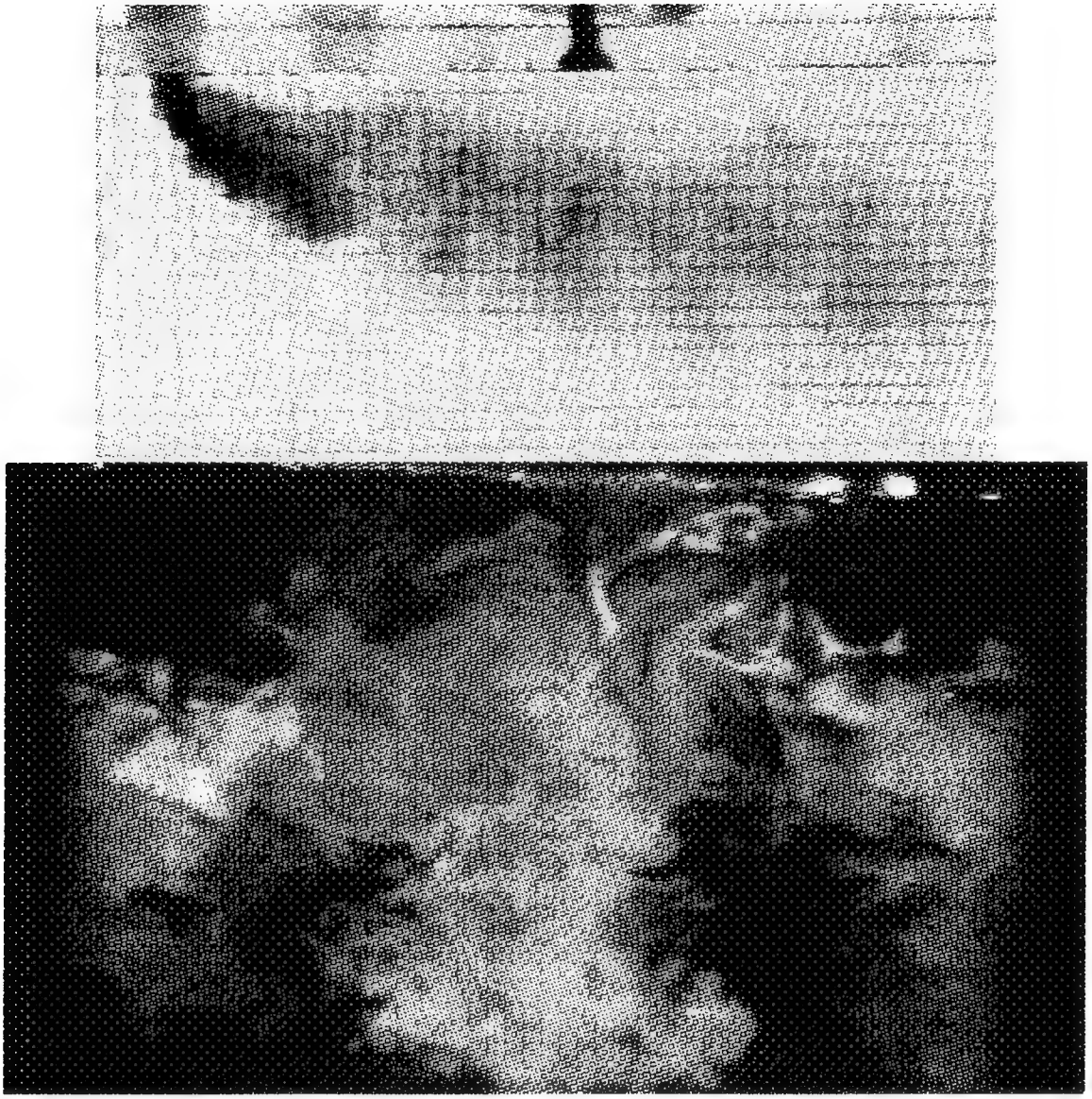

Figure A-50: In-line row injection with M_L=2.0 and M_T=2.5.

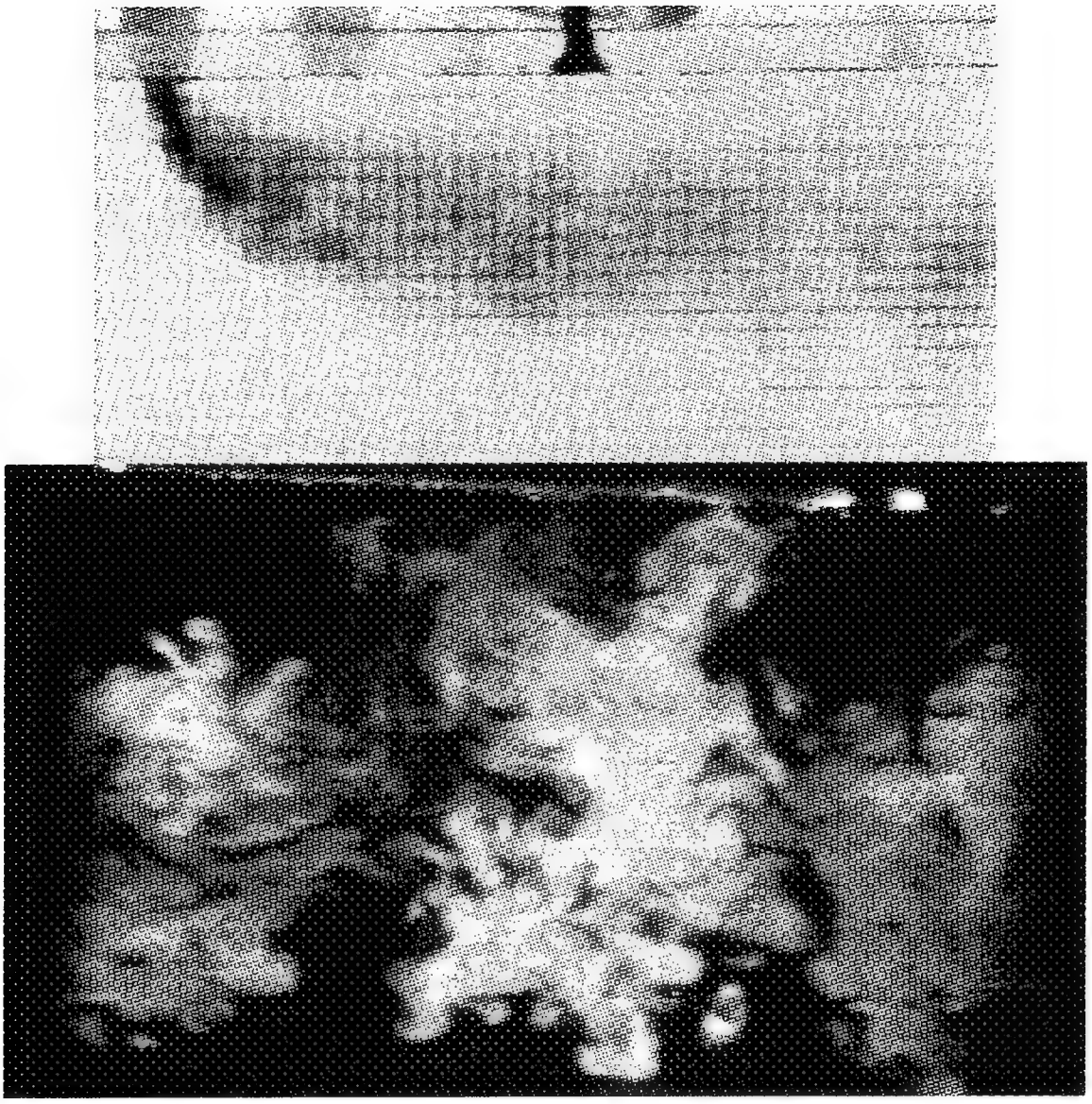

Figure A-51: In-line row injection with M_L=2.5 and M_T=0.5.

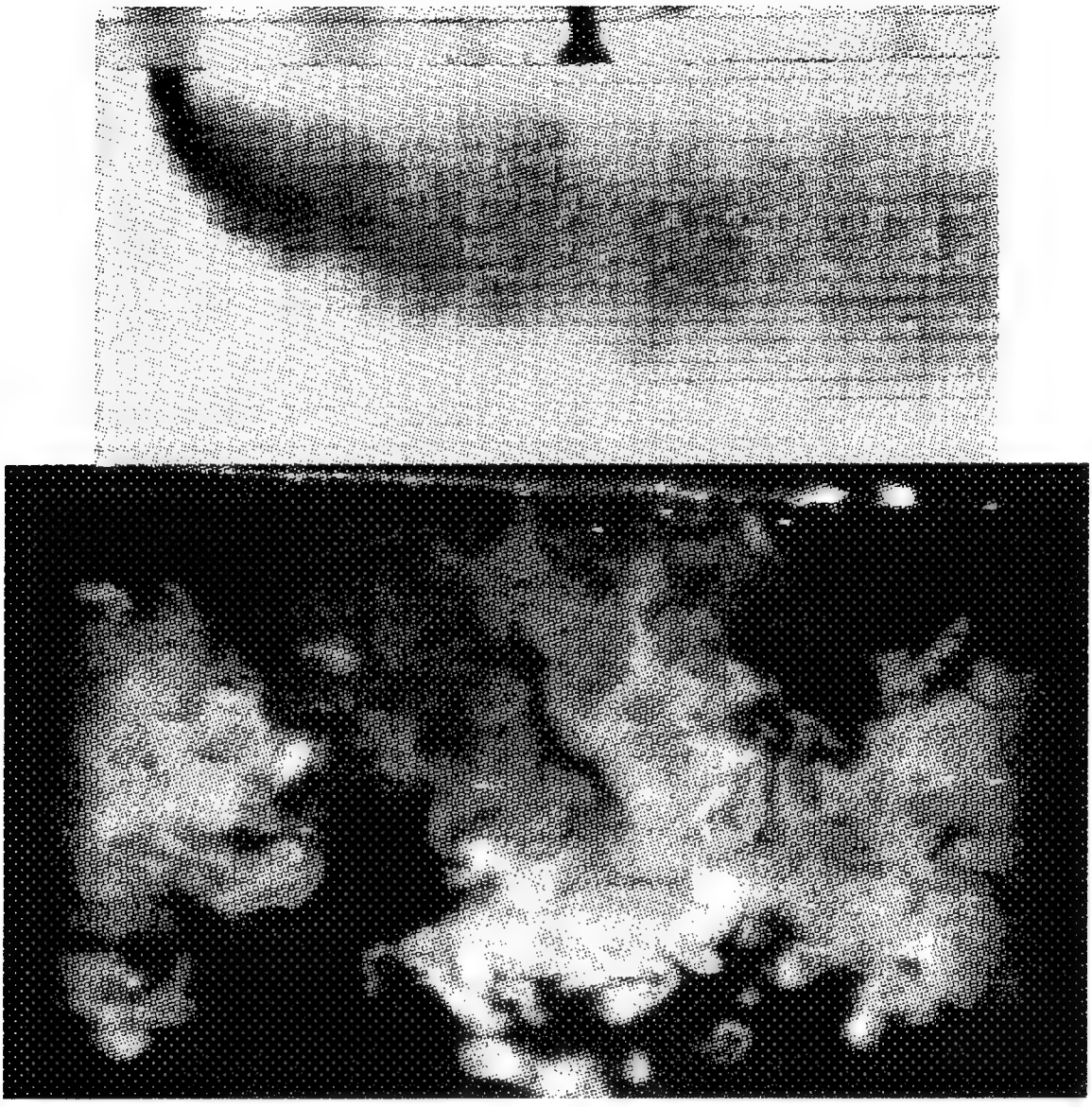

Figure A-52: In-line row injection with M_L=2.5 and M_T=1.0.

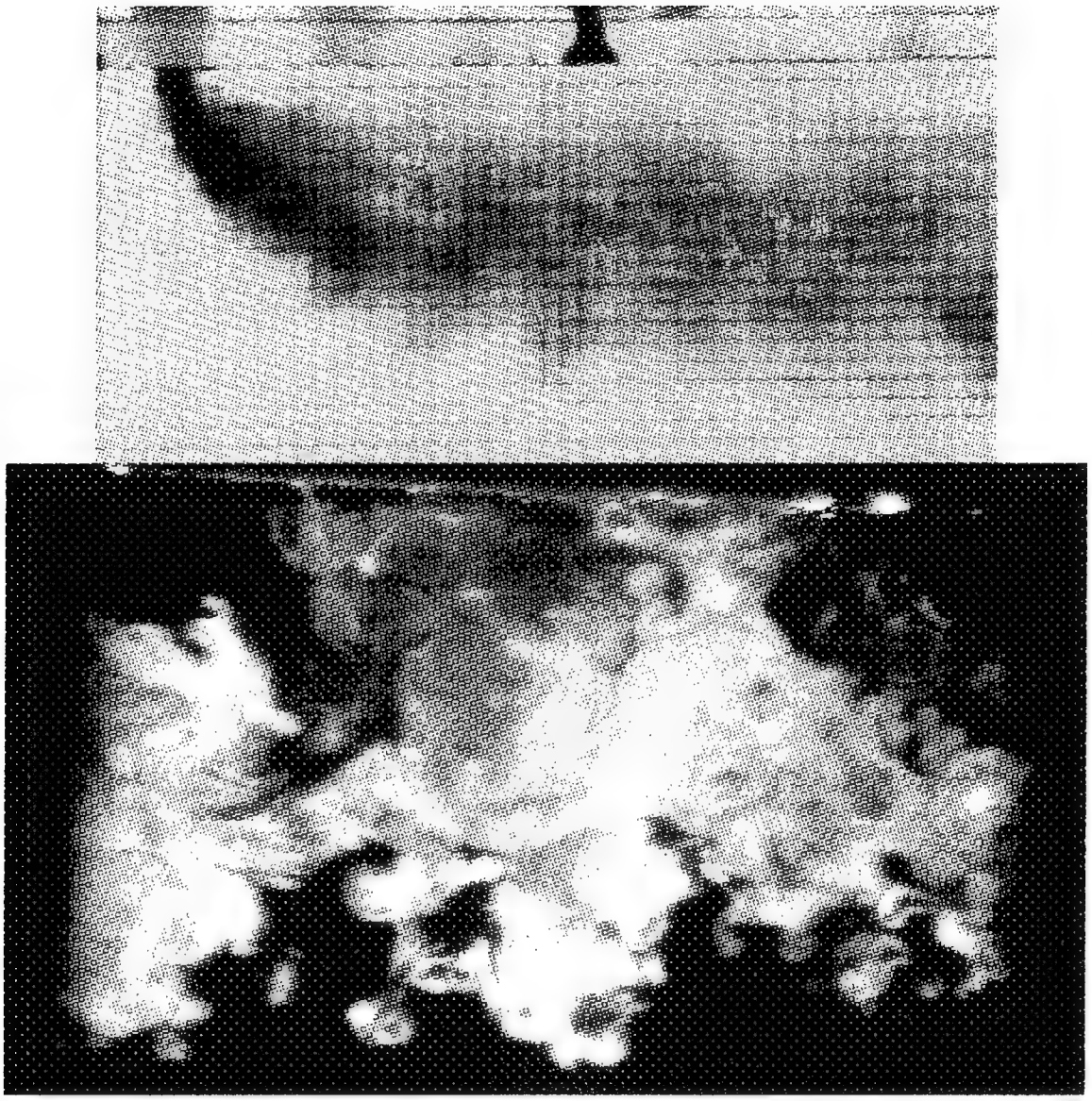

Figure A-53: In-line row injection with M_L=2.5 and M_T=1.5.

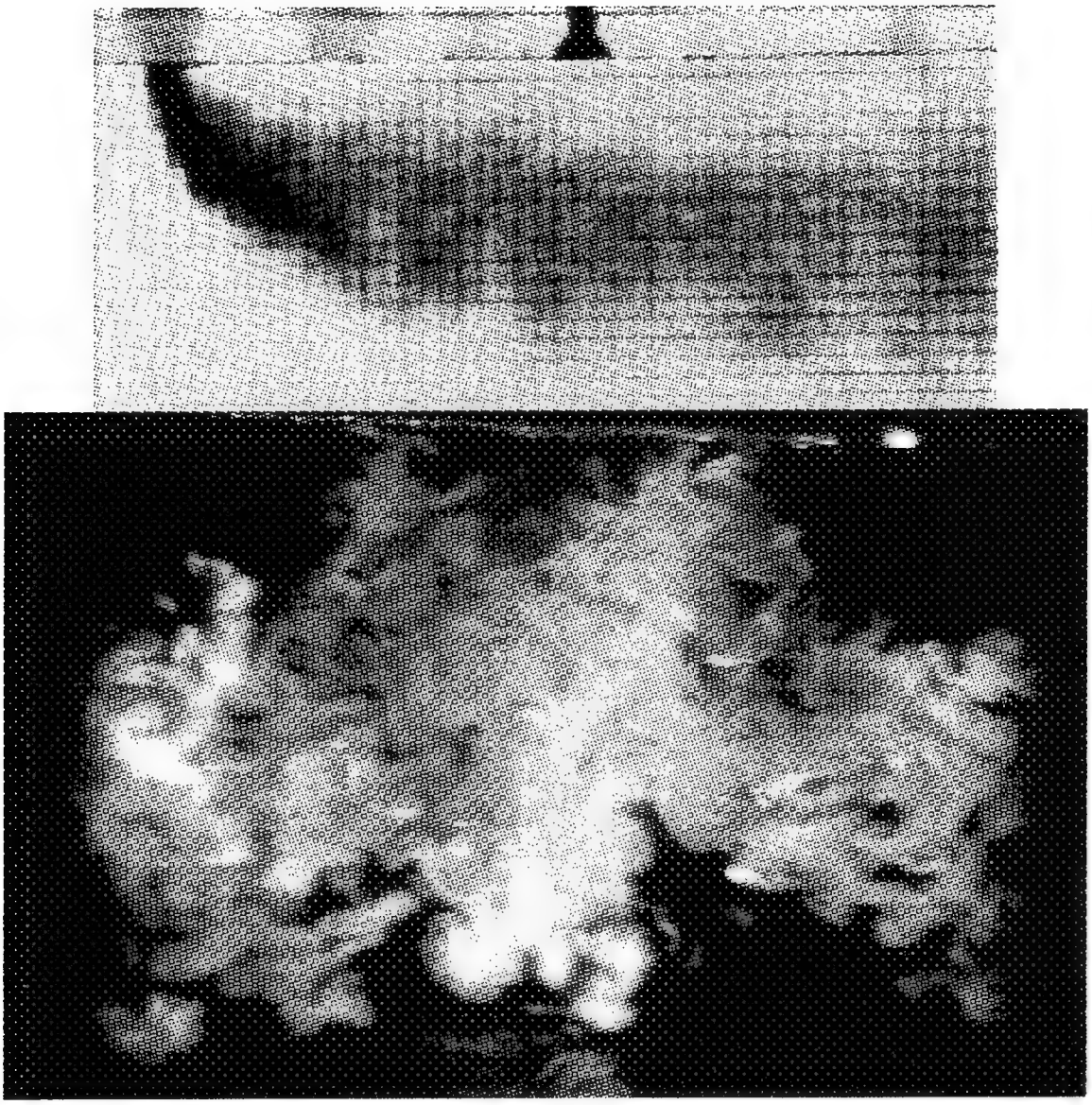

Figure A-54: In-line row injection with M_L=2.5 and M_T=2.0.

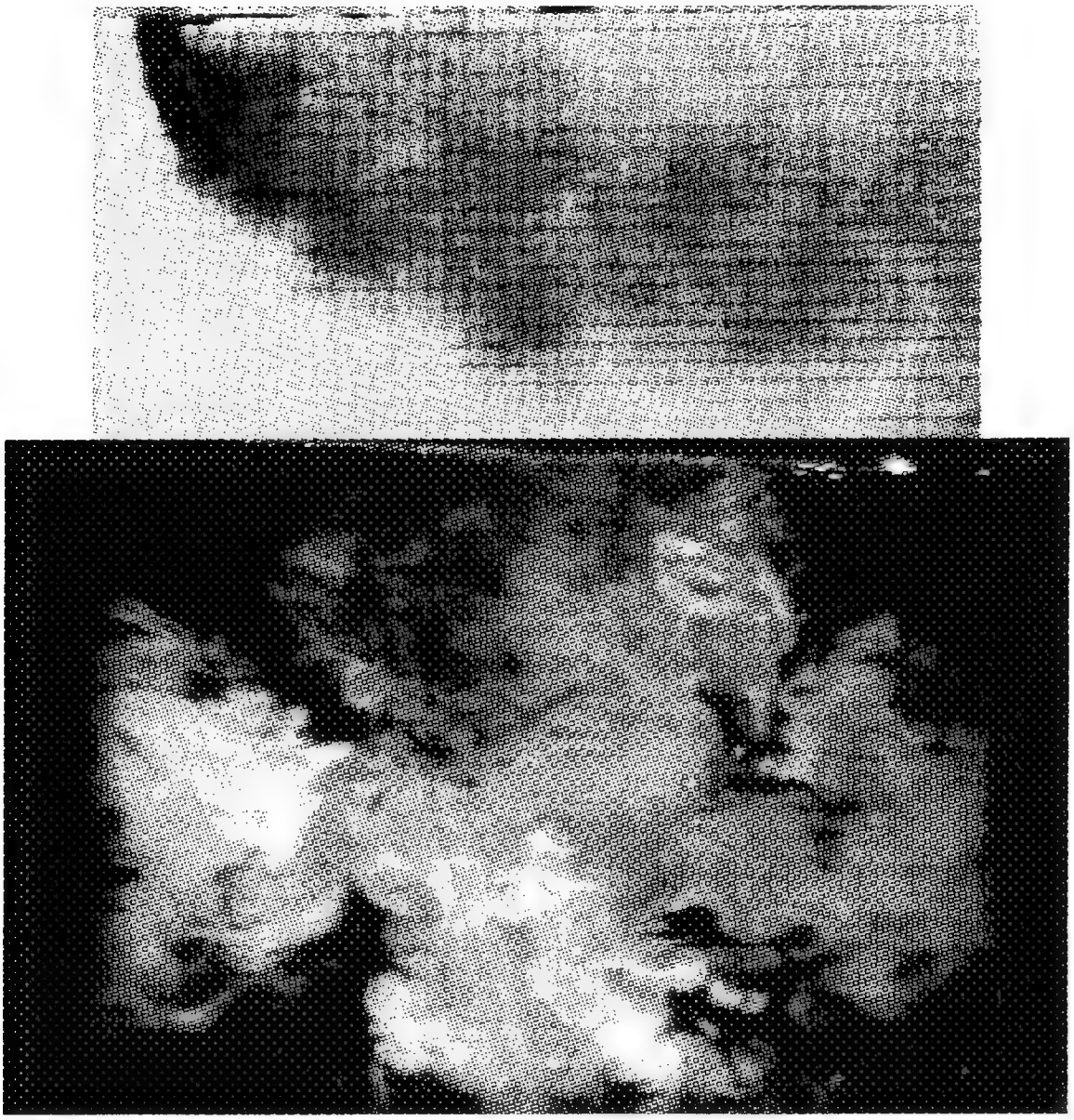

Figure A-55: In-line row injection with M_L=2.5 and M_T=2.5.

University of Washington

Abstract

Flow Visualization of Vorticity Cancellation of Jets in Crossflow

by Anthony G. Simpson

Chairperson of Supervisory Committee: Professor Mitsuru Kurosaka
Dept. of Aeronautics and Astronautics

An experimental apparatus was designed and constructed for water tunnel flow visualization of multiple, staggered and in-line row jet injection in crossflow. Specifically, a physical explanation was sought for existing film cooling performance results from turbine test rigs. Experiments were conducted in the University of Washington low-speed, free surface water tunnel facility having a 3.0x0.7x0.7 meter test section and a speed capability of up to 0.7 m/s. Jet injection was controlled for each row independently at blowing ratios from 0.5 to 2.5, with the jet development length to diameter ratio set at 6.0. Flow visualization using both colored dye and fluorescent laser sheeting was accomplished to track vortex structure and interaction in the flow. The results indicate that vorticity cancellation is a factor in improved cooling performance over single row injection through a reduction in both jet lift off from the surface and entrainment of the main flow toward the surface.

List of References

Eroglu, Adnan. "An Experimental Investigation of Entrainment and Mixing in Pulsed and Exponential Transverse Jets." diss. University of Washington, 1991.

Fric, T.F. "Structure in the Near Field of the Transverse Jet." diss. California Institute of Technology, 1990.

Haven, Brenda A. and M. Kurosaka. "Contoured 'Shaped' Holes: Improving Cooling Effectiveness & Aero Performance" White Paper Briefing to the A.F.O.S.R., 1994.

Kerrebrock, Jack L. *Aircraft Engines and Gas Turbines.* 2nd ed. Cambridge: MIT Press, 1992.

Kurosaka, M. "Contoured Holes for Film Cooling: the Effect of Kidney Shaped Vortices." Proposal for the A.F.O.S.R., 1994.

Norton, R.J.G. et.al. *Turbine Cooling System Design: Volume I - Technical Report.* Washington: GPO, 1990.

United States. *Integrated High Performance Turbine Engine Technology Initiative.* Ed. William Koop. N.p: n.p., [c. 1990].

University of Washington

Abstract

Flow Visualization of Vorticity Cancellation of Jets in Crossflow

by Anthony G. Simpson

Chairperson of Supervisory Committee: Professor Mitsuru Kurosaka
Dept. of Aeronautics and Astronautics

An experimental apparatus was designed and constructed for water tunnel flow visualization of multiple, staggered and in-line row jet injection in crossflow. Specifically, a physical explanation was sought for existing film cooling performance results from turbine test rigs. Experiments were conducted in the University of Washington low-speed, free surface water tunnel facility having a 3.0x0.7x0.7 meter test section and a speed capability of up to 0.7 m/s. Jet injection was controlled for each row independently at blowing ratios from 0.5 to 2.5, with the jet development length to diameter ratio set at 6.0. Flow visualization using both colored dye and fluorescent laser sheeting was accomplished to track vortex structure and interaction in the flow. The results indicate that vorticity cancellation is a factor in improved cooling performance over single row injection through a reduction in both jet lift off from the surface and entrainment of the main flow toward the surface.

List of References

Eroglu, Adnan. "An Experimental Investigation of Entrainment and Mixing in Pulsed and Exponential Transverse Jets." diss. University of Washington, 1991.

Fric, T.F. "Structure in the Near Field of the Transverse Jet." diss. California Institute of Technology, 1990.

Haven, Brenda A. and M. Kurosaka. "Contoured 'Shaped' Holes: Improving Cooling Effectiveness & Aero Performance" White Paper Briefing to the A.F.O.S.R., 1994.

Kerrebrock, Jack L. *Aircraft Engines and Gas Turbines.* 2nd ed. Cambridge: MIT Press, 1992.

Kurosaka, M. "Contoured Holes for Film Cooling: the Effect of Kidney Shaped Vortices." Proposal for the A.F.O.S.R., 1994.

Norton, R.J.G. et.al. *Turbine Cooling System Design: Volume I - Technical Report.* Washington: GPO, 1990.

United States. *Integrated High Performance Turbine Engine Technology Initiative.* Ed. William Koop. N.p: n.p., [c. 1990].